UNIVERSITY OF CALIFORNIA SAN DIEGO

Membrane potential dynamics of the endoplasmic reticulum in neurons

A dissertation submitted in partial satisfaction of the
requirements for the degree Doctor of Philosophy

in

Biology with a Specialization in Multi-Scale Biology

by

Evan Campbell

Committee in charge:

Professor Brenda Bloodgood, Chair
Professor David Kleinfeld
Professor Andrew McCulloch
Professor Gulcin Pekkurnaz
Professor Padmini Rangamani
Professor Charles Stevens

2022

The dissertation of Evan Campbell is approved, and it is acceptable in quality and form for publication on microfilm and electronically.

University of California San Diego

2022

EPIGRAPH

Science is built up with facts, as a house is with stones.
But a collection of facts is no more a science than a heap of stones is a house

- Henri Poncare, 1901

TABLE OF CONTENTS

LIST OF ABBREVIATIONS

ANOVA	Analysis of variance
AP	Action potentials, also called spikes
ASAP3	Accelerated sensor of action potentials 3
$ASAP3_{ER}$	Endoplasmic reticulum targeted accelerated sensor of action potentials 3
$ASAP3_{PM}$	Plasma membrane targeted accelerated sensor of action potentials 3
ATP	Adenosine triphosphate
au	Arbitrary units
Avg	Average
bAP	Back-propagating action potentials
BSA	Bovine serum albumin
caff	Caffeine
CC	Correlation coefficient
CICR	Calcium induced calcium release
CMOS	Complementary metal-oxide-semiconductor
cpGFP	Circularly permuted green fluorescent protein
DIC	Infrared differential interference contrast
DIV	Days in vitro
DMEM	Dulbecco's Modified Eagle medium
DPT	Days post-transfection
EMCCD	Electron multiplying charge coupled device
ER	Endoplasmic reticulum
ER-GFP	Endoplasmic reticulum targeted green fluorescent protein
GEVI	Genetically encoded voltage indicator
HBSS	Hank's Balanced Salt Solution

Hz	Hertz
IP3	Inositol 1,4,5-triphosphate
IP3R	Inositol 1,4,5-triphosphate receptor
LTCC	L-type calcium channels
mA	Milliamp
mGluR	Metabotropic glutamate receptor
$mGluR_1$	Type 1 metabotropic glutamate receptor
$mGluR_5$	Type 5 metabotropic glutamate receptor
min	Minute
μm	Micrometer
μM	Micromolar
mm	Millimeter
mM	Millimolar
ms	Millisecond
mm^2	Square millimeter
mOsm	Milliosmoles
NCP-$ASAP_{ER}$	Endoplasmic reticulum targeted accelerated sensor of action potentials with a non-circularly permuted green fluorescent protein
NDSEG	National Defense Science and Engineering Graduate
NGS	Normal goat solution
NIBIB	National Institute of Biomedical Imaging and Bioengineering
NIH	National Institute of Health
NINDS	National Institute of Neurological Disorders and Stroke
nm	Nanometer
non-perm	Not permeabilized
P0-1	Postnatal day zero to one
pA	Picoamp

Pax	Paxilline
PBS	Phosphate buffered solution
PCC	Pearson’s correlation coefficient
Pen	Penitrem
perm	Permeabilized
PM	Plasma membrane
PTX	Picrotoxin
RMSE	Root mean square error
ROI	Region of interest
RRID	Research. Resource identifier
Ry	Ryanodine
RyR	Ryanodine receptor
s	Second
SD	Standard deviation
SEM	Standard error of the mean
SOCE	Store operated calcium entry
SR	Sarcoplasmic reticulum
tdT-ER	Endoplasmic reticulum targeted tdTomato
TTX	Tetrodotoxin
WT	Wild-type

LIST OF SYMBOLS

$a_{(x)}$	Linear coefficient that is a function of one-dimensional space
β	Scaling term
BK	Large potassium conductance
$b_{(x)}$	Exponential coefficient that is a function of one-dimensional space
Ca^{2+}	Calcium
CI	Confidence interval
Cl^-	Chloride
C_m	Membrane capacitance
CO_2	Carbon dioxide
CPCCOEt	7-(Hydroxyimino)cyclopropa[b]chromen-1a-carboxylate ethyl ester
°C	Degrees Celsius
ΔF/F	Change in fluorescence divided by baseline fluorescence
DHPG	(RS)-3,5-Dihydroxyphenylglycine
F	Faraday's constant
%F	Percent baseline fluorescence
H^+	Protons
$I_{(x,t)}$	Dimensionless function of both one-dimensional space and time, obtained from Alexa-594 dye fluorescence
$I_{0(x,t)}$	Input current
K^+	Potassium
λ	Length constant
MPEP	2-Methyl-6-(phenylethynyl)pyridine hydrochloride
Na^+	Sodium
MΩ	Mega ohms
mV	Millivolt

N	Number of experimental trials
OH^-	Hydroxide
p	Probability that a statistical measure will be greater than or equal to
pH	Potential of hydrogen measure of acidity
P_x	Permeability of an ion “X’ across a membrane
R	The universal gas constant
R^2	Statistical measure of fit
R_i	Resistivity of the volume within a membrane
R_m	Membrane resistance
R_s	Series resistance
T	Temperature in Kelvin
τ	Time constant
t	Time dimension
V	Voltage
V_{in}	Electrical potential within a membrane
V_m	Membrane potential
V_{out}	Electrical potential outside of a membrane
V_{eq}	The equilibrium potential, also called reversal potential or Nernst potential
x	One dimensional space
$[X]_{in}$	Concentration of ion species “X” inside of a membrane
$[X]_{out}$	Concentration of ion species “X” outside of a membrane
z	Valence of the charge on a free ion

LIST OF FIGURES

LIST OF TABLES

ACKNOWLEDGEMENTS

With tremendous gratitude to:

Brenda Bloodgood, who has an effusive love of science that is infectious to all whom work with her. Her creative yet rigorous study of biology has served as a great inspiration and guide. The ideas and studies presented in this dissertation have been borne out by many evolving hypothesis and conversations with Brenda.

The current and past members of the Bloodgood laboratory who have provided lively insight, assistance, comradery, and inspiration. Especially to my students who devoted countless hours to mastering methods of scientific investigation themselves, and whom I am immensely proud to have worked with.

The members of my committee, David Kleinfeld, Andrew McCulloch, Gulcin Pekkurnaz, Padmini Rangamani, and Chuck Stevens who have served as formal or informal collaborators and have been instrumental in developing the techniques and direction of this study. Especially to David Kleinfeld who has somehow withstood the full force of my inquisitive curiosity for optics and has consistently been an encouraging and brilliantly humorous guide for exploring biophysics and neurophysiology.

Chapter 2 is material appearing in E.P. Campbell, A.A. Abushawish, M.K. Bell, M. Haryono, P. Rangamani, B.L. Bloodgood. Electrical signals in neuronal ER: large, linear, and spatially restricted. In revision. The dissertation author was the primary investigator and author of this paper.

VITA

2008-2010 Research Assistant, Abramson Lab, Portland State University

2010-2014 Research Assistant, Kintner Lab, Salk Institute for Biological Studies

2010 Bachelor of Science, Chemistry: Biochemistry, Portland State University

2022 Doctorate of Philosophy, Biology with a Specialization in Multi-Scale Biology, University of California, San Diego

PUBLICATIONS:

E.P. Campbell, A.A. Abushawish, M.K. Bell, M. Haryono, P. Rangamani, B.L. Bloodgood. Electrical signals in neuronal ER: large, linear, and spatially restricted – manuscript in review.

M.G. Haberl, J. Laughlin, E.P. Campbell, K. Robinson, Y. Wang, L. Makrakis, A. Nguyen, J. Oshiro, S. Phan, E. Bushong, T.D. Deerinck, M.H. Ellisman, P. Rangamani, B.L. Bloodgood. Somatic ultrastructure compartmentalizes cerebellar neurons and guides intracellular Ca2+ flux – manuscript in preparation.

F. Puppo, S. Sadegh, C.A. Trujillo, M. Thunemann, E.P. Campbell, M. Vandenberghe, X. Shan, I.A. Akkouh, E.W. Miller, B.L.Bloodgood, G.A. Silva, A.M. Dale, G.T. Einevoll, S.Djurovic, O.A. Andreassen, A.R. Muotri, A. Devor (2021) All-optical electrophysiology in hiPSC-derived neurons with synthetic voltage sensors. Front. Cell. Neurosci. DOI: 10.3389/fncel.2021.671549.

A. Wu, B. Yu, Q. Chen, G.A. Matthews, C. Lu, E. Campbell, K.M. Tye, T. Komiyama (2020) Context dependent plasticity of adult-born neurons regulated by cortical feedback. Sci. Adv. DOI: 10.1126/sciadv.abc8319.

E.P. Campbell, I.K. Quigley, C. Kintner (2016). Foxn4 promotes gene expression required for the formation of multiple motile cilia. Development, DOI: 10.1242/dev.143859.

Acknowledgement for technical assistance in - J.L. Stubbs, E.K. Vladar, J.D. Axelrod, C. Kintner (2012) Multicilin promotes centriole assembly and ciliogenesis during multiciliate cell differentiation. Nat. Cell Biol., DOI: 10.1038/ncb2406.

ABSTRACT OF THE DISSERTATION

Membrane potential dynamics of the endoplasmic reticulum in neurons

by

Evan Campbell

Doctor of Philosophy in Biology with a Specialization in Multi-Scale Biology

University of California San Diego, 2022

Professor Brenda Bloodgood, Chair

The endoplasmic reticulum (ER) is a highly tortuous organelle that spans throughout a cell with a continuous membrane containing ion channels, pumps, and transporters. It is unknown if stimuli that gate ER ion channels can trigger substantial membrane potential fluctuations and if those fluctuations spread beyond their site of origin. Here, we visualize ER membrane potential dynamics in cultured rat hippocampal neurons by targeting a genetically-encoded voltage indicator specifically to the ER. We report a polarized ER membrane potential that bidirectionally responds to synaptic activity over hundreds of milliseconds.

Direct stimulation of ER ion channels generates depolarizations that scale with stimulus strength and reach tens of millivolts in amplitude. However, ER potentials do not spread beyond the site of receptor activation, exhibiting steep attenuation that is exacerbated by BK channels. Thus, segments of ER can generate large depolarizations that are actively restricted from impacting nearby, contiguous regions of membrane.

Chapter I: Introduction

The use of understanding biophysical properties in neurons is the basis they provide for clarifying higher scale functions of the nervous system. Insights at the molecular and cellular level are the first steps toward understanding mechanisms of cognitive functions like learning and memory, or dysfunctions that may manifest in neurological diseases. With this intent, I have concentrated the focus of my doctoral studies on describing a fundamental cellular property of neurons that was previously unknown and may broadly underpin signaling and functions of the nervous system. Namely, I have adapted an optical technique and have used it to specifically probe the endoplasmic reticulum (ER) organelle membrane for voltage signals.

In this dissertation, Chapter I will survey the contemporary scientific understanding of membrane potential in biological systems, ER structure and function, and methods of measuring voltage dynamics in organelles. Chapter II will present the original research performed during my doctoral studies, which is currently in review for publication in a scientific journal. Lastly, Chapter III will discuss the implications of the findings from my doctoral research and how they apply to the border body of scientific knowledge.

Membrane potential is central to neuronal signaling:

Membrane potential is a fundamental property of any membrane that separates electrical charge. In living cells, membrane potential is established by charged molecules as well as cations and anions that are separated by relatively impermeable phospholipid membranes (Overton 1899; Gorter and Grendel 1925; J. Bernstein 1868; Julius Bernstein 1902). Asymmetric distributions of ions on either side of these membranes are set by their relative permeabilities, which can be controlled by a variety of proteins embedded within membrane structures acting as ion pumps, transporters, or channels (Singer and Nicolson 1972; Hodgkin

and Keynes 1955; Caldwell et al. 1960; Hille 1975, 1978). The electrical charge generated by these asymmetric clouds of ions builds a net voltage associated with compartments on the inside and outside of membranes. The difference between which, determines the membrane's transmembrane voltage potential, which is also called membrane potential, and can be described by the equation:

$$V_m = V_{in} - V_{out}$$

Where V_m is the membrane potential, and V_{in} and V_{out} are the voltage values inside and outside of biological membranes, respectively (Overton 1899; Gorter and Grendel 1925; J. Bernstein 1868; Julius Bernstein 1902).

Membrane potentials in biological systems are often many tens of millivolts (mV) in amplitude, and in excitable membrane systems, can change rapidly when cellular activity stimulates conductance of ions across the membrane (Julius Bernstein 1902; K. S. Cole and Curtis 1939; Hodgkin and Huxley 1945, 1952). The most rapid of these changes can occur when membrane resistance suddenly decreases for a specific ion species, which is enacted by the opening of transmembrane ion channels and subsequent flow of ions through their channel pores along ionic electrical and chemical gradients (K. S. Cole and Baker 1941; Hodgkin 1951; Katz and Miledi 1970; Landau and Ben-Haim 1974; Jiang, Lee, et al. 2003). The driving force for ion diffusion through such pores is founded on the electrical charge of ions, as well as differences in concentrations of each ion species inside and outside of the membrane. If only one species of ion were present, the driving force from its charge and the driving force from its concentrations would sway ionic flux across a membrane until an equilibrium were reached between these two driving forces. The membrane potential at this equilibrium is defined as the reversal potential (or Nernst potential, or equilibrium potential) for that species of ion and is defined by the Nernst equation:

$$V_{eq} = \frac{RT}{zF} ln\left(\frac{[X]_{out}}{[X]_{in}}\right)$$

Where V_{eq} is the reversal (or equilibrium) potential, R is the universal gas constant, T is the temperature in Kelvin, z is the valence of the ion, F is Faraday's constant, and $[X]_{out}$ and $[X]_{in}$ are the concentrations of ions outside and inside of a biological membrane (W. Nernst 1888; Walther Nernst 1889). However, within biological systems where many ionic species are present, relative contributions of several ionic species govern the overall membrane potential. For example, potassium (K^+), sodium (Na^+), and chloride (Cl^-) ions primarily define the plasma membrane (PM) potential of neurons, and their combined membrane potential may be calculated by:

$$V_m = \frac{RT}{F} ln\left(\frac{P_K[K^+]_{out} + P_{Na}[Na^+]_{out} + P_{Cl}[Cl^-]_{out}}{P_K[K^+]_{in} + P_{Na}[Na^+]_{in} + P_{Cl}[Cl^-]_{in}}\right)$$

Where respectively, V_m is the membrane potential, R, T, and F are again the universal gas constant, temperature in Kelvin, and Faraday constant, and P_X, $[X]_{out}$, and $[X]_{in}$ are the permeability, the outside concentrations, and the inside concentrations of ion species "X", which may be either Na^+, K^+, or Cl^- (Goldman 1943; Hodgkin and Katz 1949). This equation commonly referred to as the Goldman, Hodgkin, Katz equation illustrates the contribution of each species of ion, and its concentration gradient, to establishing membrane potential across the PM. In biological membrane systems such as this, where multiple ion species present, the driving force acting on each type of ion is shaped by the difference between the overall membrane potential and its own reversal potential. Thus in living cells, the dynamics of charged ions form a circuitous interplay between overall membrane potential, the driving force for their own flux across membranes, and the driving force for the flux of other ion species as well.

In excitable membranes like the PM of neurons, increasing membrane potential can also trigger dramatic electrical fluctuations called action potentials (APs, or spikes), which rapidly rise and fall well over 100 mV in total amplitude (Hodgkin and Huxley 1939; Kenneth Stewart Cole 1949). These explosive fluctuations in membrane potential are triggered by the shift of voltage-sensitive protein domains in transmembrane ion channels, which changes their conformations and opens their ion-specific pores to allow ion conductance (Hille 1975; Jiang, Lee, et al. 2003; Jiang, Ruta, et al. 2003; Payandeh et al. 2011, 2012).

Conductance through voltage gated ion channels can alter membrane potential and stimulate other voltage gated ion channels, thus providing regenerative cascades of ion flux and predictable sequences of ion currents. For instance, APs in the PM of neurons are chiefly defined by Na^+ currents that depolarize the PM, followed by potassium K^+ currents that repolarize it (Hodgkin and Huxley 1952; Coombs, Eccles, and Fatt 1955). Here, the specific voltage sensitivity of Na^+ channels also defines an all-or-nothing activation threshold in membrane potential that, once passed, spurs the cascade of Na^+ and K^+ currents that make up a spike (Hodgkin and Huxley 1952; Armstrong and Bezanilla 1973). In this light, voltage sensitive protein domains dictate the initiation and dynamism of ion currents involved in APs. Proteins that can detect and change membrane potential, such as voltage gated ion channels, are thus central to defining the electrical properties of biological membrane systems.

A feature of APs that has been noted since the earliest studies of membrane potential in neurons is their capacity to rapidly spread across cellular membranes (Hodgkin 1937; Hodgkin and Huxley 1945). Indeed in neurons, APs are triggered at the initial segment of axons (or axon hillock), where voltage gated Na^{2+} channels are highest in density, then propagate throughout entire axonal projections by activating Na^+ and K^+ currents in successive lengths of axon (Hodgkin and Huxley 1945; Coombs, Curtis, and Eccles 1957; Colbert and Johnston 1996). Conduction velocities of APs along axon structures can approach 150 meters per second (s) in myelinated axons (Hursh 1939; Boyd and Davey 1968). The speed of this transmission is particularly important for neurons, which require efficient communication along elaborate axon projections that stretch many centimeters away from neuron somas (Ramón y Cajal 1899). At these widely distributed axon terminals, APs stimulate voltage gated calcium (Ca^{2+}) channels, which flux Ca^{2+} and coordinate the synchronous release of synaptic vesicles to conduct synaptic transmission between cells (KATZ and B 1969; Takahashi and Momiyama 1993; Verhage et al. 2000; Han and Jackson 2006; Ramón y Cajal 1899). In this way, propagation of membrane potential provides a basis for fast communication between cells separated by long distances via APs and synaptic communication. Accordingly, APs in neurons are the nervous system's primary method for detecting and relaying information such as sensory

experience (Adrian and Zotterman 1926a, [b] 1926). Thus, the biophysical properties of membrane potential in neurons effectively define the rate at which organisms can detect stimuli and mount behavioral responses (Sabatini and Regehr 1999).

Membrane potential dynamics provide input processing in neurons:

Whereas the axon hillock is usually the singular point of triggering AP output, most neurons receive thousands of synaptic inputs that generate excitatory or inhibitory postsynaptic potentials spread out along their intricate dendritic trees (Bannister and Larkman 1995a, [b] 1995; Larkman 1991). Summation of these postsynaptic potentials at the axon hillock determines the pattern and frequency of spiking. Thus, integration of postsynaptic potentials in dendrites is central to determining AP output and neurotransmission (Magee 2000; Häusser, Spruston, and Stuart 2000).

The broad spatial distributions and high numbers of synaptic inputs along dendritic branches provides neurons with an immense capacity to integrate postsynaptic potentials even due to passive propagation along complex dendrite structures. This form of passive propagation in can be described by what are known as cable properties of dendrites (W. Rall 1962). Cable properties describe the summation and spread of electrical signals along cellular structures by equating them to mathematical models of electrical circuits. Model complexity can be added to account for geometric and membrane complexity of cellular structures such as membrane surface area at branching structures, volumes enclosed by cylindrical or spherical structures, membrane resistances, membrane capacitances, resistivity of the material enclosed by membranes, or ionic conductances past membranes (W. Rall et al. 1992; Wilfrid Rall 1995). Imbuing such models with realistic parameters measured at dendrites can derive the passive electrical properties of dendrite membrane systems, such as the distance and times at which electrical impulses diminish while spreading due to passive propagation alone. These qualities are described by parameters known as length and time constants, respectively defined as the distance and time at which electrical impulses decrease to

37% of their original magnitude. Cable properties can also illustrate differences in magnitude and duration of electrical signals that arise in different cellular compartments or combine across intricate dendritic structures. These many measures describe the filtering effects due to generation, dispersion, combination of electrical charges in dendrites (W. Rall 1967; Jack and Redman 1971; Rinzel and Rall 1974; Mainen et al. 1996). Thus cable properties can influence how electrical signals combine and transmit to the axon hillock where they determine cellular output.

In concert with cable properties, specific ion channel compositions at synapses or along regions of dendrites can modify amplitude and duration of postsynaptic potentials. Indeed a large variety of receptor activities in dendrites can increase or decrease the amplitude, kinetics, and spread of postsynaptic potentials (Lipowsky, Gillessen, and Alzheimer 1996; Hoffman et al. 1997; Geiger et al. 1997; Spruston 1999). In many cases, active input processing overcomes the effects of dendritic filtering (Magee and Cook 2000; S. R. Williams and Stuart 2000; Cook and Johnston 1999; Magee 1999). In fact, active input processing in dendrites can effectuate a range of sublinear or superlinear electrical responses depending on factors like cell type, dendritic region, synaptic receptor composition, and stimulation timing (Cash and Yuste 1999; Polsky, Mel, and Schiller 2004; Losonczy and Magee 2006; M. E. Larkum, Zhu, and Sakmann 1999; Schiller et al. 2000; Gasparini and Magee 2006; Roth and Häusser 2001). APs that initiate at the axon hillock can even be propagated back into dendrites through the action of voltage gated Na^{+} and Ca^{2+} channels (backpropagating action potentials, or bAPs; G. J. Stuart and Sakmann 1994; G. Stuart, Schiller, and Sakmann 1997; Schiller et al. 1997). Unsurprisingly, these broad arrays of membrane potential responses are important for a variety of local functions such as synaptic plasticity (Kim et al. 2015; Losonczy, Makara, and Magee 2008; Wei et al. 2001; Bicknell and Häusser 2021), as well as global functions like controlling spike frequency (Stephen R. Williams and Stuart 2002; M. E. Larkum, Zhu, and Sakmann 1999; Golding and Spruston 1998).

Dendritic integration has clear implications for cognitive functions as well. An elegant example of this is the observation that dendritic plateau potentials which trigger bust spiking in CA1 pyramidal neurons

of the hippocampus, can also encode neurons to fire in one area of an external environment from only a single bursting event. The rapid form of plasticity that generates these "place cells" is believed to generate underlie associative learning and conjunctive memory formation (Bittner et al. 2015, 2017; Hsu et al. 2018).

Membrane potential is also essential at intracellular membranes:

Like at the PM, membrane potential and current flow across internal membranes have demonstrable impacts on the function of several organelles. For example, mitochondria have a highly polarized membrane potential that is largely generated by proton (H^+) transporters (Sorgato, Keller, and Stühmer 1987; Tedeschi, Mannella, and Bowman 1987; for review see Zorova et al. 2018) and is essential for the synthesis of adenosine triphosphate (ATP; Mitchell 1961; Stock, Leslie, and Walker 1999; for review see Mitchell 1966; Zorova et al. 2018). While mitochondria are the primary source of ATP to power cellular functions, they can also participate in Ca^{2+} and stress response signaling (Vasington and Murphy 1962; Ishii, Hirose, and Iino 2006; for review see Rosario Rizzuto et al. 2012; Eisner, Picard, and Hajnóczky 2018). To meet these many functions, the mitochondrial membranes contain a variety of selective and non-selective ion channels, including voltage sensitive channels that contribute to the transport of metabolites (Colombini 1979; Novgorodov et al. 1991; A. C. Lee et al. 1998), Ca^{2+} uptake (Kirichok, Krapivinsky, and Clapham 2004), volume regulation (Garlid 1996), and apoptosis (Vander Heiden et al. 2000). Regulation of mitochondrial membrane potential by large conductance K^+ channels (BK) is also suggested to be important for broader physiological functions, such as increasing the resilience of cardiac cells to ischemia (Bentzen et al. 2009; Soltysinska et al. 2014; Gałecka et al. 2021) and inhibiting production of harmful reactive oxygen species in neurons (Kulawiak et al. 2008). Taken together, membrane potential is essential for several essential mitochondrial functions.

Lysosomes also possess plentiful mechanisms of regulating membrane potential and applications of it to their functions. The lysosomal membrane potential is predominantly set by Na^+ and H^+ gradients

(X. Wang et al. 2012). Lysosomal two-pore channels, that are gated by PI(3,5)P2 and modulated by mTOR signaling, generate Na^+ currents which increase the fusogenic potential of the organelle membrane (X. Wang et al. 2012; Cang et al. 2013). While H^+ pumps and non selective cation channels in lysosomes are required for release of Ca^{2+} (Churchill et al. 2002; Cao et al. 2015, 2017). Still further channels, which are gated by voltage, drive Ca^{2+} efflux and refilling of lysosomal stores (Tian et al. 2015; W. Wang et al. 2017). Thus while some functions of membrane potential in lysosomes are consistent with other organelles, such as regulation of Ca^{2+} handling, the lysosome also uses membrane potential for novel functions such as regulation of membrane fusion.

Nuclear membrane potential is determined by its stringent regulation of structure and transport. The nuclear membrane comprises a membranous subnetwork of the ER that encloses the genetic material of eukaryotic cells. It does so using two concentric sets of membranes called the nuclear envelope, and a series of nuclear pores that bridge the cytoplasm and nucleoplasm (Watson 1955; Mazzanti, Bustamante, and Oberleithner 2001). While the nucleus invariably encloses electrical charges associated with the moieties of nucleic acids and proteins, the nucleoplasm also contains a number of asymmetric ion compositions with those of the cytoplasm (Oberleithner et al. 1993; Century, Fenichel, and Horowitz 1970; Century and Horowitz 1974). Nuclear membrane potential is therefore thought to be established from the combination of fixed changes associated with genomic and protein material as well as ionic gradients set through nuclear pores and by the nuclear envelope (Mazzanti et al. 1990; Mazzanti, Bustamante, and Oberleithner 2001). Indeed the nuclear envelope encloses a many ion channels, including large conductance K^+ channels that are Ca^{2+} or voltage gated (Mazzanti et al. 1990; Maruyama, Shimada, and Taniguchi 1995; O. Fedorenko et al. 2010; O. A. Fedorenko and Marchenko 2014). In addition to shaping nuclear membrane potential, these channels are proposed to facilitate Ca^{2+} release into the nucleus through inositol 1,4,5-triphosphate receptors (IP3Rs) and ryanodine receptors (RyRs; O. A. Fedorenko and Marchenko 2014; Mak and Foskett 1994; Marchenko et al. 2005; Mak, McBride, and Foskett 1998; Taufiq-Ur-Rahman et al. 2009). Nuclear Ca^{2+} in turn mediates essential functions such as nuclear membrane fusion (Sullivan, Busa,

and Wilson 1993), and CREB activation that controls gene expression for late-phase plasticity and neuronal survival (O. A. Fedorenko and Marchenko 2014; Hardingham et al. 1997; Hardingham, Arnold, and Bading 2001; Papadia et al. 2005). By similar mechanisms, nuclear BK channels in hippocampal neurons and macrophages have been shown to modulate nuclear membrane potential and are believed to be necessary for proper CREB phosphorylation and translocation to the nucleus (Li et al. 2014; Selezneva et al. 2021). Clearly, when examined, the electrical signaling repertoire of organelles is multifaceted, and essential.

The ER is heterogeneous in structure and function:

The ER is a tortuous organelle that extends throughout a cell as a continuous anastomosing network of membranes (Dayel, Hom, and Verkman 1999; Martone et al. 1993). In neurons, the ER is particularly elaborate as emanates from the outer nuclear lamina and reaches into axons, dendrites, and dendritic spines, often crossing many hundreds of micrometers in total distance (Terasaki et al. 1994; Tsukita and Ishikawa 1976; Martone et al. 1993; Spacek and Harris 1997; Y. Wu et al. 2017; Cui-Wang et al. 2012). The ER has a rich diversity of structural subdomains including the nuclear envelope, large sheet-like cisternae, and dense polygonal grids of tubules (Watson 1955; Porter and Yamada 1960; Snapp et al. 2003; Shibata et al. 2008; Nixon-Abell et al. 2016; for review see Goyal and Blackstone 2013). In neurons, which have highly heterogeneous morphology themselves (Ramón y Cajal 1899), the specialization of ER structural subdomains is particularly distinctive. For example, dense grids of ER tubules that have high proportions of membrane surface area form at dendritic branch points and along stretches of highly active dendrite (Cui-Wang et al. 2012). Also, within the largest and most active dendritic spine compartments large stacks of flat ER sheets form bulky structures called spine apparatuses (Spacek and Harris 1997; Y. Wu et al. 2017). Here, the vast range of motifs in ER membrane ultrastructure are laid bare by the elongated and compartmentalized morphology of neurons.

A rich diversity of functions have also been attributed to the many structural domains of the ER, which can be both cell type and compartment specific. Rough ER, so called because it is studded with ribosomes, predominantly forms large sheets-like cisternae near the nucleus, which are the most concentrated sites of protein synthesis, modification, and quality control in a cell (Redman and Sabatini 1966; Dallner, Orrenius, and Bergstrand 1963; Shibata et al. 2010). Conversely, smooth ER that lacks significant ribosome incorporation, predominantly forms ER tubules and is the cell's primary source of lipid synthesis (Dallner, Orrenius, and Bergstrand 1963; Shibata et al. 2010; Higgins 1974). In neurons, ER that enters dendrites and axons is predominantly smooth ER, which can serve numerous functions (Broadwell and Cataldo 1983; Pozzo-Miller et al. 1997). For example, the ER also encloses the largest intracellular deposits of Ca^{2+}, which are encapsulated by massive cisterns of smooth ER and occur frequently in axons and at dendrites, providing local Ca^{2+} release and buffering (Hales et al. 1974; McGraw, Somlyo, and Blaustein 1980; Pozzo-Miller et al. 1997; for review see Lynes and Simmen 2011). Further, dense sinuous grids of ER tubules that form adjacent to dendritic spines or at branch points in response to group I metabotropic glutamate receptor (mGluR) signaling can slow diffusion along the ER and effectively increasing delivery of proteins and cellular resources into active sections of dendrites (Cui-Wang et al. 2012). Lastly, spine apparatuses may also assemble in response to rapid Ca^{2+} transients in active dendritic spines. Within these spine compartments the spine apparatus facilitates both rapid and slow forms of signal transduction across the compartment volume (Basnayake et al. 2019, 2021). These examples in neurons illustrate how adaptively and precisely the ER is integrated into cellular functions and signaling.

The ER is also unique in that it contacts every other organelle type, earning it distinction as the central hub for the organelle "interactome" (Valm et al. 2017; H. Wu, Carvalho, and Voeltz 2018). Contact points between the ER and other membrane systems can exhibit unique membrane phase behavior and may be coordinated by an array of contact-specific tethering proteins (King et al. 2020). Through these contact points the ER facilitates a range of organelle functions like mitochondrial division and DNA replication (Friedman et al. 2011; Ryu et al. 2012; Lewis, Uchiyama, and Nunnari 2016), mitochondrial Ca^{2+} uptake

(R. Rizzuto et al. 1998), phospholipid transfer with the golgi or peroxisomes (Peretti et al. 2008; Raychaudhuri and Prinz 2008), and endosome fission (Rowland et al. 2014; Hoyer et al. 2018; for review of all ER contact points see H. Wu, Carvalho, and Voeltz 2018). In neurons, ER contact points with every other organelle are evident across dendritic, somatic, and axonal compartments, including abundant contacts with the highly active PM (Spacek and Harris 1997; Y. Wu et al. 2017). ER contact points in neurons are known to regulate endosome mediated neurite outgrowth (Raiborg et al. 2015) and subcellular trafficking of organelles such as lysosomes along axons (Özkan et al. 2021). The sheer variety of contributions the ER makes to organelle functions clarifies its role as the central hub of the organelle interactome.

The ER's contribution to subcellular trafficking of organelles may hold special significance in neurons, which have elongated structures requiring metabolic and signaling demands at regions far removed from neuron somas. Indeed, dendrites have been shown to utilize various mechanisms for shuttling Golgi and mitochondria to highly active dendrite regions (Horton and Ehlers 2003; Chang, Honick, and Reynolds 2006; Pekkurnaz et al. 2014; Basu et al. 2021). The ER's influence on organelle trafficking in neurons may be understood through its many contact points (Özkan et al. 2021) as well as its ability to interpret the cytoskeletal "tubulin code" per selective binding between ER proteins and subsets of post-translationally modified microtubules. Groundbreaking work has recently shown that this role of the ER is necessary for distributing all organelle types throughout cells (Zheng et al. 2021). Though investigation in this area is still early, these mechanisms may have important implications for activity-dependent trafficking of smooth ER and polyribosomes to active spines and dendrite, where they enlarge synaptic structures and promote spine clustering (Chirillo et al. 2019; Ostroff et al. 2002). Similarly, ER interpretation of the tubulin code may underlie subcellular trafficking of Golgi, recycling endosomes, mitochondria, and lysosomes in neurons, which orchestrate protein synthesis and structural plasticity in dendrites (Horton and Ehlers 2003; Park et al. 2006; Chang, Honick, and Reynolds 2006; Goo et al. 2017). These mechanisms may add to the explanatory power to synaptic remodeling and spine plasticity regulated by microtubule dynamics

(Jaworski et al. 2009; Gu, Firestein, and Zheng 2008), and provide yet further catalogs of how ER biology is essential to neuronal functions.

The ER widely mediates Ca^{2+} signaling within neurons:

Dynamics of Ca^{2+} ions in the cytosol of cells is a ubiquitous and vital form of second messenger signaling that controls functions ranging from cellular excitability to exocytosis, structural plasticity, and transcription (for review see Clapham 2007; Ross 2012). Across all cell types, the ER is well established as the primary organelle involved in intracellular Ca^{2+} signaling. The lumen of the ER contains stores of Ca^{2+} that can reach millimolar concentrations, which are roughly 10^4 fold higher in concentration than Ca^{2+} in the cytoplasm. These represent the largest and most abundant Ca^{2+} stores within cells (Hales et al. 1974; Pozzo-Miller et al. 1997; Somlyo et al. 1981). From its massive intracellular Ca^{2+} stores, the ER can both release Ca^{2+} into the cytosol through IP3Rs or RyRs (Hales et al. 1974; Streb et al. 1983; Fleischer et al. 1985; for review see Ross 2012), or remove Ca^{2+} by pumping it back into ER stores using SERCA pumps (Hasselbach and Makinose 1961, 1963). Multiple modes of ER release through IP3Rs and RyRs can also generate Ca^{2+} transients with different concentrations, spatial scales, and kinetics (Lock and Parker 2020; Parker and Yao 1991). For example, small localized Ca^{2+} transients called "puffs" last for tens of milliseconds and remain restricted within a few micrometers or less (Yao, Choi, and Parker 1995; M. Bootman et al. 1997). In contrast, larger Ca^{2+} signals can last for several seconds and sweep through entire cells as regenerative propagating waves (Woods, Cuthbertson, and Cobbold 1986; Parker and Yao 1991; M. D. Bootman, Berridge, and Lipp 1997). These Ca^{2+} waves can transmit information across cellular compartments and repeat with frequencies that depend on cell type and stimulation. However, a common feature that is shared by all Ca^{2+} waves is their dependence on Ca^{2+} induced Ca^{2+} release (CICR) by IP3Rs and RyRs, or G protein signal transduction that stimulates IP3Rs (Nash et al. 2001; Cobbold et al. 1988; Kawabata et al. 1996; Parker and Ivorra 1990; Bezprozvanny, Watras, and Ehrlich 1991; for review see

Smedler and Uhlén 2014; Cheng and Lederer 2008). Thus, the ER can orchestrate Ca^{2+} signaling across many spatiotemporal scales and it is the principal organelle that controls Ca^{2+} dynamics.

The ER in neurons mediates a constellation of Ca^{2+} signaling across axons, somas, and dendrites. Activation of IP3Rs and RyRs during spontaneous neuronal activity gives rise to small Ca^{2+} transients that last for less than 100 milliseconds (ms), which resemble Ca^{2+} puffs described in other cell types, and do not coincide with PM depolarizations. These elementary Ca^{2+} events occur at consistent dendritic locations, most frequently located at dendritic branch points, and spread 2 micrometers (μm) along dendrites on average. The concentrations of Ca^{2+} puffs can be 10-70% of the Ca^{2+} concentrations that are generated by conductance through PM channels during bAPs in the same locations (Manita and Ross 2009; G. J. Stuart and Sakmann 1994; Schiller et al. 1997). In contrast to puffs, large sweeping waves of Ca^{2+} waves can also be generated by ER in dendritic branches. These waves can be spurred by coordinated stimulation of IP3Rs and depolarization of the PM, and can spread hundreds of μm along dendritic trees. Concentrations of Ca^{2+} waves in dendrites can reach 5 micromolar (μM), more than 15 fold greater than Ca^{2+} concentrations observed from conductance through PM channels during bAPs alone (Pozzo Miller et al. 1996; Matthew E. Larkum et al. 2003; T. Nakamura et al. 2000; Helmchen, Imoto, and Sakmann 1996). Ca^{2+} waves also persist for many seconds, significantly longer than Ca^{2+} puffs, but require many minutes (min) of recovery before initiating again. While these waves propagate at approximate speeds of 100 micrometers per second, roughly 2000 fold slower than bAP propagation, they can invade the somatic compartment and increase excitability and spike rate (Takeshi Nakamura et al. 2002; Hagenston, Fitzpatrick, and Yeckel 2008). Therefore, despite arising within the same dendritic compartments, Ca^{2+} waves are generated by different receptor activities than Ca^{2+} puffs and have diametrically distinct concentration scales, spread, kinetics, and influence on cell spiking. Waves and puffs of Ca^{2+} denote the ER's extensive range of Ca^{2+} signaling scales in neurons.

Ca^{2+} signaling from the ER also has an expansive repertoire of functional applications in neurons. In axon terminals, the Ca^{2+} concentration of ER stores is associated with presynaptic release probability (de

Juan-Sanz et al. 2017). Here, mobilization of Ca^{2+} from the ER does not directly coordinate synchronous fusion of presynaptic vesicles, which happens at more rapid and focal scales at activity zones (Dodge and Rahamimoff 1967), but instead increases the baseline of spontaneous release. This form of scaling-up the probability of presynaptic release is primarily attributed to neuromodulator signaling to the ER enacted by receptors such as muscarinic acetylcholine receptors (Sharma and Vijayaraghavan 2003; Llano et al. 2000). Within the somatic compartments of neurons, CICR enacted through RyRs the ER is associated with amplifying Ca^{2+} signals arising from conductance through channels at the PM (Sandler and Barbara 1999). Similar mechanisms of CICR via RyRs of the ER also enhance Ca^{2+} signals from synaptic activity within dendritic spines compartments (Emptage, Bliss, and Fine 1999). These functions of the ER show its involvement with Ca^{2+} signaling and excitability across every compartment of neurons.

Within the same compartment of neurons, the ER may also provide multiple Ca^{2+} signaling functions and adapt them as signaling requirements change. Such adaptable functions may be enacted by unique receptors or structures of the ER. For example, in spine compartments Ca^{2+} conductance through RyRs of the ER is associated with specific forms of short-lasting synaptic potentiation. Whereas Ca^{2+} conductance through IP3Rs is associated with intermediate and long-term forms of potentiation (Raymond and Redman 2006; Fernández de Sevilla et al. 2008). The presence and prominence of ER structures within spine compartments also seems to have dependence on spine size, activity level, and receptor compositions. Within large spines that contain strong synapses, the ER forms stable long lasting structures that are associated with substantial Ca^{2+} transients and are required for long term depression mediated by mGluRs (Holbro, Grunditz, and Oertner 2009). Within smaller less-active spines, the ER does not establish permanent structures, but instead enters them temporarily. Here, thin ribbons of ER transiently enter smaller spine compartments in response to heightened synaptic activity and stabilize Ca^{2+} dynamics to prevent runaway excitation (Perez-Alvarez et al. 2020). This demonstrates the adaptable functionality of ER Ca^{2+} signaling, which can provide specific utilities for the individual requirements of each synapse.

Ca^{2+} signaling machinery of the ER is cell type and compartment specific:

Modalities of ER Ca^{2+} signaling can also be unique within neuronal cell types. For example, although the ER is integrated tremendously with Ca^{2+} signaling in Purkinje cells of the cerebellum (Finch and Augustine 1998; Takechi, Eilers, and Konnerth 1998; S. S. Wang, Denk, and Häusser 2000), these neurons do not have regenerative Ca^{2+} waves that propagate across their dendritic arbors, as have been observed in pyramidal neurons in the hippocampus (Jaffe and Brown 1994; T. Nakamura et al. 1999). One explanation for cell type specific Ca^{2+} signaling by the ER may be dissimilar expression of ER receptors and proteins. Indeed, even similar cell types can differ in their relative expression of ER Ca^{2+} receptors. In the hippocampus, pyramidal neurons of the CA1 region express IP3Rs more abundantly than those of the CA3 region. Conversely, CA3 pyramidal neurons express RyRs more highly than CA1 pyramidal neurons (Nakanishi, Kuwajima, and Mikoshiba 1992; Sharp et al. 1993). In addition to ER Ca^{2+} channels, different cell types of neurons also express varying levels of Ca^{2+} binding proteins (Arai et al. 1991; Laube et al. 2002; Mulder et al. 2009; for review see Andressen, Blümcke, and Celio 1993), including proteins that chelate Ca^{2+} inside ER stores (Villa et al. 1992; Furlan et al. 2020; Hagiwara et al. 2012). These Ca^{2+} binding proteins within ER stores maintain their high Ca^{2+} concentrations and determine the amount of Ca^{2+} readily mobilized for signaling (Nakanishi, Kuwajima, and Mikoshiba 1992; Sharp et al. 1993). Therefore Ca^{2+} signaling from the ER may greatly differ across neuronal cell types based on the presence and relative abundance of Ca^{2+} release and storage proteins.

Subcellular trafficking of Ca^{2+} handling proteins in the ER may also account for differences in ER Ca^{2+} signaling across neuronal cell types. In CA3 pyramidal neurons of the hippocampus, RyRs localize to the ER in the soma and in dendritic spines, whereas IP3Rs preferentially inhabit the ER in dendritic shafts and are absent within the soma (Nakanishi, Kuwajima, and Mikoshiba 1992; Sharp et al. 1993). This contrasts receptor distributions in Purkinje neurons, where RyRs only localize to the ER in somas and dendritic shafts, and are conspicuously absence from ER within spine compartments, whereas IP3Rs inhabit ER in both dendritic shafts and spines (Walton et al. 1991; Sharp et al. 1993). Further, IP3Rs in the ER

localize at subsets of Ca^{2+} stores in the ER, which themselves are heterogeneously distributed within neuronal structures (Takei et al. 1992; Villa et al. 1991). Indeed, ER Ca^{2+} stores have asymmetric cellular distributions, as well as unique protein populations within their lumens, which can differ from other ER stores in the same cell (Macer and Koch 1988; Gatti et al. 2001; for review, see Koch 1990). The functional significance of such pairings between specific Ca^{2+} release channels and stores in the ER is supported by observations that IP3Rs and RyRs can mobilize Ca^{2+} from separate sources neuronal ER, which are in turn replenished by unique refilling mechanisms (Chen-Engerer et al. 2019). Thus, compartmentalization of particular ER receptors and Ca^{2+} deposits may comprise one basis for generating the vast diversity of ER Ca^{2+} signaling in neurons.

Coupling between Ca^{2+} signaling proteins at the ER and the PM can also patently shape Ca^{2+} dynamics mediated by the ER. Interactions between proteins of the ER and the PM are prolific and occur at close appositions between the two membranes. These ER-PM contact points typically come within 30 nanometers (nm) or less, and serve functions ranging from lipid synthesis and transfer (Pichler et al. 2001; Hoffmann et al. 2019), to maintenance of ER morphology (Manford et al. 2012), and various modes of Ca^{2+} handling (Perni et al. 2015; for review see Saheki and De Camilli 2017). One of the most abundant forms of ER-PM contacts are areas of store operated Ca^{2+} entry (SOCE). SOCE is an ER Ca^{2+} store refilling process, which is initiated by transmembrane Ca^{2+} sensor proteins STIM1 or STIM2 when they detect low Ca^{2+} concentrations at their domains in the ER lumen (Liou et al. 2005; Zhang et al. 2005; Stathopulos et al. 2008; Gudlur et al. 2018). STIM proteins translocate to ER near the PM and form complexes with a number of proteins including SERCA pumps in the ER, and Orai Ca^{2+} channels in the PM (Feske et al. 2006; Sampieri et al. 2009; Srikanth et al. 2012). At these ER-PM contact points STIMs directly gate Orai channels to influx Ca^{2+} from the extracellular space, which is simultaneously pumped into nearby Ca^{2+} stores of the ER (Prakriya et al. 2006; Sampieri et al. 2009). RyRs too can couple with SOCE protein complexes, which serve to prolong STIM1 activation and Ca^{2+} uptake (Thakur, Dadsetan, and Fomina 2012). In a similar way, IP3Rs associate with these contact points, which enhances SOCE (Boulay et al.

1999; Sampieri et al. 2018), but more importantly, stabilizes IP3Rs and licenses them to become active (Thillaiappan et al. 2017, 2021). Thus SOCE protein complexes control both influx and efflux of Ca^{2+} from the ER.

RyRs of the ER are also highly associated with ER-PM contact points that are stabilized by K^+ channels of the PM. The best-known examples of these are contacts made between RyRs in the ER and clusters of Kv2.1 channels as well as voltage gated L-type Ca^{2+} channels (LTCCs) in the PM (Fox et al. 2015; Kirmiz et al. 2018; Vierra et al. 2019). In neurons, these complexes amplify Ca^{2+} signals from LTCCs in the PM via CICR from RyRs at the ER and generate local somatodendritic Ca^{2+} signals independent of APs (Vierra et al. 2019). Clustering of RyRs, Kv2.1 channels, and LTCCs is also necessary for zinc-based stress responses enacted by of Kv2.1 channel trafficking, as well as LTCC dependent activation of CREB for gene expression (Schulien et al. 2016; Vierra et al. 2021). In the somatic compartments of inhibitory neurons of the cochlear nucleus, RyRs can also couple with BK channels and voltage gated P/Q Ca^{2+} channels at the PM. Here, CICR by RyRs enables burst spiking activity in these neurons (Irie and Trussell 2017). Therefore, in view of the ER's many forms of Ca^{2+} signaling, coupling between PM and ER proteins provides yet another mechanism to alter Ca^{2+} signaling for cell type and compartment specific functions.

There is a strong biophysical basis for membrane potential of the ER and its involvement in signaling:

Despite the numerous vital functions of the ER and its highly dynamic conductance of ions like Ca^{2+}, membrane potential dynamics of the ER are yet to be definitively described. Early calculations made from studies of cardiomyocytes have shown that regulation of membrane potential is necessary to compensate for the charge generated by Ca^{2+} release from the ER (or sarcoplasmic reticulum, SR, in the case of cardiac cells; Oetliker 1989). The ER also maintains concentration gradients for many ion species, which change in composition in response to cellular activity (Pozzo-Miller et al. 1997; Somlyo et al. 1981). Furthermore, in addition to Ca^{2+} channels, the ER has a variety of resident cation and anion channels,

including some that are gated by voltage (Miller 1978; Tanifuji, Sokabe, and Kasai 1987; Townsend and Rosenberg 1995; Buyse et al. 1998; Yazawa et al. 2007; Zhu, Yan, and Thornhill 2014), ions (Ahern and Laver 1998; Kuum et al. 2012), or ligands (Kawano et al. 1992; Duncan et al. 1997; Ashrafpour et al. 2008). These features of the ER demonstrate its inherent capacity to maintain and regulate membrane potential.

The ER's ion channel compositions and ionic gradients across its membrane give rise to the prospect of highly dynamic electrical signaling within its membrane system. This concept could have profound implications for signaling in neurons. Efforts to model membrane potential in the ER even suggest that electrical signals may spread across its membrane structure, as occurs at the PM (Shemer et al. 2008). If changes in membrane potential can propagate along the ER's structure, they could facilitate rapid signaling between distant regions of a cell. An alternative hypothesis to this may be that changes in ER membrane potential are compartmentalized. If this were the case, changes in membrane potential may represent a mechanism for providing region-specific control of driving force for Ca^{2+} release from the ER (Oetliker 1989). Yet in spite of these compelling biological possibilities, the fundamental electrical signaling capabilities of the ER membrane have yet to be unambiguously measured.

Methods of measuring organelle membrane potential are rapidly advancing:

Organelle membrane potential has been measured using a variety of strategies. Direct recordings with electrodes are feasible for organelles that are large, like the nucleus (Mak and Foskett 1994; Stehno-Bittel, Lückhoff, and Clapham 1995), or that have relatively large volumes like mitochondria, chloroplasts, vacuoles, endosomes, and lysosomes (Tedeschi, Mannella, and Bowman 1987; Sorgato, Keller, and Stühmer 1987; Pottosin 1992; Bertl et al. 1998; Saito, Hanson, and Schlesinger 2007; Xu et al. 2007). In contrast, the ribbons and tubules that make up the ER may be only tens of nanometers in diameter (Y. Wu et al. 2017; Spacek and Harris 1997) and can be highly dynamic (C. Lee and Chen 1988; Nixon-Abell et al. 2016; Perez-Alvarez et al. 2020), prohibiting access with recording electrodes.

In recent decades, a prime focus for molecular tool development has been generating fluorescent sensors to optically measure membrane potential. These efforts have seen the development of an exhaustive variety of fluorophore-based tools built on scaffolds of chemicals, proteins, or a hybrid of the two (Huang, Walker, and Miller 2015; Siegel and Isacoff 1997; Sakai et al. 2001; Grenier et al. 2019; Abdelfattah et al. 2019). However, all of these techniques utilize the same principle of modulating fluorescence intensity in response to changes in voltage across cellular membranes. The creative design of these tools has produced sensors that emit at wavelengths covering nearly the entire spectrum of light, and that report voltage through fluorescence changes that increase, decrease, or differ between two fluorophores (Piatkevich et al. 2018; Alich et al. 2021; Beck and Gong 2019; for review see Knöpfel and Song 2019; Mollinedo-Gajate, Song, and Knöpfel 2021). Genetically encoded voltage indicators (GEVIs) have gained particular traction due to their ability to be selectively expressed in neuronal cell types, their compatibility other fluorescent tools such as fluorescent Ca^{2+} indicators, and their ability to be targeted to specific cellular regions such as dendritic spines or somas using endogenous mechanisms of protein trafficking (Platisa et al. 2022; Bando, Wenzel, and Yuste 2021; Cornejo, Ofer, and Yuste 2021; Villette et al. 2019). These advancements have provided a suite of novel tools to study membrane potential in living cellular systems.

Recently, several techniques have been developed that enable the visualization of organelle membrane potential in living cells (Saminathan et al. 2021; Matamala et al. 2021; Sepehri Rad et al. 2018; Sanchez et al. 2018). Efforts to optically measure membrane potential in the ER (or SR in cardiac cells) have hinted that the ER may be highly polarized (Matamala et al. 2021; but see Sanchez et al. 2018) and rapidly follow changes in the PM potential (Sepehri Rad et al. 2018; but see Sanchez et al. 2018). While these reports of ER membrane potential are intriguing, they are limited by either lack of specificity in the subcellular targeting of the voltage sensor, uncertainty about the orientation of the sensor, or high variability in measurements.

Concluding perspective:

The focus of my doctoral studies has been investigating membrane potential dynamics of the ER in neurons. This is due to the likelihood that regulation of membrane potential contributes to some, if not all of the ER's vital roles in neuronal signaling and functions. In particular, I have been fascinated by the capacity of the ER's membrane potential for signaling either across long distances, or within local compartments of neurons. To my mind, the important emphasis of this question is how changes in ER membrane potential may alter the driving force for Ca^{2+} release across these spatial scales, and thus global or compartmentalized forms of Ca^{2+} signaling. However, the electrical properties of the ER membrane may have far-reaching implications for a number of essential functions in neurons, which I will discuss at further length in the Chapter III of this dissertation.

To conduct my studies, I selectively targeted the localization of a GEVI, the Accelerated Sensor of Action Potentials 3 (ASAP3; Villette et al. 2019), to the ER membrane through the addition of an ER retention peptide signal. In brief, imaging of $ASAP3_{ER}$ in dissociated neurons from the rat hippocampus revealed that the ER membrane is highly polarized and that its membrane potential changes many tens of millivolts in response to network activity, mGluR signaling, or direct activation of RyRs. Moreover, by focally activating RyRs, I found that the ER membrane potential responds linearly to increases in stimulus strength, and that despite the large magnitude of these changes, they are tightly restricted to the cellular regions that were stimulated directly. A passive cable model of the ER membrane, constructed through a collaboration with the Rangamani group at UC San Diego, predicts that ER membrane resistance and luminal resistivity are the most likely properties that restrict the spread of electrical activity. This led me to test the involvement of BK channels in lowering ER membrane resistance and restricting electrical spread along ER membrane. When BK channels were blocked, I observed an increased spread of depolarizations along the ER membrane in response to RyR stimulation. Which demonstrated that active conductance through BK channels is one of the ER membrane's features that limits the spread of electrical signals. Together, the findings of my doctoral work suggests that membrane potential in the ER is highly dynamic

and responsive to cellular stimuli. Yet, electrical changes in the ER membrane are prevented from spreading along its structure, and thus preserve the driving force for Ca^{2+} release from ER in directly adjoining regions of neurons. I propose that this may be a mechanism that contributes to regional control of Ca^{2+} signaling mediated by the ER. The full extent of these studies is presented in Chapter II of this dissertation.

References:

Abdelfattah A. S., Kawashima T., Singh A., Novak O., Liu H., Shuai Y., Huang Y. C., Campagnola L., Seeman S. C., Yu J., Zheng J., Grimm J. B., Patel R., Friedrich J., Mensh B. D., Paninski L., Macklin J. J., Murphy G. J., Podgorski K., Lin B. J., Chen T. W., Turner G. C., Liu Z., Koyama M., Svoboda K., Ahrens M. B., Lavis L. D., & Schreiter E. R. (2019). Bright and photostable chemigenetic indicators for extended in vivo voltage imaging. *Science*, *365*(6454), 699–704.

Adrian, E. D., & Zotterman, Y. (1926a). The impulses produced by sensory nerve-endings: Part II. The response of a Single End-Organ. *The Journal of Physiology*, *61*(2), 151–171.

Adrian, E. D., & Zotterman, Y. (1926b). The impulses produced by sensory nerve endings: Part 3. Impulses set up by Touch and Pressure. *The Journal of Physiology*, *61*(4), 465–483.

Ahern, G. P., & Laver, D. R. (1998). ATP inhibition and rectification of a Ca2+-activated anion channel in sarcoplasmic reticulum of skeletal muscle. *Biophysical Journal*, *74*(5), 2335–2351.

Alich, T. C., Pabst, M., Pothmann, L., Szalontai, B., Faas, G. C., & Mody, I. (2021). A dark quencher genetically encodable voltage indicator (dqGEVI) exhibits high fidelity and speed. *Proceedings of the National Academy of Sciences of the United States of America*, *118*(6). https://doi.org/10.1073/pnas.2020235118

Andressen, C., Blümcke, I., & Celio, M. R. (1993). Calcium-binding proteins: selective markers of nerve cells. *Cell and Tissue Research*, *271*(2), 181–208.

Arai, R., Winsky, L., Arai, M., & Jacobowitz, D. M. (1991). Immunohistochemical localization of calretinin in the rat hindbrain. *The Journal of Comparative Neurology*, *310*(1), 21–44.

Armstrong, C. M., & Bezanilla, F. (1973). Currents related to movement of the gating particles of the sodium channels. *Nature*, *242*(5398), 459–461.

Ashrafpour, M., Eliassi, A., Sauve, R., Sepehri, H., & Saghiri, R. (2008). ATP regulation of a large conductance voltage-gated cation channel in rough endoplasmic reticulum of rat hepatocytes. *Archives of Biochemistry and Biophysics*, *471*(1), 50–56.

Bando, Y., Wenzel, M., & Yuste, R. (2021). Simultaneous two-photon imaging of action potentials and subthreshold inputs in vivo. *Nature Communications*, *12*(1), 7229.

Bannister, N. J., & Larkman, A. U. (1995a). Dendritic morphology of CA1 pyramidal neurones from the rat hippocampus: I. Branching patterns. *The Journal of Comparative Neurology*, *360*(1), 150–160.

Bannister, N. J., & Larkman, A. U. (1995b). Dendritic morphology of CA1 pyramidal neurones from the rat hippocampus: II. Spine distributions. *The Journal of Comparative Neurology*, *360*(1), 161–171.

Basnayake, K., Mazaud, D., Bemelmans, A., Rouach, N., Korkotian, E., & Holcman, D. (2019). Fast calcium transients in dendritic spines driven by extreme statistics. *PLoS Biology*, *17*(6), e2006202.

Basnayake, K., Mazaud, D., Kushnireva, L., Bemelmans, A., Rouach, N., Korkotian, E., & Holcman, D. (2021). Nanoscale molecular architecture controls calcium diffusion and ER replenishment in dendritic spines. *Science Advances*, *7*(38), eabh1376.

Basu, H., Pekkurnaz, G., Falk, J., Wei, W., Chin, M., Steen, J., & Schwarz, T. L. (2021). FHL2 anchors mitochondria to actin and adapts mitochondrial dynamics to glucose supply. *The Journal of Cell Biology*, *220*(10). https://doi.org/10.1083/jcb.201912077

Beck, C., & Gong, Y. (2019). A high-speed, bright, red fluorescent voltage sensor to detect neural activity. *Scientific Reports*, *9*(1), 15878.

Bentzen, B. H., Osadchii, O., Jespersen, T., Hansen, R. S., Olesen, S.-P., & Grunnet, M. (2009). Activation of big conductance Ca(2+)-activated K (+) channels (BK) protects the heart against ischemia-reperfusion injury. *Pflugers Archiv: European Journal of Physiology*, *457*(5), 979–988.

Bernstein, J. (1868). Ueber den zeitlichen Verlauf der negativen Schwankung des Nervenstroms. *Pflugers Archiv fur die gesamte Physiologie des Menschen und der Tiere*, *1*(1), 173–207.

Bernstein, J. (1902). Untersuchungen zur Thermodynamik der bioelektrischen Ströme. *Pflugers Archiv fur die gesamte Physiologie des Menschen und der Tiere*, *92*(10), 521–562.

Bertl, A., Bihler, H., Kettner, C., & Slayman, C. L. (1998). Electrophysiology in the eukaryotic model cell Saccharomyces cerevisiae. *Pflugers Archiv: European Journal of Physiology*, *436*(6), 999–1013.

Bezprozvanny, I., Watras, J., & Ehrlich, B. E. (1991). Bell-shaped calcium-response curves of Ins(1,4,5)P3- and calcium-gated channels from endoplasmic reticulum of cerebellum. *Nature*, *351*(6329), 751–754.

Bicknell, B. A., & Häusser, M. (2021). A synaptic learning rule for exploiting nonlinear dendritic computation. *Neuron*, *109*(24), 4001–4017.e10.

Bittner, K. C., Grienberger, C., Vaidya, S. P., Milstein, A. D., Macklin, J. J., Suh, J., Tonegawa, S., & Magee, J. C. (2015). Conjunctive input processing drives feature selectivity in hippocampal CA1 neurons. *Nature Neuroscience*, *18*(8), 1133–1142.

Bittner, K. C., Milstein, A. D., Grienberger, C., Romani, S., & Magee, J. C. (2017). Behavioral time scale synaptic plasticity underlies CA1 place fields. *Science*, *357*(6355), 1033–1036.

Bootman, M. D., Berridge, M. J., & Lipp, P. (1997). Cooking with calcium: the recipes for composing global signals from elementary events. *Cell*, *91*(3), 367–373.

Bootman, M., Niggli, E., Berridge, M., & Lipp, P. (1997). Imaging the hierarchical Ca2+ signalling system in HeLa cells. *The Journal of Physiology*, *499 (Pt 2)*, 307–314.

Boulay, G., Brown, D. M., Qin, N., Jiang, M., Dietrich, A., Zhu, M. X., Chen, Z., Birnbaumer, M., Mikoshiba, K., & Birnbaumer, L. (1999). Modulation of Ca(2+) entry by polypeptides of the inositol 1,4, 5-trisphosphate receptor (IP3R) that bind transient receptor potential (TRP): evidence for roles of TRP and IP3R in store depletion-activated Ca(2+) entry. *Proceedings of the National Academy of Sciences of the United States of America*, *96*(26), 14955–14960.

Boyd, I. A., & Davey, M. R. (1968). *Composition of peripheral nerves*. Churchill Livingstone.

Broadwell, R. D., & Cataldo, A. M. (1983). The neuronal endoplasmic reticulum: its cytochemistry and contribution to the endomembrane system. I. Cell bodies and dendrites. *The Journal of Histochemistry and Cytochemistry: Official Journal of the Histochemistry Society*, *31*(9), 1077–1088.

Buyse, G., Trouet, D., Voets, T., Missiaen, L., Droogmans, G., Nilius, B., & Eggermont, J. (1998). Evidence for the intracellular location of chloride channel (ClC)-type proteins: co-localization of ClC-6a and ClC-6c with the sarco/endoplasmic-reticulum Ca2+ pump SERCA2b. *Biochemical Journal*, *330 (Pt 2)*, 1015–1021.

Caldwell, P. C., Hodgkin, A. L., Keynes, R. D., & Shaw, T. L. (1960). The effects of injecting "energy-rich" phosphate compounds on the active transport of ions in the giant axons of Loligo. *The Journal of Physiology*, *152*, 561–590.

Cang, C., Zhou, Y., Navarro, B., Seo, Y.-J., Aranda, K., Shi, L., Battaglia-Hsu, S., Nissim, I., Clapham, D. E., & Ren, D. (2013). mTOR regulates lysosomal ATP-sensitive two-pore Na(+) channels to adapt to metabolic state. *Cell*, *152*(4), 778–790.

Cao, Q., Yang, Y., Zhong, X. Z., & Dong, X.-P. (2017). The lysosomal Ca2+ release channel TRPML1 regulates lysosome size by activating calmodulin. *The Journal of Biological Chemistry*, *292*(20), 8424–8435.

Cao, Q., Zhong, X. Z., Zou, Y., Murrell-Lagnado, R., Zhu, M. X., & Dong, X.-P. (2015). Calcium release through P2X4 activates calmodulin to promote endolysosomal membrane fusion. *The Journal of Cell Biology*, *209*(6), 879–894.

Cash, S., & Yuste, R. (1999). Linear summation of excitatory inputs by CA1 pyramidal neurons. *Neuron*, *22*(2), 383–394.

Century, T. J., Fenichel, I. R., & Horowitz, S. B. (1970). The concentrations of water, sodium and potassium in the nucleus and cytoplasm of amphibian oocytes. *Journal of Cell Science*, *7*(1), 5–13.

Century, T. J., & Horowitz, S. B. (1974). Sodium exchange in the cytoplasm and nucleus of amphibian oocytes. *Journal of Cell Science*, *16*(2), 465–471.

Chang, D. T. W., Honick, A. S., & Reynolds, I. J. (2006). Mitochondrial trafficking to synapses in cultured primary cortical neurons. *The Journal of Neuroscience: The Official Journal of the Society for Neuroscience*, *26*(26), 7035–7045.

Chen-Engerer, H.-J., Hartmann, J., Karl, R. M., Yang, J., Feske, S., & Konnerth, A. (2019). Two types of functionally distinct Ca2+ stores in hippocampal neurons. *Nature Communications*, *10*(1), 3223.

Cheng, H., & Lederer, W. J. (2008). Calcium sparks. *Physiological Reviews*, *88*(4), 1491–1545.

Chirillo, M. A., Waters, M. S., Lindsey, L. F., Bourne, J. N., & Harris, K. M. (2019). Local resources of polyribosomes and SER promote synapse enlargement and spine clustering after long-term potentiation in adult rat hippocampus. *Scientific Reports*, *9*(1), 3861.

Churchill, G. C., Okada, Y., Thomas, J. M., Genazzani, A. A., Patel, S., & Galione, A. (2002). NAADP Mobilizes Ca2+ from Reserve Granules, Lysosome-Related Organelles, in Sea Urchin Eggs. *Cell*, *111*(5), 703–708.

Clapham, D. E. (2007). Calcium signaling. *Cell*, *131*(6), 1047–1058.

Cobbold, P., Woods, N., Wainwright, J., & Cuthbertson, R. (1988). Single cell measurements in research on calcium-mobilising purinoceptors. *Journal of Receptor Research*, *8*(1-4), 481–491.

Colbert, C. M., & Johnston, D. (1996). Axonal action-potential initiation and Na+ channel densities in the soma and axon initial segment of subicular pyramidal neurons. *The Journal of Neuroscience: The Official Journal of the Society for Neuroscience*, *16*(21), 6676–6686.

Cole, K. S. (1949). Dynamic electrical characteristics of the squid axon membrane. *Archives Des Sciences Physiologiques*, *3*(2), 253–258.

Cole, K. S., & Baker, R. F. (1941). LONGITUDINAL IMPEDANCE OF THE SQUID GIANT AXON. *The Journal of General Physiology*, *24*(6), 771–788.

Cole, K. S., & Curtis, H. J. (1939). ELECTRIC IMPEDANCE OF THE SQUID GIANT AXON DURING ACTIVITY. *The Journal of General Physiology*, *22*(5), 649–670.

Colombini, M. (1979). A candidate for the permeability pathway of the outer mitochondrial membrane. *Nature*, *279*(5714), 643–645.

Cook, E. P., & Johnston, D. (1999). Voltage-dependent properties of dendrites that eliminate location-dependent variability of synaptic input. *Journal of Neurophysiology*, *81*(2), 535–543.

Coombs, J. S., Curtis, D. R., & Eccles, J. C. (1957). The interpretation of spike potentials of motoneurones. *The Journal of Physiology*, *139*(2), 198–231.

Coombs, J. S., Eccles, J. C., & Fatt, P. (1955). The electrical properties of the motoneurone membrane. *The Journal of Physiology*, *130*(2), 291–325.

Cornejo, V. H., Ofer, N., & Yuste, R. (2021). Voltage compartmentalization in dendritic spines in vivo. *Science*, eabg0501.

Cui-Wang, T., Hanus, C., Cui, T., Helton, T., Bourne, J., Watson, D., Harris, K. M., & Ehlers, M. D. (2012). Local zones of endoplasmic reticulum complexity confine cargo in neuronal dendrites. *Cell*, *148*(1-2), 309–321.

Dallner, G., Orrenius, S., & Bergstrand, A. (1963). Isolation and properties of rough and smooth vesicles from rat liver. *The Journal of Cell Biology*, *16*, 426–430.

Dayel, M. J., Hom, E. F., & Verkman, A. S. (1999). Diffusion of green fluorescent protein in the aqueous-phase lumen of endoplasmic reticulum. *Biophysical Journal*, *76*(5), 2843–2851.

de Juan-Sanz, J., Holt, G. T., Schreiter, E. R., de Juan, F., Kim, D. S., & Ryan, T. A. (2017). Axonal Endoplasmic Reticulum Ca2+ Content Controls Release Probability in CNS Nerve Terminals. *Neuron*, *93*(4), 867–881.e6.

Dodge, F. A., Jr, & Rahamimoff, R. (1967). Co-operative action a calcium ions in transmitter release at the neuromuscular junction. *The Journal of Physiology*, *193*(2), 419–432.

Duncan, R. R., Westwood, P. K., Boyd, A., & Ashley, R. H. (1997). Rat brain p64H1, expression of a new member of the p64 chloride channel protein family in endoplasmic reticulum. *The Journal of Biological Chemistry*, *272*(38), 23880–23886.

Eisner, V., Picard, M., & Hajnóczky, G. (2018). Mitochondrial dynamics in adaptive and maladaptive cellular stress responses. *Nature Cell Biology*, *20*(7), 755–765.

Emptage, N., Bliss, T. V., & Fine, A. (1999). Single synaptic events evoke NMDA receptor-mediated release of calcium from internal stores in hippocampal dendritic spines. *Neuron*, *22*(1), 115–124.

Fedorenko, O. A., & Marchenko, S. M. (2014). Ion channels of the nuclear membrane of hippocampal neurons. *Hippocampus*, *24*(7), 869–876.

Fedorenko, O., Yarotskyy, V., Duzhyy, D., & Marchenko, S. (2010). The large-conductance ion channels in the nuclear envelope of central neurons. *Pflugers Archiv: European Journal of Physiology*, *460*(6), 1045–1050.

Fernández de Sevilla, D., Núñez, A., Borde, M., Malinow, R., & Buño, W. (2008). Cholinergic-mediated IP3-receptor activation induces long-lasting synaptic enhancement in CA1 pyramidal neurons. *The Journal of Neuroscience: The Official Journal of the Society for Neuroscience*, *28*(6), 1469–1478.

Feske, S., Gwack, Y., Prakriya, M., Srikanth, S., Puppel, S.-H., Tanasa, B., Hogan, P. G., Lewis, R. S., Daly, M., & Rao, A. (2006). A mutation in Orai1 causes immune deficiency by abrogating CRAC channel function. *Nature*, *441*(7090), 179–185.

Finch, E. A., & Augustine, G. J. (1998). Local calcium signalling by inositol-1,4,5-trisphosphate in Purkinje cell dendrites. *Nature*, *396*(6713), 753–756.

Fleischer, S., Ogunbunmi, E. M., Dixon, M. C., & Fleer, E. A. (1985). Localization of Ca2+ release channels with ryanodine in junctional terminal cisternae of sarcoplasmic reticulum of fast skeletal muscle. *Proceedings of the National Academy of Sciences of the United States of America*, *82*(21), 7256–7259.

Fox, P. D., Haberkorn, C. J., Akin, E. J., Seel, P. J., Krapf, D., & Tamkun, M. M. (2015). Induction of stable ER-plasma-membrane junctions by Kv2.1 potassium channels. *Journal of Cell Science*, *128*(11), 2096–2105.

Friedman, J. R., Lackner, L. L., West, M., DiBenedetto, J. R., Nunnari, J., & Voeltz, G. K. (2011). ER tubules mark sites of mitochondrial division. *Science*, *334*(6054), 358–362.

Furlan, S., Campione, M., Murgia, M., Mosole, S., Argenton, F., Volpe, P., & Nori, A. (2020). Calsequestrins New Calcium Store Markers of Adult Zebrafish Cerebellum and Optic Tectum. *Frontiers in Neuroanatomy*, *14*, 15.

Gałecka, S., Kulawiak, B., Bednarczyk, P., Singh, H., & Szewczyk, A. (2021). Single channel properties of mitochondrial large conductance potassium channel formed by BK-VEDEC splice variant. *Scientific Reports*, *11*(1), 10925.

Garlid, K. D. (1996). Cation transport in mitochondria--the potassium cycle. *Biochimica et Biophysica Acta*, *1275*(1-2), 123–126.

Gasparini, S., & Magee, J. C. (2006). State-Dependent Dendritic Computation in Hippocampal CA1 Pyramidal Neurons. *The Journal of Neuroscience: The Official Journal of the Society for Neuroscience*, *26*(7), 2088–2100.

Gatti, G., Trifari, S., Mesaeli, N., Parker, J. M., Michalak, M., & Meldolesi, J. (2001). Head-to-tail oligomerization of calsequestrin: a novel mechanism for heterogeneous distribution of endoplasmic reticulum luminal proteins. *The Journal of Cell Biology*, *154*(3), 525–534.

Geiger, J. R., Lübke, J., Roth, A., Frotscher, M., & Jonas, P. (1997). Submillisecond AMPA receptor-mediated signaling at a principal neuron-interneuron synapse. *Neuron*, *18*(6), 1009–1023.

Golding, N. L., & Spruston, N. (1998). Dendritic sodium spikes are variable triggers of axonal action potentials in hippocampal CA1 pyramidal neurons. *Neuron*, *21*(5), 1189–1200.

Goldman, D. E. (1943). POTENTIAL, IMPEDANCE, AND RECTIFICATION IN MEMBRANES. *The Journal of General Physiology*, *27*(1), 37–60.

Goo, M. S., Sancho, L., Slepak, N., Boassa, D., Deerinck, T. J., Ellisman, M. H., Bloodgood, B. L., & Patrick, G. N. (2017). Activity-dependent trafficking of lysosomes in dendrites and dendritic spines. *The Journal of Cell Biology*, *216*(8), 2499–2513.

Gorter, E., & Grendel, F. (1925). ON BIMOLECULAR LAYERS OF LIPOIDS ON THE CHROMOCYTES OF THE BLOOD. *The Journal of Experimental Medicine*, *41*(4), 439–443.

Goyal, U., & Blackstone, C. (2013). Untangling the web: mechanisms underlying ER network formation. *Biochimica et Biophysica Acta*, *1833*(11), 2492–2498.

Grenier, V., Daws, B. R., Liu, P., & Miller, E. W. (2019). Spying on Neuronal Membrane Potential with Genetically Targetable Voltage Indicators. *Journal of the American Chemical Society*, *141*(3), 1349–1358.

Gudlur, A., Zeraik, A. E., Hirve, N., Rajanikanth, V., Bobkov, A. A., Ma, G., Zheng, S., Wang, Y., Zhou, Y., Komives, E. A., & Hogan, P. G. (2018). Calcium sensing by the STIM1 ER-luminal domain. *Nature Communications*, *9*(1), 4536.

Gu, J., Firestein, B. L., & Zheng, J. Q. (2008). Microtubules in dendritic spine development. *The Journal of Neuroscience: The Official Journal of the Society for Neuroscience*, *28*(46), 12120–12124.

Hagenston, A. M., Fitzpatrick, J. S., & Yeckel, M. F. (2008). MGluR-mediated calcium waves that invade the soma regulate firing in layer V medial prefrontal cortical pyramidal neurons. *Cerebral Cortex* , *18*(2), 407–423.

Hagiwara, D., Arima, H., Morishita, Y., Goto, M., Banno, R., Sugimura, Y., & Oiso, Y. (2012). BiP mRNA expression is upregulated by dehydration in vasopressin neurons in the hypothalamus in mice. *Peptides*, *33*(2), 346–350.

Hales, C. N., Luzio, J. P., Chandler, J. A., & Herman, L. (1974). Localization of calcium in the smooth endoplasmic reticulum of rat isolated fat cells. *Journal of Cell Science*, *15*(1), 1–15.

Han, X., & Jackson, M. B. (2006). Structural transitions in the synaptic SNARE complex during Ca2+-triggered exocytosis. *The Journal of Cell Biology*, *172*(2), 281–293.

Hardingham, G. E., Arnold, F. J., & Bading, H. (2001). Nuclear calcium signaling controls CREB-mediated gene expression triggered by synaptic activity. *Nature Neuroscience*, *4*(3), 261–267.

Hardingham, G. E., Chawla, S., Johnson, C. M., & Bading, H. (1997). Distinct functions of nuclear and cytoplasmic calcium in the control of gene expression. *Nature*, *385*(6613), 260–265.

Hasselbach, W., & Makinose, M. (1961). [The calcium pump of the "relaxing granules" of muscle and its dependence on ATP-splitting]. *Biochemische Zeitschrift*, *333*, 518–528.

Hasselbach, W., & Makinose, M. (1963). [ON THE MECHANISM OF CALCIUM TRANSPORT ACROSS THE MEMBRANE OF THE SARCOPLASMIC RETICULUM]. *Biochemische Zeitschrift*, *339*, 94–111.

Häusser, M., Spruston, N., & Stuart, G. J. (2000). Diversity and Dynamics of Dendritic Signaling. *Science*, *290*(5492), 739–744.

Helmchen, F., Imoto, K., & Sakmann, B. (1996). Ca2+ buffering and action potential-evoked Ca2+ signaling in dendrites of pyramidal neurons. *Biophysical Journal*, *70*(2), 1069–1081.

Higgins, J. A. (1974). Studies on the biogenesis of smooth endoplasmic reticulum membranes in hepatocytes of phenobarbital-treated rats. II. The site of phospholipid synthesis in the initial phase of membrane proliferation. *The Journal of Cell Biology*, *62*(3), 635–646.

Hille, B. (1975). Ionic selectivity, saturation, and block in sodium channels. A four-barrier model. *The Journal of General Physiology*, *66*(5), 535–560.

Hille, B. (1978). Ionic channels in excitable membranes. Current problems and biophysical approaches. *Biophysical Journal*, *22*(2), 283–294.

Hodgkin, A. L. (1937). Evidence for electrical transmission in nerve: Part I. *The Journal of Physiology*, *90*(2), 183–210.

Hodgkin, A. L. (1951). The ionic basis of electrical activity in nerve and muscle. *Biological Reviews of the Cambridge Philosophical Society*. https://doi.org/10.1111/j.1469-185X.1951.tb01204.x

Hodgkin, A. L., & Huxley, A. F. (1939). Action Potentials Recorded from Inside a Nerve Fibre. *Nature*, *144*(3651), 710–711.

Hodgkin, A. L., & Huxley, A. F. (1945). Resting and action potentials in single nerve fibres. *The Journal of Physiology*, *104*(2), 176–195.

Hodgkin, A. L., & Huxley, A. F. (1952). A quantitative description of membrane current and its application to conduction and excitation in nerve. *The Journal of Physiology*, *117*(4), 500–544.

Hodgkin, A. L., & Katz, B. (1949). The effect of sodium ions on the electrical activity of giant axon of the squid. *The Journal of Physiology*, *108*(1), 37–77.

Hodgkin, A. L., & Keynes, R. D. (1955). Active transport of cations in giant axons from Sepia and Loligo. *The Journal of Physiology*, *128*(1), 28–60.

Hoffman, D. A., Magee, J. C., Colbert, C. M., & Johnston, D. (1997). K+ channel regulation of signal propagation in dendrites of hippocampal pyramidal neurons. *Nature*, *387*(6636), 869–875.

Hoffmann, P. C., Bharat, T. A. M., Wozny, M. R., Boulanger, J., Miller, E. A., & Kukulski, W. (2019). Tricalbins Contribute to Cellular Lipid Flux and Form Curved ER-PM Contacts that Are Bridged by Rod-Shaped Structures. *Developmental Cell*, *51*(4), 488–502.e8.

Holbro, N., Grunditz, A., & Oertner, T. G. (2009). Differential distribution of endoplasmic reticulum controls metabotropic signaling and plasticity at hippocampal synapses. *Proceedings of the National Academy of Sciences of the United States of America*, *106*(35), 15055–15060.

Horton, A. C., & Ehlers, M. D. (2003). Dual modes of endoplasmic reticulum-to-Golgi transport in dendrites revealed by live-cell imaging. *The Journal of Neuroscience: The Official Journal of the Society for Neuroscience*, *23*(15), 6188–6199.

Hoyer, M. J., Chitwood, P. J., Ebmeier, C. C., Striepen, J. F., Qi, R. Z., Old, W. M., & Voeltz, G. K. (2018). A Novel Class of ER Membrane Proteins Regulates ER-Associated Endosome Fission. *Cell*, *175*(1), 254–265.e14.

Hsu, C.-L., Zhao, X., Milstein, A. D., & Spruston, N. (2018). Persistent Sodium Current Mediates the Steep Voltage Dependence of Spatial Coding in Hippocampal Pyramidal Neurons. *Neuron*, *99*(1), 147–162.e8.

Huang, Y.-L., Walker, A. S., & Miller, E. W. (2015). A Photostable Silicon Rhodamine Platform for Optical Voltage Sensing. *Journal of the American Chemical Society*, *137*(33), 10767–10776.

Hursh, J. B. (1939). CONDUCTION VELOCITY AND DIAMETER OF NERVE FIBERS. *American Journal of Physiology-Legacy Content*, *127*(1), 131–139.

Irie, T., & Trussell, L. O. (2017). Double-Nanodomain Coupling of Calcium Channels, Ryanodine Receptors, and BK Channels Controls the Generation of Burst Firing. *Neuron*, *96*(4), 856–870.e4.

Ishii, K., Hirose, K., & Iino, M. (2006). Ca2+ shuttling between endoplasmic reticulum and mitochondria underlying Ca2+ oscillations. *EMBO Reports*, *7*(4), 390–396.

Jack, J. J., & Redman, S. J. (1971). The propagation of transient potentials in some linear cable structures. *The Journal of Physiology*, *215*(2), 283–320.

Jaffe, D. B., & Brown, T. H. (1994). Metabotropic glutamate receptor activation induces calcium waves within hippocampal dendrites. *Journal of Neurophysiology*, *72*(1), 471–474.

Jaworski, J., Kapitein, L. C., Gouveia, S. M., Dortland, B. R., Wulf, P. S., Grigoriev, I., Camera, P., Spangler, S. A., Di Stefano, P., Demmers, J., Krugers, H., Defilippi, P., Akhmanova, A., & Hoogenraad, C. C. (2009). Dynamic microtubules regulate dendritic spine morphology and synaptic plasticity. *Neuron*, *61*(1), 85–100.

Jiang, Y., Lee, A., Chen, J., Ruta, V., Cadene, M., Chait, B. T., & MacKinnon, R. (2003). X-ray structure of a voltage-dependent K+ channel. *Nature*, *423*(6935), 33–41.

Jiang, Y., Ruta, V., Chen, J., Lee, A., & MacKinnon, R. (2003). The principle of gating charge movement in a voltage-dependent K+ channel. *Nature*, *423*(6935), 42–48.

KATZ, & B. (1969). The release of neural transmitter substances. *Liverpool University Press*, 5–39.

Katz, B., & Miledi, R. (1970). Membrane noise produced by acetylcholine. *Nature*, *226*(5249), 962–963.

Kawabata, S., Tsutsumi, R., Kohara, A., Yamaguchi, T., Nakanishi, S., & Okada, M. (1996). Control of calcium oscillations by phosphorylation of metabotropic glutamate receptors. *Nature*, *383*(6595), 89–92.

Kawano, S., Nakamura, F., Tanaka, T., & Hiraoka, M. (1992). Cardiac sarcoplasmic reticulum chloride channels regulated by protein kinase A. *Circulation Research*, *71*(3), 585–589.

Kim, Y., Hsu, C.-L., Cembrowski, M. S., Mensh, B. D., & Spruston, N. (2015). Dendritic sodium spikes are required for long-term potentiation at distal synapses on hippocampal pyramidal neurons. *eLife*, *4*. https://doi.org/10.7554/eLife.06414

King, C., Sengupta, P., Seo, A. Y., & Lippincott-Schwartz, J. (2020). ER membranes exhibit phase behavior at sites of organelle contact. *Proceedings of the National Academy of Sciences of the United States of America*, *117*(13), 7225–7235.

Kirichok, Y., Krapivinsky, G., & Clapham, D. E. (2004). The mitochondrial calcium uniporter is a highly selective ion channel. *Nature*, *427*(6972), 360–364.

Kirmiz, M., Palacio, S., Thapa, P., King, A. N., Sack, J. T., & Trimmer, J. S. (2018). Remodeling neuronal ER-PM junctions is a conserved nonconducting function of Kv2 plasma membrane ion channels. *Molecular Biology of the Cell*, *29*(20), 2410–2432.

Knöpfel, T., & Song, C. (2019). Optical voltage imaging in neurons: moving from technology development to practical tool. *Nature Reviews. Neuroscience*, *20*(12), 719–727.

Koch, G. L. (1990). The endoplasmic reticulum and calcium storage. *BioEssays: News and Reviews in Molecular, Cellular and Developmental Biology*, *12*(11), 527–531.

Kulawiak, B., Kudin, A. P., Szewczyk, A., & Kunz, W. S. (2008). BK channel openers inhibit ROS production of isolated rat brain mitochondria. *Experimental Neurology*, *212*(2), 543–547.

Kuum, M., Veksler, V., Liiv, J., Ventura-Clapier, R., & Kaasik, A. (2012). Endoplasmic reticulum potassium-hydrogen exchanger and small conductance calcium-activated potassium channel activities are essential for ER calcium uptake in neurons and cardiomyocytes. *Journal of Cell Science*, *125*(Pt 3), 625–633.

Landau, E. M., & Ben-Haim, D. (1974). Acetylcholine noise: analysis after chemical modification of receptor. *Science*, *185*(4155), 944–946.

Larkman, A. U. (1991). Dendritic morphology of pyramidal neurones of the visual cortex of the rat: III. Spine distributions. *The Journal of Comparative Neurology*, *306*(2), 332–343.

Larkum, M. E., Watanabe, S., Nakamura, T., Lasser-Ross, N., & Ross, W. N. (2003). Synaptically activated Ca2+ waves in layer 2/3 and layer 5 rat neocortical pyramidal neurons. *The Journal of Physiology*, *549*(Pt 2), 471–488.

Larkum, M. E., Zhu, J. J., & Sakmann, B. (1999). A new cellular mechanism for coupling inputs arriving at different cortical layers. *Nature*, *398*(6725), 338–341.

Laube, G., Seidenbecher, C. I., Richter, K., Dieterich, D. C., Hoffmann, B., Landwehr, M., Smalla, K. H., Winter, C., Böckers, T. M., Wolf, G., Gundelfinger, E. D., & Kreutz, M. R. (2002). The neuron-specific Ca2+-binding protein caldendrin: gene structure, splice isoforms, and expression in the rat central nervous system. *Molecular and Cellular Neurosciences*, *19*(3), 459–475.

Lee, A. C., Xu, X., Blachly-Dyson, E., Forte, M., & Colombini, M. (1998). The role of yeast VDAC genes on the permeability of the mitochondrial outer membrane. *The Journal of Membrane Biology*, *161*(2), 173–181.

Lee, C., & Chen, L. B. (1988). Dynamic behavior of endoplasmic reticulum in living cells. *Cell*, *54*(1), 37–46.

Lewis, S. C., Uchiyama, L. F., & Nunnari, J. (2016). ER-mitochondria contacts couple mtDNA synthesis with mitochondrial division in human cells. *Science*, *353*(6296), aaf5549.

Li, B., Jie, W., Huang, L., Wei, P., Li, S., Luo, Z., Friedman, A. K., Meredith, A. L., Han, M.-H., Zhu, X.-H., & Gao, T.-M. (2014). Nuclear BK channels regulate gene expression via the control of nuclear calcium signaling. *Nature Neuroscience*, *17*(8), 1055–1063.

Liou, J., Kim, M. L., Heo, W. D., Jones, J. T., Myers, J. W., Ferrell, J. E., Jr, & Meyer, T. (2005). STIM is a Ca2+ sensor essential for Ca2+-store-depletion-triggered Ca2+ influx. *Current Biology: CB*, *15*(13), 1235–1241.

Lipowsky, R., Gillessen, T., & Alzheimer, C. (1996). Dendritic Na+ channels amplify EPSPs in hippocampal CA1 pyramidal cells. *Journal of Neurophysiology*, *76*(4), 2181–2191.

Llano, I., González, J., Caputo, C., Lai, F. A., Blayney, L. M., Tan, Y. P., & Marty, A. (2000). Presynaptic calcium stores underlie large-amplitude miniature IPSCs and spontaneous calcium transients. *Nature Neuroscience*, *3*(12), 1256–1265.

Lock, J. T., & Parker, I. (2020). IP3 mediated global Ca2+ signals arise through two temporally and spatially distinct modes of Ca2+ release. *eLife*, *9*. https://doi.org/10.7554/eLife.55008

Losonczy, A., & Magee, J. C. (2006). Integrative properties of radial oblique dendrites in hippocampal CA1 pyramidal neurons. *Neuron*, *50*(2), 291–307.

Losonczy, A., Makara, J. K., & Magee, J. C. (2008). Compartmentalized dendritic plasticity and input feature storage in neurons. *Nature*, *452*(7186), 436–441.

Lynes, E. M., & Simmen, T. (2011). Urban planning of the endoplasmic reticulum (ER): how diverse mechanisms segregate the many functions of the ER. *Biochimica et Biophysica Acta*, *1813*(10), 1893–1905.

Macer, D. R., & Koch, G. L. (1988). Identification of a set of calcium-binding proteins in reticuloplasm, the luminal content of the endoplasmic reticulum. *Journal of Cell Science*, *91 (Pt 1)*, 61–70.

Magee, J. C. (1999). Dendritic lh normalizes temporal summation in hippocampal CA1 neurons. *Nature Neuroscience*, *2*(6), 508–514.

Magee, J. C. (2000). Dendritic integration of excitatory synaptic input. *Nature Reviews. Neuroscience*, *1*(3), 181–190.

Magee, J. C., & Cook, E. P. (2000). Synaptic weight is independent of synapse location in CA1 pyramidal neurons. *Nature Neuroscience*, *3*, 895–903.

Mainen, Z. F., Carnevale, N. T., Zador, A. M., Claiborne, B. J., & Brown, T. H. (1996). Electrotonic architecture of hippocampal CA1 pyramidal neurons based on three-dimensional reconstructions. *Journal of Neurophysiology*, *76*(3), 1904–1923.

Mak, D. O., & Foskett, J. K. (1994). Single-channel inositol 1,4,5-trisphosphate receptor currents revealed by patch clamp of isolated Xenopus oocyte nuclei. *The Journal of Biological Chemistry*, *269*(47), 29375–29378.

Mak, D. O., McBride, S., & Foskett, J. K. (1998). Inositol 1,4,5-trisphosphate [correction of tris-phosphate] activation of inositol trisphosphate [correction of tris-phosphate] receptor Ca2+ channel by ligand tuning of Ca2+ inhibition. *Proceedings of the National Academy of Sciences of the United States of America*, *95*(26), 15821–15825.

Manford, A. G., Stefan, C. J., Yuan, H. L., Macgurn, J. A., & Emr, S. D. (2012). ER-to-plasma membrane tethering proteins regulate cell signaling and ER morphology. *Developmental Cell*, *23*(6), 1129–1140.

Manita, S., & Ross, W. N. (2009). Synaptic activation and membrane potential changes modulate the frequency of spontaneous elementary Ca2+ release events in the dendrites of pyramidal neurons. *The Journal of Neuroscience: The Official Journal of the Society for Neuroscience*, *29*(24), 7833–7845.

Marchenko, S. M., Yarotskyy, V. V., Kovalenko, T. N., Kostyuk, P. G., & Thomas, R. C. (2005). Spontaneously active and InsP3-activated ion channels in cell nuclei from rat cerebellar Purkinje and granule neurones. *The Journal of Physiology*, *565*(Pt 3), 897–910.

Martone, M. E., Zhang, Y., Simpliciano, V. M., Carragher, B. O., & Ellisman, M. H. (1993). Three-dimensional visualization of the smooth endoplasmic reticulum in Purkinje cell dendrites. *The Journal of Neuroscience: The Official Journal of the Society for Neuroscience*, *13*(11), 4636–4646.

Maruyama, Y., Shimada, H., & Taniguchi, J. (1995). Ca(2+)-activated K(+)-channels in the nuclear envelope isolated from single pancreatic acinar cells. *Pflugers Archiv: European Journal of Physiology*, *430*(1), 148–150.

Matamala, E., Castillo, C., Vivar, J. P., Rojas, P. A., & Brauchi, S. E. (2021). Imaging the electrical activity of organelles in living cells. *Communications Biology*, *4*(1), 389.

Mazzanti, M., Bustamante, J. O., & Oberleithner, H. (2001). Electrical dimension of the nuclear envelope. *Physiological Reviews*, *81*(1), 1–19.

Mazzanti, M., DeFelice, L. J., Cohn, J., & Malter, H. (1990). Ion channels in the nuclear envelope. *Nature*, *343*(6260), 764–767.

McGraw, C. F., Somlyo, A. V., & Blaustein, M. P. (1980). Localization of calcium in presynaptic nerve terminals. An ultrastructural and electron microprobe analysis. *The Journal of Cell Biology*, *85*(2), 228–241.

Miller, C. (1978). Voltage-gated cation conductance channel from fragmented sarcoplasmic reticulum: steady-state electrical properties. *The Journal of Membrane Biology*, *40*(1), 1–23.

Mitchell, P. (1961). Coupling of phosphorylation to electron and hydrogen transfer by a chemi-osmotic type of mechanism. *Nature*, *191*, 144–148.

Mitchell, P. (1966). Chemiosmotic coupling in oxidative and photosynthetic phosphorylation. *Biological Reviews of the Cambridge Philosophical Society*, *41*(3), 445–502.

Mollinedo-Gajate, I., Song, C., & Knöpfel, T. (2021). Genetically Encoded Voltage Indicators. *Advances in Experimental Medicine and Biology*, *1293*, 209–224.

Mulder, J., Zilberter, M., Spence, L., Tortoriello, G., Uhlén, M., Yanagawa, Y., Aujard, F., Hökfelt, T., & Harkany, T. (2009). Secretagogin is a Ca2+-binding protein specifying subpopulations of telencephalic neurons. *Proceedings of the National Academy of Sciences of the United States of America*, *106*(52), 22492–22497.

Nakamura, T., Barbara, J. G., Nakamura, K., & Ross, W. N. (1999). Synergistic release of Ca2+ from IP3-sensitive stores evoked by synaptic activation of mGluRs paired with backpropagating action potentials. *Neuron*, *24*(3), 727–737.

Nakamura, T., Lasser-Ross, N., Nakamura, K., & Ross, W. N. (2002). Spatial segregation and interaction of calcium signalling mechanisms in rat hippocampal CA1 pyramidal neurons. *The Journal of Physiology*, *543*(Pt 2), 465–480.

Nakamura, T., Nakamura, K., Lasser-Ross, N., Barbara, J. G., Sandler, V. M., & Ross, W. N. (2000). Inositol 1,4,5-trisphosphate (IP3)-mediated Ca2+ release evoked by metabotropic agonists and backpropagating action potentials in hippocampal CA1 pyramidal neurons. *The Journal of Neuroscience: The Official Journal of the Society for Neuroscience*, *20*(22), 8365–8376.

Nakanishi, S., Kuwajima, G., & Mikoshiba, K. (1992). Immunohistochemical localization of ryanodine receptors in mouse central nervous system. *Neuroscience Research*, *15*(1-2), 130–142.

Nash, M. S., Young, K. W., Challiss, R. A., & Nahorski, S. R. (2001). Intracellular signalling. Receptor-specific messenger oscillations. *Nature*, *413*(6854), 381–382.

Nernst, W. (1888). Zur Kinetik der in Lösung befindlichen Körper. *Zeitschrift für Physikalische Chemie*, *2U*(1), 613–637.

Nernst, W. (1889). Die elektromotorische Wirksamkeit der Jonen. *Zeitschrift für Physikalische Chemie*, *4U*(1), 129–181.

Nixon-Abell, J., Obara, C. J., Weigel, A. V., Li, D., Legant, W. R., Xu, C. S., Pasolli, H. A., Harvey, K., Hess, H. F., Betzig, E., Blackstone, C., & Lippincott-Schwartz, J. (2016). Increased spatiotemporal resolution reveals highly dynamic dense tubular matrices in the peripheral ER. *Science*, *354*(6311). https://doi.org/10.1126/science.aaf3928

Novgorodov, S. A., Gudz, T. I., Kushnareva, Y. E., Eriksson, O., & Leikin, Y. N. (1991). Effects of the membrane potential upon the Ca2+ - and cumene hydroperoxide-induced permeabilization of the inner mitochondrial membrane. *FEBS Letters*, *295*(1-3), 77–80.

Oberleithner, H., Schuricht, B., Wünsch, S., Schneider, S., & Püschel, B. (1993). Role of H+ ions in volume and voltage of epithelial cell nuclei. *Pflugers Archiv: European Journal of Physiology*, *423*(1-2), 88–96.

Oetliker, H. (1989). Energetical considerations related to calcium release from the sarcoplasmic reticulum in skeletal muscle. *Biomedica Biochimica Acta*, *48*(5-6), S313–S318.

Ostroff, L. E., Fiala, J. C., Allwardt, B., & Harris, K. M. (2002). Polyribosomes redistribute from dendritic shafts into spines with enlarged synapses during LTP in developing rat hippocampal slices. *Neuron*, *35*(3), 535–545.

Overton, E. (1899). *Ueber die allgemeinen osmotischen Eigenschaften der Zelle, ihre vermutlichen Ursachen u. ihre Bedeutg fd Physiologie*. Fäsi & Beer.

Özkan, N., Koppers, M., van Soest, I., van Harten, A., Jurriens, D., Liv, N., Klumperman, J., Kapitein, L. C., Hoogenraad, C. C., & Farías, G. G. (2021). ER - lysosome contacts at a pre-axonal region regulate axonal lysosome availability. *Nature Communications*, *12*(1), 4493.

Papadia, S., Stevenson, P., Hardingham, N. R., Bading, H., & Hardingham, G. E. (2005). Nuclear Ca2+ and the cAMP response element-binding protein family mediate a late phase of activity-dependent neuroprotection. *The Journal of Neuroscience: The Official Journal of the Society for Neuroscience*, *25*(17), 4279–4287.

Parker, I., & Ivorra, I. (1990). Inhibition by Ca2+ of inositol trisphosphate-mediated Ca2+ liberation: a possible mechanism for oscillatory release of Ca2+. *Proceedings of the National Academy of Sciences of the United States of America*, *87*(1), 260–264.

Parker, I., & Yao, Y. (1991). Regenerative release of calcium from functionally discrete subcellular stores by inositol trisphosphate. *Proceedings. Biological Sciences / The Royal Society*, *246*(1317), 269–274.

Park, M., Salgado, J. M., Ostroff, L., Helton, T. D., Robinson, C. G., Harris, K. M., & Ehlers, M. D. (2006). Plasticity-induced growth of dendritic spines by exocytic trafficking from recycling endosomes. *Neuron*, *52*(5), 817–830.

Payandeh, J., Gamal El-Din, T. M., Scheuer, T., Zheng, N., & Catterall, W. A. (2012). Crystal structure of a voltage-gated sodium channel in two potentially inactivated states. *Nature*, *486*(7401), 135–139.

Payandeh, J., Scheuer, T., Zheng, N., & Catterall, W. A. (2011). The crystal structure of a voltage-gated sodium channel. *Nature*, *475*(7356), 353–358.

Pekkurnaz, G., Trinidad, J. C., Wang, X., Kong, D., & Schwarz, T. L. (2014). Glucose regulates mitochondrial motility via Milton modification by O-GlcNAc transferase. *Cell*, *158*(1), 54–68.

Peretti, D., Dahan, N., Shimoni, E., Hirschberg, K., & Lev, S. (2008). Coordinated lipid transfer between the endoplasmic reticulum and the Golgi complex requires the VAP proteins and is essential for Golgi-mediated transport. *Molecular Biology of the Cell*, *19*(9), 3871–3884.

Perez-Alvarez, A., Yin, S., Schulze, C., Hammer, J. A., Wagner, W., & Oertner, T. G. (2020). Endoplasmic reticulum visits highly active spines and prevents runaway potentiation of synapses. *Nature Communications*, *11*(1), 5083.

Perni, S., Dynes, J. L., Yeromin, A. V., Cahalan, M. D., & Franzini-Armstrong, C. (2015). Nanoscale patterning of STIM1 and Orai1 during store-operated Ca2+ entry. *Proceedings of the National Academy of Sciences of the United States of America*, *112*(40), E5533–E5542.

Piatkevich, K. D., Jung, E. E., Straub, C., Linghu, C., Park, D., Suk, H.-J., Hochbaum, D. R., Goodwin, D., Pnevmatikakis, E., Pak, N., Kawashima, T., Yang, C.-T., Rhoades, J. L., Shemesh, O., Asano, S., Yoon, Y.-G., Freifeld, L., Saulnier, J. L., Riegler, C., Engert F., Hughes T., Drobizhev M., Szabo B., Ahrens M. B., Flavell S. W., Sabatini B. L., Boyden, E. S. (2018). A robotic multidimensional directed evolution approach applied to fluorescent voltage reporters. *Nature Chemical Biology*, *14*(4), 352–360.

Pichler, H., Gaigg, B., Hrastnik, C., Achleitner, G., Kohlwein, S. D., Zellnig, G., Perktold, A., & Daum, G. (2001). A subfraction of the yeast endoplasmic reticulum associates with the plasma membrane and has a high capacity to synthesize lipids. *European Journal of Biochemistry / FEBS*, *268*(8), 2351–2361.

Platisa, J., Zeng, H., Madisen, L., Cohen, L. B., Pieribone, V. A., & Storace, D. A. (2022). Voltage imaging in the olfactory bulb using transgenic mouse lines expressing the genetically encoded voltage indicator ArcLight. *Scientific Reports*, *12*(1), 1875.

Polsky, A., Mel, B. W., & Schiller, J. (2004). Computational subunits in thin dendrites of pyramidal cells. *Nature Neuroscience*, *7*(6), 621–627.

Porter, K. R., & Yamada, E. (1960). Studies on the endoplasmic reticulum. V. Its form and differentiation in pigment epithelial cells of the frog retina. *The Journal of Biophysical and Biochemical Cytology*, *8*, 181–205.

Pottosin, I. I. (1992). Single channel recording in the chloroplast envelope. *FEBS Letters*, *308*(1), 87–90.

Pozzo Miller, L. D., Petrozzino, J. J., Golarai, G., & Connor, J. A. (1996). Ca2+ release from intracellular stores induced by afferent stimulation of CA3 pyramidal neurons in hippocampal slices. *Journal of Neurophysiology*, *76*(1), 554–562.

Pozzo-Miller, L. D., Pivovarova, N. B., Leapman, R. D., Buchanan, R. A., Reese, T. S., & Andrews, S. B. (1997). Activity-dependent calcium sequestration in dendrites of hippocampal neurons in brain slices. *The Journal of Neuroscience: The Official Journal of the Society for Neuroscience*, *17*(22), 8729–8738.

Prakriya, M., Feske, S., Gwack, Y., Srikanth, S., Rao, A., & Hogan, P. G. (2006). Orai1 is an essential pore subunit of the CRAC channel. *Nature*, *443*(7108), 230–233.

Raiborg, C., Wenzel, E. M., Pedersen, N. M., Olsvik, H., Schink, K. O., Schultz, S. W., Vietri, M., Nisi, V., Bucci, C., Brech, A., Johansen, T., & Stenmark, H. (2015). Repeated ER-endosome contacts promote endosome translocation and neurite outgrowth. *Nature*, *520*(7546), 234–238.

Rall, W. (1962). Theory of physiological properties of dendrites. *Annals of the New York Academy of Sciences*, *96*, 1071–1092.

Rall, W. (1967). Distinguishing theoretical synaptic potentials computed for different soma-dendritic distributions of synaptic input. *Journal of Neurophysiology*, *30*(5), 1138–1168.

Rall, W. (1995). Perspective on neuron model complexity. *The Handbook of Brain Theory and Neural Networks*, 728–732.

Rall, W., Burke, R. E., Holmes, W. R., Jack, J. J., Redman, S. J., & Segev, I. (1992). Matching dendritic neuron models to experimental data. *Physiological Reviews*, *72*(4 Suppl), S159–S186.

Ramón y Cajal, S. (1899). *Textura del sistema nervioso del hombre y de los vertebrados: estudios sobre el plan estructural y composición histológica de los centros nerviosos adicionados de consideraciones fisiológicas fundadas en los nuevos descubrimientos*. Moya.

Raychaudhuri, S., & Prinz, W. A. (2008). Nonvesicular phospholipid transfer between peroxisomes and the endoplasmic reticulum. *Proceedings of the National Academy of Sciences of the United States of America*, *105*(41), 15785–15790.

Raymond, C. R., & Redman, S. J. (2006). Spatial segregation of neuronal calcium signals encodes different forms of LTP in rat hippocampus. *The Journal of Physiology*, *570*(Pt 1), 97–111.

Redman, C. M., & Sabatini, D. D. (1966). Vectorial discharge of peptides released by puromycin from attached ribosomes. *Proceedings of the National Academy of Sciences of the United States of America*, *56*(2), 608–615.

Rinzel, J., & Rall, W. (1974). Transient response in a dendritic neuron model for current injected at one branch. *Biophysical Journal*, *14*(10), 759–790.

Rizzuto, R., De Stefani, D., Raffaello, A., & Mammucari, C. (2012). Mitochondria as sensors and regulators of calcium signalling. *Nature Reviews. Molecular Cell Biology*, *13*(9), 566–578.

Rizzuto, R., Pinton, P., Carrington, W., Fay, F. S., Fogarty, K. E., Lifshitz, L. M., Tuft, R. A., & Pozzan, T. (1998). Close contacts with the endoplasmic reticulum as determinants of mitochondrial Ca2+ responses. *Science*, *280*(5370), 1763–1766.

Ross, W. N. (2012). Understanding calcium waves and sparks in central neurons. *Nature Reviews. Neuroscience*, *13*(3), 157–168.

Roth, A., & Häusser, M. (2001). Compartmental models of rat cerebellar Purkinje cells based on simultaneous somatic and dendritic patch-clamp recordings. *The Journal of Physiology*, *535*(Pt 2), 445–472.

Rowland, A. A., Chitwood, P. J., Phillips, M. J., & Voeltz, G. K. (2014). ER contact sites define the position and timing of endosome fission. *Cell*, *159*(5), 1027–1041.

Ryu, S.-W., Choi, K., Yoon, J., Kim, S., & Choi, C. (2012). Endoplasmic reticulum-specific BH3-only protein BNIP1 induces mitochondrial fragmentation in a Bcl-2- and Drp1-dependent manner. *Journal of Cellular Physiology*, *227*(8), 3027–3035.

Sabatini, B. L., & Regehr, W. G. (1999). Timing of synaptic transmission. *Annual Review of Physiology*, *61*, 521–542.

Saheki, Y., & De Camilli, P. (2017). Endoplasmic Reticulum-Plasma Membrane Contact Sites. *Annual Review of Biochemistry*, *86*, 659–684.

Saito, M., Hanson, P. I., & Schlesinger, P. (2007). Luminal chloride-dependent activation of endosome calcium channels: patch clamp study of enlarged endosomes. *The Journal of Biological Chemistry*, *282*(37), 27327–27333.

Sakai, R., Repunte-Canonigo, V., Raj, C. D., & Knöpfel, T. (2001). Design and characterization of a DNA-encoded, voltage-sensitive fluorescent protein. *The European Journal of Neuroscience*, *13*(12), 2314–2318.

Saminathan, A., Devany, J., Veetil, A. T., Suresh, B., Pillai, K. S., Schwake, M., & Krishnan, Y. (2021). A DNA-based voltmeter for organelles. *Nature Nanotechnology*, *16*(1), 96–103.

Sampieri, A., Santoyo, K., Asanov, A., & Vaca, L. (2018). Association of the IP3R to STIM1 provides a reduced intraluminal calcium microenvironment, resulting in enhanced store-operated calcium entry. *Scientific Reports*, *8*(1), 13252.

Sampieri, A., Zepeda, A., Asanov, A., & Vaca, L. (2009). Visualizing the store-operated channel complex assembly in real time: identification of SERCA2 as a new member. *Cell Calcium*, *45*(5), 439–446.

Sanchez, C., Berthier, C., Allard, B., Perrot, J., Bouvard, C., Tsutsui, H., Okamura, Y., & Jacquemond, V. (2018). Tracking the sarcoplasmic reticulum membrane voltage in muscle with a FRET biosensor. *The Journal of General Physiology*, *150*(8), 1163–1177.

Sandler, V. M., & Barbara, J. G. (1999). Calcium-induced calcium release contributes to action potential-evoked calcium transients in hippocampal CA1 pyramidal neurons. *The Journal of Neuroscience: The Official Journal of the Society for Neuroscience*, *19*(11), 4325–4336.

Schiller, J., Major, G., Koester, H. J., & Schiller, Y. (2000). NMDA spikes in basal dendrites of cortical pyramidal neurons. *Nature*, *404*(6775), 285–289.

Schiller, J., Schiller, Y., Stuart, G., & Sakmann, B. (1997). Calcium action potentials restricted to distal apical dendrites of rat neocortical pyramidal neurons. *The Journal of Physiology*, *505 (Pt 3)*, 605–616.

Schulien, A. J., Justice, J. A., Di Maio, R., Wills, Z. P., Shah, N. H., & Aizenman, E. (2016). Zn(2+) - induced Ca(2+) release via ryanodine receptors triggers calcineurin-dependent redistribution of cortical neuronal Kv2.1 K(+) channels. *The Journal of Physiology*, *594*(10), 2647–2659.

Selezneva, A., Yoshida, M., Gibb, A., & Willis, D. (2021). Nuclear BK channels regulate CREB phosphorylation in RAW264.7 macrophages. *Pharmacological Reports: PR*, *73*(3), 881–890.

Sepehri Rad, M., Cohen, L. B., Braubach, O., & Baker, B. J. (2018). Monitoring voltage fluctuations of intracellular membranes. *Scientific Reports*, *8*(1), 6911.

Sharma, G., & Vijayaraghavan, S. (2003). Modulation of presynaptic store calcium induces release of glutamate and postsynaptic firing. *Neuron*, *38*(6), 929–939.

Sharp, A. H., McPherson, P. S., Dawson, T. M., Aoki, C., Campbell, K. P., & Snyder, S. H. (1993). Differential immunohistochemical localization of inositol 1,4,5-trisphosphate- and ryanodine-sensitive Ca2+ release channels in rat brain. *The Journal of Neuroscience: The Official Journal of the Society for Neuroscience*, *13*(7), 3051–3063.

Shemer, I., Brinne, B., Tegnér, J., & Grillner, S. (2008). Electrotonic signals along intracellular membranes may interconnect dendritic spines and nucleus. *PLoS Computational Biology*, *4*(3), e1000036.

Shibata, Y., Shemesh, T., Prinz, W. A., Palazzo, A. F., Kozlov, M. M., & Rapoport, T. A. (2010). Mechanisms determining the morphology of the peripheral ER. *Cell*, *143*(5), 774–788.

Shibata, Y., Voss, C., Rist, J. M., Hu, J., Rapoport, T. A., Prinz, W. A., & Voeltz, G. K. (2008). The reticulon and DP1/Yop1p proteins form immobile oligomers in the tubular endoplasmic reticulum. *The Journal of Biological Chemistry*, *283*(27), 18892–18904.

Siegel, M. S., & Isacoff, E. Y. (1997). A genetically encoded optical probe of membrane voltage. *Neuron*, *19*(4), 735–741.

Singer, S. J., & Nicolson, G. L. (1972). The fluid mosaic model of the structure of cell membranes. *Science*, *175*(4023), 720–731.

Smedler, E., & Uhlén, P. (2014). Frequency decoding of calcium oscillations. *Biochimica et Biophysica Acta*, *1840*(3), 964–969.

Snapp, E. L., Hegde, R. S., Francolini, M., Lombardo, F., Colombo, S., Pedrazzini, E., Borgese, N., & Lippincott-Schwartz, J. (2003). Formation of stacked ER cisternae by low affinity protein interactions. *The Journal of Cell Biology*, *163*(2), 257–269.

Soltysinska, E., Bentzen, B. H., Barthmes, M., Hattel, H., Thrush, A. B., Harper, M.-E., Qvortrup, K., Larsen, F. J., Schiffer, T. A., Losa-Reyna, J., Straubinger, J., Kniess, A., Thomsen, M. B., Brüggemann, A., Fenske, S., Biel, M., Ruth, P., Wahl-Schott, C., Boushel, R. C., Olesen, S.P., Lukowski, R. (2014). KCNMA1 encoded cardiac BK channels afford protection against ischemia-reperfusion injury. *PloS One*, *9*(7), e103402.

Somlyo, A. V., Gonzalez-Serratos, H. G., Shuman, H., McClellan, G., & Somlyo, A. P. (1981). Calcium release and ionic changes in the sarcoplasmic reticulum of tetanized muscle: an electron-probe study. *The Journal of Cell Biology*, *90*(3), 577–594.

Sorgato, M. C., Keller, B. U., & Stühmer, W. (1987). Patch-clamping of the inner mitochondrial membrane reveals a voltage-dependent ion channel. *Nature*, *330*(6147), 498–500.

Spacek, J., & Harris, K. M. (1997). Three-dimensional organization of smooth endoplasmic reticulum in hippocampal CA1 dendrites and dendritic spines of the immature and mature rat. *The Journal of Neuroscience: The Official Journal of the Society for Neuroscience*, *17*(1), 190–203.

Spruston, N. (1999). *Dendritic integration. Ch 10 in Stuart G, Spruston N, Hausser M, eds*. Dendrites Oxford University Press.

Srikanth, S., Jew, M., Kim, K.-D., Yee, M.-K., Abramson, J., & Gwack, Y. (2012). Junctate is a Ca2+-sensing structural component of Orai1 and stromal interaction molecule 1 (STIM1). *Proceedings of the National Academy of Sciences of the United States of America*, *109*(22), 8682–8687.

Stathopulos, P. B., Zheng, L., Li, G.-Y., Plevin, M. J., & Ikura, M. (2008). Structural and mechanistic insights into STIM1-mediated initiation of store-operated calcium entry. *Cell*, *135*(1), 110–122.

Stehno-Bittel, L., Lückhoff, A., & Clapham, D. E. (1995). Calcium release from the nucleus by InsP3 receptor channels. *Neuron*, *14*(1), 163–167.

Stock, D., Leslie, A. G., & Walker, J. E. (1999). Molecular architecture of the rotary motor in ATP synthase. *Science*, *286*(5445), 1700–1705.

Streb, H., Irvine, R. F., Berridge, M. J., & Schulz, I. (1983). Release of Ca2+ from a nonmitochondrial intracellular store in pancreatic acinar cells by inositol-1,4,5-trisphosphate. *Nature*, *306*(5938), 67–69.

Stuart, G. J., & Sakmann, B. (1994). Active propagation of somatic action potentials into neocortical pyramidal cell dendrites. *Nature*, *367*(6458), 69–72.

Stuart, G., Schiller, J., & Sakmann, B. (1997). Action potential initiation and propagation in rat neocortical pyramidal neurons. *The Journal of Physiology*, *505 (Pt 3)*, 617–632.

Sullivan, K. M., Busa, W. B., & Wilson, K. L. (1993). Calcium mobilization is required for nuclear vesicle fusion in vitro: implications for membrane traffic and IP3 receptor function. *Cell*, *73*(7), 1411–1422.

Takahashi, T., & Momiyama, A. (1993). Different types of calcium channels mediate central synaptic transmission. *Nature*, *366*(6451), 156–158.

Takechi, H., Eilers, J., & Konnerth, A. (1998). A new class of synaptic response involving calcium release in dendritic spines. *Nature*, *396*(6713), 757–760.

Takei, K., Stukenbrok, H., Metcalf, A., Mignery, G. A., Südhof, T. C., Volpe, P., & De Camilli, P. (1992). Ca2+ stores in Purkinje neurons: endoplasmic reticulum subcompartments demonstrated by the heterogeneous distribution of the InsP3 receptor, Ca(2+)-ATPase, and calsequestrin. *The Journal of Neuroscience: The Official Journal of the Society for Neuroscience*, *12*(2), 489–505.

Tanifuji, M., Sokabe, M., & Kasai, M. (1987). An anion channel of sarcoplasmic reticulum incorporated into planar lipid bilayers: single-channel behavior and conductance properties. *The Journal of Membrane Biology*, *99*(2), 103–111.

Taufiq-Ur-Rahman, Skupin, A., Falcke, M., & Taylor, C. W. (2009). Clustering of InsP3 receptors by InsP3 retunes their regulation by InsP3 and Ca2+. *Nature*, *458*(7238), 655–659.

Tedeschi, H., Mannella, C. A., & Bowman, C. L. (1987). Patch clamping the outer mitochondrial membrane. *The Journal of Membrane Biology*, *97*(1), 21–29.

Terasaki, M., Slater, N. T., Fein, A., Schmidek, A., & Reese, T. S. (1994). Continuous network of endoplasmic reticulum in cerebellar Purkinje neurons. *Proceedings of the National Academy of Sciences of the United States of America*, *91*(16), 7510–7514.

Thakur, P., Dadsetan, S., & Fomina, A. F. (2012). Bidirectional coupling between ryanodine receptors and Ca2+ release-activated Ca2+ (CRAC) channel machinery sustains store-operated Ca2+ entry in human T lymphocytes. *The Journal of Biological Chemistry*, *287*(44), 37233–37244.

Thillaiappan, N. B., Chavda, A. P., Tovey, S. C., Prole, D. L., & Taylor, C. W. (2017). Ca2+ signals initiate at immobile IP3 receptors adjacent to ER-plasma membrane junctions. *Nature Communications*, *8*(1), 1505.

Thillaiappan, N. B., Smith, H. A., Atakpa-Adaji, P., & Taylor, C. W. (2021). KRAP tethers IP3 receptors to actin and licenses them to evoke cytosolic Ca2+ signals. *Nature Communications*, *12*(1), 4514.

Tian, X., Gala, U., Zhang, Y., Shang, W., Nagarkar Jaiswal, S., di Ronza, A., Jaiswal, M., Yamamoto, S., Sandoval, H., Duraine, L., Sardiello, M., Sillitoe, R. V., Venkatachalam, K., Fan, H., Bellen, H. J., & Tong, C. (2015). A voltage-gated calcium channel regulates lysosomal fusion with endosomes and autophagosomes and is required for neuronal homeostasis. *PLoS Biology*, *13*(3), e1002103.

Townsend, C., & Rosenberg, R. L. (1995). Characterization of a chloride channel reconstituted from cardiac sarcoplasmic reticulum. *The Journal of Membrane Biology*, *147*(2), 121–136.

Tsukita, S., & Ishikawa, H. (1976). THREE-DIMENSIONAL DISTRIBUTIONOF SMOOTH ENDOPLASMIC RETICULUM IN MYELINATED AXONS. *Journal of Electron Microscopy*, *25*(3), 141–149.

Valm, A. M., Cohen, S., Legant, W. R., Melunis, J., Hershberg, U., Wait, E., Cohen, A. R., Davidson, M. W., Betzig, E., & Lippincott-Schwartz, J. (2017). Applying systems-level spectral imaging and analysis to reveal the organelle interactome. *Nature*, *546*(7656), 162–167.

Vander Heiden, M. G., Chandel, N. S., Li, X. X., Schumacker, P. T., Colombini, M., & Thompson, C. B. (2000). Outer mitochondrial membrane permeability can regulate coupled respiration and cell survival. *Proceedings of the National Academy of Sciences of the United States of America*, *97*(9), 4666–4671.

Vasington, F. D., & Murphy, J. V. (1962). Ca ion uptake by rat kidney mitochondria and its dependence on respiration and phosphorylation. *The Journal of Biological Chemistry*, *237*, 2670–2677.

Verhage, M., Maia, A. S., Plomp, J. J., Brussaard, A. B., Heeroma, J. H., Vermeer, H., Toonen, R. F., Hammer, R. E., van den Berg, T. K., Missler, M., Geuze, H. J., & Südhof, T. C. (2000). Synaptic assembly of the brain in the absence of neurotransmitter secretion. *Science*, *287*(5454), 864–869.

Vierra, N. C., Kirmiz, M., van der List, D., Santana, L. F., & Trimmer, J. S. (2019). Kv2.1 mediates spatial and functional coupling of L-type calcium channels and ryanodine receptors in mammalian neurons. *eLife*, *8*. https://doi.org/10.7554/eLife.49953

Vierra, N. C., O'Dwyer, S. C., Matsumoto, C., Santana, L. F., & Trimmer, J. S. (2021). Regulation of neuronal excitation-transcription coupling by Kv2.1-induced clustering of somatic L-type Ca2+ channels at ER-PM junctions. *Proceedings of the National Academy of Sciences of the United States of America*, *118*(46). https://doi.org/10.1073/pnas.2110094118

Villa, A., Podini, P., Clegg, D. O., Pozzan, T., & Meldolesi, J. (1991). Intracellular Ca2+ stores in chicken Purkinje neurons: differential distribution of the low affinity-high capacity Ca2+ binding protein, calsequestrin, of Ca2+ ATPase and of the ER lumenal protein, Bip. *The Journal of Cell Biology*, *113*(4), 779–791.

Villa, A., Sharp, A. H., Racchetti, G., Podini, P., Bole, D. G., Dunn, W. A., Pozzan, T., Snyder, S. H., & Meldolesi, J. (1992). The endoplasmic reticulum of Purkinje neuron body and dendrites: molecular identity and specializations for Ca2+ transport. *Neuroscience*, *49*(2), 467–477.

Villette, V., Chavarha, M., Dimov, I. K., Bradley, J., Pradhan, L., Mathieu, B., Evans, S. W., Chamberland, S., Shi, D., Yang, R., Kim, B. B., Ayon, A., Jalil, A., St-Pierre, F., Schnitzer, M. J., Bi, G., Toth, K., Ding, J., Dieudonné, S., & Lin, M. Z. (2019). Ultrafast Two-Photon Imaging of a High-Gain Voltage Indicator in Awake Behaving Mice. *Cell*, *179*(7), 1590–1608.e23.

Walton, P. D., Airey, J. A., Sutko, J. L., Beck, C. F., Mignery, G. A., Südhof, T. C., Deerinck, T. J., & Ellisman, M. H. (1991). Ryanodine and inositol trisphosphate receptors coexist in avian cerebellar Purkinje neurons. *The Journal of Cell Biology*, *113*(5), 1145–1157.

Wang, S. S., Denk, W., & Häusser, M. (2000). Coincidence detection in single dendritic spines mediated by calcium release. *Nature Neuroscience*, *3*(12), 1266–1273.

Wang, W., Zhang, X., Gao, Q., Lawas, M., Yu, L., Cheng, X., Gu, M., Sahoo, N., Li, X., Li, P., Ireland, S., Meredith, A., & Xu, H. (2017). A voltage-dependent K+ channel in the lysosome is required for refilling lysosomal Ca2+ stores. *The Journal of Cell Biology*, *216*(6), 1715–1730.

Wang, X., Zhang, X., Dong, X.-P., Samie, M., Li, X., Cheng, X., Goschka, A., Shen, D., Zhou, Y., Harlow, J., Zhu, M. X., Clapham, D. E., Ren, D., & Xu, H. (2012). TPC proteins are phosphoinositide-activated sodium-selective ion channels in endosomes and lysosomes. *Cell*, *151*(2), 372–383.

Watson, M. L. (1955). The nuclear envelope; its structure and relation to cytoplasmic membranes. *The Journal of Biophysical and Biochemical Cytology*, *1*(3), 257–270.

Wei, D. S., Mei, Y. A., Bagal, A., Kao, J. P., Thompson, S. M., & Tang, C. M. (2001). Compartmentalized and binary behavior of terminal dendrites in hippocampal pyramidal neurons. *Science*, *293*(5538), 2272–2275.

Williams, S. R., & Stuart, G. J. (2000). Site independence of EPSP time course is mediated by dendritic I(h) in neocortical pyramidal neurons. *Journal of Neurophysiology*, *83*(5), 3177–3182.

Williams, S. R., & Stuart, G. J. (2002). Dependence of EPSP efficacy on synapse location in neocortical pyramidal neurons. *Science*, *295*(5561), 1907–1910.

Woods, N. M., Cuthbertson, K. S., & Cobbold, P. H. (1986). Repetitive transient rises in cytoplasmic free calcium in hormone-stimulated hepatocytes. *Nature*, *319*(6054), 600–602.

Wu, H., Carvalho, P., & Voeltz, G. K. (2018). Here, there, and everywhere: The importance of ER membrane contact sites. *Science*, *361*(6401). https://doi.org/10.1126/science.aan5835

Wu, Y., Whiteus, C., Xu, C. S., Hayworth, K. J., Weinberg, R. J., Hess, H. F., & De Camilli, P. (2017). Contacts between the endoplasmic reticulum and other membranes in neurons. *Proceedings of the National Academy of Sciences of the United States of America*, *114*(24), E4859–E4867.

Xu, H., Delling, M., Li, L., Dong, X., & Clapham, D. E. (2007). Activating mutation in a mucolipin transient receptor potential channel leads to melanocyte loss in varitint-waddler mice. *Proceedings of the National Academy of Sciences of the United States of America*, *104*(46), 18321–18326.

Yao, Y., Choi, J., & Parker, I. (1995). Quantal puffs of intracellular Ca2+ evoked by inositol trisphosphate in Xenopus oocytes. *The Journal of Physiology*, *482 (Pt 3)*, 533–553.

Yazawa, M., Ferrante, C., Feng, J., Mio, K., Ogura, T., Zhang, M., Lin, P.-H., Pan, Z., Komazaki, S., Kato, K., Nishi, M., Zhao, X., Weisleder, N., Sato, C., Ma, J., & Takeshima, H. (2007). TRIC channels are essential for Ca2+ handling in intracellular stores. *Nature*, *448*(7149), 78–82.

Zhang, S. L., Yu, Y., Roos, J., Kozak, J. A., Deerinck, T. J., Ellisman, M. H., Stauderman, K. A., & Cahalan, M. D. (2005). STIM1 is a Ca2+ sensor that activates CRAC channels and migrates from the Ca2+ store to the plasma membrane. *Nature*, *437*(7060), 902–905.

Zheng, P., Obara, C. J., Szczesna, E., Nixon-Abell, J., Mahalingan, K. K., Roll-Mecak, A., Lippincott-Schwartz, J., & Blackstone, C. (2021). ER proteins decipher the tubulin code to regulate organelle distribution. *Nature*. https://doi.org/10.1038/s41586-021-04204-9

Zhu, J., Yan, J., & Thornhill, W. B. (2014). The Kv1.3 potassium channel is localized to the cis-Golgi and Kv1.6 is localized to the endoplasmic reticulum in rat astrocytes. *The FEBS Journal*, *281*(15), 3433–3445.

Zorova, L. D., Popkov, V. A., Plotnikov, E. Y., Silachev, D. N., Pevzner, I. B., Jankauskas, S. S., Babenko, V. A., Zorov, S. D., Balakireva, A. V., Juhaszova, M., Sollott, S. J., & Zorov, D. B. (2018). Mitochondrial membrane potential. *Analytical Biochemistry*, *552*, 50–59.

Chapter II: Investigations and Findings

Introduction:

The ER is a massive organelle that extends throughout a cell as a continuous anastomosing network of membranes (Martone et al. 1993; Dayel, Hom, and Verkman 1999). In neurons, the ER is particularly striking as it reaches into axons, dendrites, and dendritic spines, which can be hundreds of microns from the ER origin at the outer nuclear envelope (Tsukita and Ishikawa 1976; Terasaki et al. 1994; Spacek and Harris 1997). Among its many functions, the ER plays a fundamental role in intracellular signaling as it fluxes Ca^{2+} ions across its membrane via conductance through IP3Rs and RyRs (for review see Ross 2012). In addition to these receptors, the ER has a variety of resident ion channels, including some that are gated by voltage, ions, or ligands (Miller 1978; Yazawa et al. 2007; Tanifuji, Sokabe, and Kasai 1987; Duncan et al. 1997; Kuum et al. 2012; Ahern and Laver 1998; Ashrafpour et al. 2008; Kawano et al. 1992). Moreover, the ionic composition of the ER lumen is distinct from that of the cytoplasm and changes in response to activity (Pozzo-Miller et al. 1997; Somlyo et al. 1981). Because of its morphology and repertoire of ion channels, the ER can be considered as a "cell within a cell". Yet, electrical signaling along this intracellular membrane system has not been characterized.

The ER's ion channel composition and ionic gradients across the membrane open the possibility that the ER membrane may be a site of highly dynamic electrical signaling. For example, if electrical signals actively propagate along the ER membrane, this could facilitate rapid intracellular signaling or change the driving force on Ca^{2+} efflux from the ER in distant regions of a cell (Shemer et al. 2008). If ER membrane electrical signals are spatially restricted, this could reflect mechanisms that enable stretches of the ER to function independently of adjacent, contiguous segments. Yet, the fundamental electrical signaling capabilities of the ER membrane have remained elusive: it remains unknown if the ER is a passive or active membrane system.

The ribbons and tubules that make up the ER may be only tens of nanometers in diameter (Wu et al. 2017) prohibiting access with electrodes. Recently, several tools have been developed that enable live visualization of organelle membrane potential (Saminathan et al. 2021; Matamala et al. 2021). Efforts to optically measure membrane potential in the ER (or the SR) have hinted that the ER membrane may be polarized and rapidly follow voltage changes in the PM (Sepehri Rad et al. 2018; Matamala et al. 2021; but see Sanchez et al. 2018). While these reports of ER membrane potential are intriguing, they are limited by either lack of specificity in the subcellular targeting of the voltage sensor, uncertainty about the orientation of the sensor, or high variability in measurements.

We have selectively targeted the genetically encoded fluorescent voltage indicator, ASAP3 (Villette et al. 2019), to the ER membrane through the addition of an ER retention sequence ($ASAP3_{ER}$). Imaging of $ASAP3_{ER}$ in dissociated neurons from the rat hippocampus reveals that the ER membrane potential is highly polarized and changes by tens of millivolts in response to network activity, G_q signaling, or direct activation of RyRs. Moreover, the ER membrane potential responds linearly to increases in stimulus strength, and yet changes in membrane potential are severely restricted to the regions exposed to a stimulus, in part through the function of resident BK channels. Thus, the ER is a largely passive membrane system where electrical activity is locally restricted and the spread of membrane potential fluctuations is further limited through the action of active conductance.

Results:

ASAP3 to measure membrane potential:

To probe the ER for voltage signals we sought to target a GEVI specifically to the ER membrane. We chose ASAP3 because of its photostability, high sensitivity, and ability to linearly report voltage over a large dynamic range in the PM. ASAP3 consists of a voltage-sensing domain that spans the PM and an

extracellular, circularly permuted green fluorescent protein (cpGFP) that decreases fluorescence with depolarization (Villette et al. 2019). We first expressed ASAP3 in the PM of dissociated rat hippocampal neurons to calibrate changes in ASAP3 fluorescence with PM voltage using simultaneous imaging and whole-cell recordings (**Figure 2.1A**). Stepwise changes in membrane potential resulted in fluorescence changes that were linear over a range of -85 to +15 mV with a -1 %ΔF/F for every 2.4 mV change in PM potential (**Figure 2.1B, C**; $R^2 = 0.99$), comparable to ASAP3 responses reported by other studies (Villette et al. 2019; Cornejo, Ofer, and Yuste 2021). Thus, changes in ASAP3 fluorescence can report small changes in membrane potential with high fidelity. In addition, changes in ASAP3 fluorescence reliably reported single action potentials and followed the spontaneous firing of the neuron (**Figure 2.1D, E**), confirming that ASAP3 can resolve rapid changes in membrane potential on a single trial basis.

Targeting and validating ASAP3 localization to the ER membrane:

Several peptide sequences have been identified that retain transmembrane proteins in the ER and/or recycle them back to the ER from the golgi (Teasdale and Jackson 1996; Gao et al. 2014). We cloned the amino terminal signal Met-RRR-, or carboxy terminal signals -KKRR, -KKAA, or -KKSS onto ASAP3, all of which would maintain the position of ASAP3 with its cpGFP in the ER lumen and the retention signals in the cytoplasm (**Figure 2.2A**; Schutze, Peterson, and Jackson 1994; Gaynor et al. 1994; Andersson, Kappeler, and Hauri 1999; Gaynor et al. 1994). Each construct was transfected into HEK293T cells and cell viability was assessed via the effective exclusion of Trypan blue dye. Carboxy terminus tagged ASAP3-KKAA, hereafter referred to as $ASAP3_{ER}$, had no significant impact on the viability of cells expressing it (**Figure 2.2B, C**) and thus was used going forward.

Our ability to attribute changes in $ASAP3_{ER}$ fluorescence to changes in ER membrane potential relies on the exclusive localization of the voltage sensor to the ER. To determine if $ASAP3_{ER}$ escapes ER retention and is trafficked to the PM, HEK293 cells were transfected with either ASAP3 or $ASAP3_{ER}$. Three

days later, cells were fixed and stained for GFP in either permeabilizing or non-permeabilizing staining conditions. In cells where membranes had been permeabilized, the native fluorescence of both ASAP3 and $ASAP3_{ER}$ were readily visualized and the protein could also be detected by antibodies recognizing GFP (**Figure 2.3A, B**). By comparison, in non-permeabilized conditions, cells expressing ASAP3 in the PM showed significant GFP immunoreactivity while $ASAP3_{ER}$ was virtually undetectable (34 +/- 7.5% and 3 +/- 1.6%, respectively, of permeabilized conditions; **Figure 2.3C**), indicating nearly all $ASAP3_{ER}$ is retained intracellularly.

To determine if $ASAP3_{ER}$ is in the ER and not other organelles, HEK293 cells were co-transfected with tdTomato targeted to the ER lumen (tdT-ER) and either $ASAP3_{ER}$, ASAP3, or ASAP3 targeted to the PM by the Kv2.1 proximal retention and clustering segment ($ASAP3_{PM}$; Villette et al. 2019; Daigle et al. 2018). Immunostaining for the GFP in ASAP3 was performed and the colocalization with tdT-ER was quantified. Fluorescence from $ASAP3_{ER}$ and tdT-ER were highly correlated (Pearson's correlation coefficient, PCC = 0.855 +/- 0.007 SEM) while non-targeted ASAP3 and $ASAP3_{PM}$ showed little overlap (PCC = 0.098 +/-0.039 SEM and 0.045 +/- 035 SEM, respectively; **Figure 2.4A-C**). Next, we examined whether $ASAP3_{ER}$ signal overlapped with the golgi apparatus, as proteins trafficking from the ER to other cellular destinations transit through the golgi (Barlowe 1997; Weigel et al. 2021). We also examined $ASAP3_{ER}$ overlap with mitochondria, as mitochondria have highly polarized membrane potentials (Klier, Martin, and Miller 2021; for review see Zorova et al. 2018) and could pollute our efforts to measure ER-specific signals. Cells were transfected with $ASAP3_{ER}$ and tdT-ER and immunostained for GFP and either Golga2 or Tomm20, proteins localized to golgi apparatus and mitochondria, respectively (**Figure 2.4D, E**). Neither Golga2 nor Tomm20 were significantly correlated with $ASAP3_{ER}$ immunofluorescence (PCC: 0.12 +/- 0.022 SEM, 0.212 +/- 0.026 SEM; **Figure 2.4F**). Thus, $ASAP3_{ER}$ is localized to the ER at the exclusion of the PM, golgi apparatus, and mitochondria.

Next, to see if ER localization of $ASAP3_{ER}$ holds true in neurons, we transfected dissociated neurons with tdT-ER and either ASAP3, $ASAP3_{PM}$, or $ASAP3_{ER}$. Neurons were immunostained for GFP

and imaged with structured illumination microscopy (**Figure 2.4I, J**). Fluorescence profiles from tdT-ER and $ASAP3_{ER}$ were highly correlated along 1 μm wide segments through neuron somas (correlation coefficient, CC = 0.830 +/- 0.017 SEM), while fluorescence profiles of tdT-ER and ASAP3 or $ASAP3_{PM}$ showed little correlation (CC = 0.059 +/- 0.053 SEM and CC = -0.015 +/-0.064 SEM, respectively; **Figure 2.4K**), mirroring profiles in HEK293 cells (**Figure 2.4G, H**) and indicating that $ASAP3_{ER}$ is localized specifically to ER membrane in neurons.

$ASAP3_{ER}$ fluorescence in unmanipulated neurons:

To visualize ER membrane potential dynamics we transfected dissociated neurons with $ASAP3_{ER}$ at six days in vitro (DIV6; **Figure 2.5A**) and acquired simultaneous imaging and cell-attached patch recordings, as to not disrupt the intracellular environment and ER voltage (Perkins 2006; Sepehri Rad et al. 2018; Sanchez et al. 2018). $ASAP3_{ER}$ fluorescence did not rapidly follow the PM potential and lacked the fast transients seen when ASAP3 is expressed in the PM (**Figure 2.5B**). Yet when monitored over extended time periods with slower frame rate imaging, the fluorescence signal was not fixed but slowly undulated (**Figure 2.5C**). To ensure that changes in $ASAP3_{ER}$ fluorescence do not reflect changes in surface area, volume, or other physiological variables that can impact fluorescence such as pH, we compared $ASAP3_{ER}$ fluorescence against non-voltage sensitive control constructs; either an ER-targeted ASAP variant with a non-circularly permuted GFP ($NCP\text{-}ASAP_{ER}$; Chamberland et al. 2017; Villette et al. 2019) or GFP targeted to the lumen of the ER (ER-GFP; Holbro, Grunditz, and Oertner 2009). Fluorescence fluctuations were significantly larger in $ASAP3_{ER}$ expressing cells than those expressing either $NCP\text{-}ASAP_{ER}$ or ER-GFP, as born out by the root mean square error of the signals to baseline values (RMSE: 3.01 +/- 0.540, 1.28 +/- 0.218, and 1.07 +/- 0.177 %ΔF/F, respectively; **Figure S4A-C**). Thus, changes in $ASAP3_{ER}$ fluorescence do not reflect changes in surface area, volume, or other physiological variables that can impact fluorescence such as pH but report changes in membrane potential.

Could the fluctuations in $ASAP3_{ER}$ fluorescence be associated with broader network activity and synaptic transmission that instigate signaling to the ER? To examine this, we recorded spikes as a proxy for network activity while imaging $ASAP3_{ER}$ fluorescence. Spontaneous firing rates were calculated in 0.1 second time windows, mirroring the imaging frame rate, and the cross-correlation of the spike rate and ER fluorescence signals were assessed (**Figure 2.6A, B**). We detected a significant inverse correlation between spiking and $ASAP3_{ER}$ fluorescence that peaks when the spike rate precedes ER voltage by 33.9 seconds and is not present when spike rates were shuffled (**Figure 2.6C, D**). This relationship also held true when the spike rate was calculated in 1 and 5 second time windows (**Figure 2.6E, F**). These data suggest a coupling, albeit slow, between neuronal activity and ER membrane potential.

Stimulus-dependent changes in $ASAP3_{ER}$ fluorescence:

To obtain a more temporally controlled assessment of the relationship between network activity and ER membrane potential, we imaged $ASAP3_{ER}$ fluorescence and acquired electrical recordings from the PM while washing in a high potassium chloride (KCl; 40mM) extracellular solution. We observed dramatic and significant decreases in $ASAP3_{ER}$ fluorescence in response to global depolarization that was not observed in control conditions (KCl: 51.5 +/- 7.30 %ΔF/F; control: 6.14 +/- 2.79 %ΔF/F; **Figure 2.7A, E, and H**). This suggests the ER membrane potential may change by as much as ~120 mV in response to massive depolarization and the associated spiking and synaptic transmission.

To determine if more physiologically relevant manipulations of network activity can change the ER membrane potential we pharmacologically manipulated neuronal spiking activity. Increasing firing and synaptic transmission via bath application of the $GABA_A$ antagonist picrotoxin (PTX) led to a 33.5 +/- 3.87 %ΔF/F decrease in $ASAP3_{ER}$ fluorescence (**Figure 2.7B, F, and H**), corresponding to a ~80 mV depolarization, while DMSO alone led to 5.81 +/- 0.49 %ΔF/F decrease. Notably, in neurons transfected with NCP-$ASAP_{ER}$ or GFP-ER the responses to PTX were significantly reduced (10.5 +/- 1.85 and 8.67 +/-

2.19 %ΔF/F, respectively; **Figure 2J, K**) and were comparable to $ASAP3_{ER}$ changes observed with the application of DMSO alone or with continuous imaging (Figure 2H). In contrast, preventing action potentials with bath application of tetrodotoxin (TTX) led to a 29.6 +/- 13.5 %ΔF/F increase in fluorescence (**Figure 2.7C, G, and H**) and was able to partially reverse the effect of PTX (**Figure 2.D and I**). Thus, the ER membrane potential can be depolarized or hyperpolarized over many tens of millivolts in response to sustained changes in network activity and synaptic transmission.

Elevated extracellular potassium and PTX both lead to depolarization of the ER but have radically different impacts on the PM potential. Thus we hypothesized the mechanism driving ER depolarization was synaptic in origin. Group mGluR activation induces Ca^{2+} efflux from the ER via the G_q coupled signal transduction pathway (Sugiyama, Ito, and Hirono 1987; Schoepp et al. 1994; for review see Schoepp, Jane, and Monn 1999; Reiner and Levitz 2018). Both $mGluR_1$ and $mGluR_5$ are expressed in hippocampal pyramidal neurons. To test the respective contributions of these receptors, the selective antagonists CPCCOEt or MPEP (20 μM and 1 μM, respectively) were bath-applied and then PTX was washed in while the soma of $ASAP3_{ER}$ expressing neurons were imaged. Antagonism of $mGluR_5$ had no detectable impact on the PTX-elicited decrease in $ASAP3_{ER}$ fluorescence (33.3 +/- 4.16%, **Figure 2.7L, M**). In contrast, blocking $mGluR_1$ significantly reduced $ASAP3_{ER}$ responses to PTX (17.4 +/- 3.36), and blocking both receptor types did not lead to a further reduction (18.2 +/- 3.67%; **Figure 2.7L, M**). These data indicate that in this cell type $mGluR_1$ activation is the principal synaptic transmission driving changes in somatic ER membrane potential associated with elevated network activity and synaptic transmission.

ER membrane potential responses reflect receptor type and cellular location:

To determine if different ER receptors can elicit distinct ER voltage responses, we targeted the somas of neurons expressing $ASAP3_{ER}$ with a picospritzer and locally applied DHPG to activate type I mGluRs signaling to IP3Rs, or caffeine to directly gate RyRs (**Figure 2.8A**). Alexa-594 dye (50 μM) was

included in the pipette to enable visualization of the plume. One-second puffs of DHPG and caffeine generated 6.52 +/- 2.02 and 5.41 +/- 0.654 %ΔF/F changes in fluorescence, reflecting ~17 and ~13 mV changes in membrane potential, respectively (**Figure 2.8B, C**). In contrast, a one-second-long puff of Alexa-594 carrier solution did not generate a response (0.14 +/- 0.09%; **Figure 2.9A, B**) indicating that change in fluorescence is not an artifact of the mechanics of picospritzing. Further, DHPG failed to elicit an $ASAP3_{ER}$ response when mGluR antagonists were included in the bath (**Figure 2.9C, D**) and the caffeine response was significantly attenuated by high concentrations of Ry as seen previously (**Figure 2.9E, F**; Kong et al. 2008; Chen-Engerer et al. 2019)**,** confirming the origin of the $ASAP3_{ER}$ signals. Notably, rise time and decay time constants for responses to DHPG (7.12 +/- 2.35 s, and 11.5 +/- 3.34 s) were significantly larger than to caffeine (0.681 +/- 0.045 s, and 2.73 +/- 2.03 s; **Figure 2.9C**). These results are consistent with the expectation that DHPG initiates relatively prolonged G_q mediated responses, while caffeine activates RyRs directly.

We next sought to determine how ER voltage signals scale with the strength of a stimulus. RyRs were directly activated by focally applying caffeine for several puff durations (0.1, 0.25, 0.5, and 1 s, applied in random order; **Figure 2.8D**). Increasing the puff duration led to increased peak $ASAP3_{ER}$ fluorescence change (0.162 +/- 0.064, 1.12 +/- 0.195, 2.28 +/- 0.33, and 5.46 +/- 0.643 %ΔF/F, respectively; **Figure 2.8F**) that scaled with Alexa-594 fluorescence (**Figure 2.8G**) and fit a linear stimulus-response curve. With the longest application of caffeine (1 s), the rate of change of average $ASAP3_{ER}$ fluorescence plateaued, suggesting a possible saturation of the receptors underlying the voltage signal or an additional mechanism that limits further depolarization (**Figure 2.8H**). Finally, to ensure rapid changes in membrane potential were not obscured by low frame rate imaging, we delivered 0.5 s puffs of caffeine while imaging at 100 Hz and observed comparable $ASAP3_{ER}$ responses (**Figure 2.8E, F**). Thus, in the soma, activation of RyRs changes ER voltage proportionally to the stimulus strength.

While the ER is continuous from the soma into the dendrites, dendritic ER has characteristic structural subdomains and regions of low complexity (Spacek and Harris 1997; Pozzo-Miller et al. 1997;

Cui-Wang et al. 2012), has fewer ribosomes (Broadwell and Cataldo 1983; Martone et al. 1993), and different receptor densities (Walton et al. 1991; Takei et al. 1992; Krijnse-Locker et al., 1995). These features can affect membrane capacitance, resistance, and the generation of currents thereby altering stimulus-dependent voltage responses. We therefore sought to measure dendritic ER membrane potential changes in response to direct activation of dendritic RyRs. Caffeine was focally applied to dendritic branches approximately 50-100 μm from the soma (**Figure 2.8I**). Again, changes in peak $ASAP3_{ER}$ fluorescence scaled with puff duration and Alexa-594 fluorescence (4.44 +/- 1.12, 11.5 +/- 2.58, 13.6 +/- 1.57, and 19.8 +/- 2.55 %, respectively; **Figure 2.8J-L**). At dendrites, the longest caffeine puff led to a ~50 mV depolarization of the ER membrane. Despite this large change, we did not observe a steep increase in the rate of change in $ASAP3_{ER}$ fluorescence (**Figure 2.8M**), as would have been expected if active conductances were engaged (Losonczy and Magee 2006).

In spite of the similarities between $ASAP3_{ER}$ responses in somatic and dendritic ER, they are not identical. Dendritic ER produced significantly larger peak depolarizations than somatic ER for every caffeine puff duration (two-way ANOVA: region effect $p < 0.0001$, puff effect $p < 0.0001$; **Figure 2.8N**). It is unlikely that this difference is due to imprecision in the delivery of caffeine or gating of the receptors as the rise times of the somatic and dendritic responses did not differ at any stimulus strength (two-way ANOVA: region $p = 0.828$, puff $p < 0.0001$; **Figure 2.8O**). The decay of the $ASAP3_{ER}$ signal was also notably slower in the dendrites (**Figure 2.8P**) and scaled with the amplitude of the response in both somatic and dendritic ER (**Figure 2.8Q**). Thus, while we see no evidence of an ER membrane "action potential", strong activation of RyRs can produce a long-lasting voltage signal.

Compartmentalized ER membrane potential in dendrite during spontaneous network activity:

If the ER were assumed to have membrane resistance and lumenal resistivity similar to the PM at dendrites (Shemer et al. 2008), its small diameter tubules would dissipate electrotonic potentials with a

length constant of ~150 μm (see methods for length constant equation). In this case, changes in $ASAP3_{ER}$ fluorescence between neighboring segments of dendritic ER should be highly correlated. To examine this, we imaged $ASAP3_{ER}$ in branches of dendrites (**Figure 2.10A, D**), and first applied PTX to determine if ER membrane potential is even capable of responding across such lengths. With increased excitatory input along dendrites, we detected depolarization of the ER within 5 μm long bins spanning 55 μm total. Depolarization of the ER was highly correlated across dendrites, as demonstrated by correlation coefficients calculated from $ASAP3_{ER}$ responses between each pair of region of interest (ROI) bins (**Figure 2.10B, C**). However, without coordinated input to dendrites via PTX stimulation, $ASAP3_{ER}$ fluorescence signals from spontaneous network activity showed conspicuously less correlation (**Figure 2.10D**). We observed occasional high correlations across neighboring ROI bins (for example, see **Figure 2.10E**), but regions with $CC \geq 0.75$ were only 10 % of all neighboring bins, never extended beyond 15-20 μm, and spanned 6.88 +/- 3.72 μm on average. Overall, the voltage fluctuations measured from neighboring regions of dendrite exhibited low correlation unless simultaneously stimulated (CC = 0.209 +/- 0.035; **Figure 2.10F**). These findings indicate that although ER membrane potential is highly dynamic in dendritic compartments, it may operate independently from the ER in directly adjoining sections of dendrite.

Electrical potentials in dendritic ER are restricted to stimulated regions:

To determine the extent to which ER voltage signals spread away from a point of stimulation, we next delivered brief puffs of caffeine (0.5 s) to dendritic segments (50-100 μm from soma) and imaged $ASAP3_{ER}$ fluorescence along the length of the dendrite. Changes $ASAP3_{ER}$ and Alexa-594 fluorescence were quantified for 5 μm sliding bin ROIs starting from the center of the caffeine plume, as measured by peak Alexa-594 fluorescence, and continuing 50 μm toward the soma (**Figure 2.11A, B**). The peak $ASAP3_{ER}$ response (15.7 +/- 0.921) corresponded spatially with the peak of the Alexa-594 signal and was comparable to $ASAP3_{ER}$ responses to 0.5 s caffeine puffs we previously measured (see Figure 2.8K; **Figure**

2.11C). The amplitude of the $ASAP3_{ER}$ signal decreased rapidly over short distances, falling to 50% of its original value by ~16 μm and returning to baseline values by ~41 μm. Comparing profiles of $ASAP3_{ER}$ and Alexa-594 fluorescence peaks over 50 μm showed a near-perfect overlap (**Figure 2.11B**), indicating that the change in ER voltage is restricted to the regions directly stimulated by caffeine. Indeed, using the linear stimulus-response relationship between Alexa-594 and $ASAP3_{ER}$ fluorescence that we previously calculated in dendrites (see Figure 2.8L), and the Alexa-594 profile measured in these experiments, we calculated an "expected" $ASAP3_{ER}$ response from direct caffeine stimulus at each ROI bin. The expected $ASAP3_{ER}$ response was consistent in magnitude with measured $ASAP3_{ER}$ responses at caffeine puff centers, and recapitulated the normalized $ASAP3_{ER}$ measured response profile (CC = 0.959 +/- 0.005; **Figure 2.11D, E),** indicating there is little to no detectable propagation of ER electrical signals.

To develop an intuition of how the physical properties of the ER could shape electrical signal propagation, we constructed a passive cable model of the ER using the average Alexa-594 plume to define the current input and constraining the voltage to a 50 μm cylinder (see Methods and Supplemental material for more detail; **Figure 2.11F, Figure 2.12**). Over this distance, electrotonic spread is insensitive to realistic changes in tubule diameter but strongly influenced by membrane and axial resistance (**Figure 2.11H, Table 2.2**). Thus, we hypothesized that resident ER ion channels could impact membrane resistance and suppress the spread of stimulus-evoked ER depolarization.

BK channels are localized to organelle membranes including the ER (Shruti et al. 2012), have characterized intracellular functions (Li et al. 2014; Selezneva et al. 2021; Kulawiak et al. 2008), and are gated by concurrent depolarization and Ca^{2+}, both of which are satisfied by RyR activation. To test if BK channels contribute to restricting the spread of ER depolarization, we puffed caffeine onto dendrites as above, and compared $ASAP3_{ER}$ responses before and after application of the cell-permeant BK channel antagonists penitrem or paxilline. With penitrem the peak response was reduced compared to pre-drug application (**Figure 2.11I, J**), however with both drugs we measured a shift in $ASAP3_{ER}$ fluorescence such that depolarization was detected further away from the center of the caffeine puff (**Figure 2.11I, K**). Indeed,

the stimulus-evoked depolarization decayed to 50% of the maximum at a greater distance when BK channels were blocked (**Figure 2.11M**). Thus, BK channels in the ER membrane actively suppress the propagation of electrical signals.

Discussion:

The electrical signaling repertoire of organelles is multifaceted and essential. Our study provides a foundation for exploring electrical signaling in the ER and its impact on broader cellular functions. The -KKAA ER retention sequence that we used to target $ASAP3_{ER}$ is evolutionarily conserved (Dogic et al. 2001) and reliably retains integral proteins directly in the ER, such that the carboxy terminal -KKAA remains in the cytoplasm (Andersson, Kappeler, and Hauri 1999; Shin et al. 1991). By leveraging this biology, the location and orientation of $ASAP3_{ER}$ is predictable, which ensures that photons collected from large cellular volumes originate from the ER membrane and accurately report relative depolarizations and hyperpolarizations. While GFP fluorescence is sensitive to low pH (Kneen et al. 1998), the lumen of the ER is consistently neutral (Kim et al. 1998; for review see Casey, Grinstein, and Orlowski 2010) and stimulus-dependent changes in $ASAP3_{ER}$ fluorescence can be readily compared to NCP-$ASAP_{ER}$ and GFP-ER, to abrogate pH concerns. Thus, our strategy enables measurement of ER membrane potential changes and will be broadly applicable to other cellular systems, such as cardiomyocytes where SR membrane potential remains controversial (Oetliker 1989; Sanchez et al. 2018; Gillespie and Fill 2009).

In neurons, $ASAP3_{ER}$ reports bidirectional changes in ER membrane potential that are modest but ongoing during spontaneous activity and substantial in response to manipulations of network activity, seemingly similar to the PM and different from organelles like lysosomes and Golgi (Saminathan et al. 2021; Matamala et al. 2021). The timescales over which ER membrane potential changes, however, are much slower than those observed at the PM and more closely resemble those of lysosomes and Golgi

(Saminathan et al. 2021; Matamala et al. 2021). Clearly, the ER membrane system generates distinct electrical dynamics unique from those observed at the PM or other organelles.

Our measurements of stimulus-evoked ER membrane potential responses indicate that its dynamic range is large, on par with that of the PM. This opens the possibility that fluctuations in ER membrane potential activate resident voltage-gated ion channels in addition to BK channels as we have shown. However, increasing depolarization of the ER membrane across the range of stimuli that we provided did not trigger steep increases in the rate of $ASAP3_{ER}$ fluorescence changes, suggesting that the ER membrane does not engage active conductances to generate superlinear depolarizations akin to those at the PM (Losonczy and Magee 2006). Rather, our finding that BK channels limit the spread of electrical responses along the ER membrane demonstrates that active conductances may instead maintain linearity or even constrain electrical responses. Indeed, voltage-gated K^+ channels (Yazawa et al. 2007; Wang et al. 2019), Cl^- channels (Tanifuji, Sokabe, and Kasai 1987; Buyse et al. 1998), and even RyRs (Gillespie and Fill 2009; Gillespie, Chen, and Fill 2012) have been proposed to shunt or counteract changes in ER membrane potential. Thus, repolarization or shunting by voltage-gated ion channels may be essential to suppress spread of electrical responses and give rise to a compartmentalized ER membrane system where adjacent regions of ER can function independently.

The ER is known to compartmentalize protein distributions (Cui-Wang et al. 2012) and Ca^{2+} stores (Chen-Engerer et al. 2019), and may restrict electrical propagation through shared mechanisms. ER complexity that restricts protein diffusion at branch points and spines (Cui-Wang et al. 2012) may also shorten apparent length constants due to the intricacy of the membrane surface area. Further, the small diameter of ER tubules, which also limits diffusion (often ~50 nm; Nixon-Abell et al. 2016) will inevitably increase axial resistance and attenuate electrical propagation. This may provide a basis for independent ER electrical properties at dendritic regions like branch points where relatively high densities of IP3Rs generates Ca^{2+} signaling "hot spots" (Fitzpatrick et al. 2009), or PM-ER junctions where clustered $K_V2.1$,

LTCC, and RyRs generate Ca^{2+} "sparks" (Thillaiappan et al. 2017). In this way, ER structure and membrane potential may synergistically shape ER Ca^{2+} signaling.

Methods:

Resource Availability:

Materials availability

Plasmids generated in this study will be deposited to Addgene.

Data and code availability

All data reported in this paper will be shared by the lead contact upon request.

All original code will be deposited at Github and will be publicly available as of the date of publication. DOIs will be listed in the key resource table.

Any additional information required to reanalyze the data reported in this paper is available from the lead contact upon request.

Experimental Model Details:

Animals

All animal procedures were performed in accordance with the University of California San Diego Institutional Animal Care and Use Committee (protocol number S20032) and complied with all relevant

ethical regulations for animal research. Primary hippocampal cultures were prepared from wild-type (WT) Sprague Dawley (Envigo) rat pups on postnatal day 0-1 (P0-1). Hippocampal tissue was collected from animals of both sexes and pooled.

Primary neuronal and cell cultures

Hippocampi from P0-1 rat pups were prepared as previously described (GOSLIN and K 1998). Dissociated neurons were plated at a density of 130 cells per square millimeter (mm^2) on 12 millimeter (mm) diameter glass coverslips coated with poly-d-lysine (Neuvitro, Vancouver, WA). Neurons were grown in maintenance media consisting of Neurobasal-A media, supplemented with Glutamax, and B27 supplement (all from Thermo Fisher Scientific, Waltham, MA). Neurons were transfected with plasmid DNA as indicated using Lipofectamine 3000 (Thermo Fisher Scientific, Waltham, MA) at DIV6, according to the manufacturer's recommendations. Transfected neurons were used for experiments at 9−21 DIV, but specifically from 14-21 for KCl, PTX, or TTX experiments that manipulated network activity in cultures.

Human embryonic kidney 293 T-variant cells (HEK293T; ATCC, Manassas, VA) were plated on 12 mm glass coverslips (Neuvitro, Vancouver, WA) coated with bovine collagen I (Corning, Corning, NY) according to the manufacturer's recommendations, and maintained in Dulbecco's Modified Eagle medium (DMEM) supplemented with 10% fetal bovine serum, and penicillin-streptomycin (all from Thermo Fisher Scientific, Waltham, MA). Cells were continuously maintained at 37°C and 5% CO_2 and were passaged at 80-90% confluency. HEK293T are thought to be derived from an epithelial or neuronal lineage from female embryonic human kidney tissue. Our cell line was not authenticated. Cells were transfected using 1% Polyethylenimine Max (Polysciences Inc., Warrington, PA) according to the manufacturer's recommendations at approximately 30% confluency and were used for experimentation 2-3 days post-transfection (DPT2-3).

Method Details:

DNA construct subcloning

Plasmids were made by standard molecular biology techniques with all cloned fragments confirmed by sequencing. ASAP3 subcloned into a pcDNA3.1/Puro-CAG vector (Lam et al. 2012) was provided as a kind gift by Dr. Lin and served as a starting point for cloning putative ER retained ASAP3 variants, which were inserted between Nhe and HindIII restriction sites. The ASAP3 variant containing an amino-terminus MRRR- tag was cloned using 5'-CGCTAGCCGCCACCATGAGGAGGAGGATGGAGACGACTGTGAGGTATGAAC-3' forward primer with 5'-AAGCTTTCATTAGGTTACCACTTCAAGTTGTTTCTTCTGTG-3' reverse primer, while variants possessing carboxy-terminus tags all used 5'-CGCTAGCCGCCACCATGGA-3' forward primer, combined with reverse primers 5'-CAAGCTTTTACGCCGCCTTCTTGGTTACCACTTCAAGTTGTTTCTTCTGTG-3', 5'-CAAGCTTTCATTACCTCCTCTTCTTGGTTACCACTTCAAGTTGTTTCTTCTGTG-3', or 5'-CAAGCTTTCATTAAGAAGACTTCTTGGTTACCACTTCAAGTTGTTTCTTCTGTG-3' for -KKAA, -KKRR, or -KKSS retention tags, respectively. The NCP-ASAP1 construct (Villette et al. 2019; Chamberland et al. 2017) was cloned to generate the NCP-ASAP$_{ER}$ control construct using identical -KKAA primers as for ASAP3$_{ER}$. For expression in neurons ASAP3$_{ER}$ was cloned into pAAV.hSyn between NcoI and HindIII restriction sites using 5'-CGTCGACCGCCACCATGGAGACGACT-3' forward primer and 5'-CCGAGCTCGGTACCAAGCTT-3' reverse primer.

Trypan Blue viability staining

HEK293 cells at DPT2-3 were subjected to Trypan Blue stain (Gibco, Life Technologies) according to the manufacturer's recommendations. Bright field and 488 fluorescence images were obtained with a Zeiss, Axio Imager.M2 widefield fluorescence microscope equipped with a Zeiss, apotome2 module. Trypan Blue and GFP (ASAP3 variant) positivity were scored and % viability was calculated by:

$$\%\ viability = 100\% \times \frac{(\#\ cells\ Trypan\ Blue\ negative\ and\ fluorescence\ positive)}{(\#\ cells\ fluorescence\ positive)}$$

Immunohistochemistry

After transfection HEK293 cells or dissociated neurons were fixed with warmed (37°C) phosphate buffered saline (PBS) containing 4% paraformaldehyde (Electron Microscopy Sciences, Hatfield, PA) for 10 min. Unless otherwise stated, cells were permeabilized with PBS containing 1% Triton X-100 for 5 min at room temperature. Blocking was performed on ice for 1 hour in a PBS solution containing 3% normal goat serum (NGS), 1% bovine serum albumin (BSA), 1% gelatin from cold water fish skin, and 0.1% Triton X-100. Primary antibodies were diluted in PBS solution containing 0.3% NGS, 0.1% BSA, 0.1 % gelatin from cold water fish skin, and 0.1% Triton X-100 and applied to cultures 24 hours at 4°C. Secondary antibodies were diluted in the same solution as primaries and were added to cultures at room temperature for 1 hour. Coverslips were mounted onto glass slides using DAPI Fluoromount-G mounting media (SouthernBiotechnology, Homewood, AL) to label nuclei. Images were acquired with a Nikon Ti2-E microscope with Nikon A1R HD confocal scanning, equipped with Nikon N-SIM structured illumination and an Andor iXon Ultra 897 EMCCD camera.

For non-permeabilized staining of HEK293 cells expressing ASAP3 or ASAP3$_{ER}$, cultures were fixed as above, but permeabilization with Triton X-100 was skipped and Triton X-100 was excluded from all solutions. Antibody concentrations and procedures were otherwise identical. For imaging permeabilized

and non-permeabilized cultures, microscope and imaging settings were established while imaging permeabilized cultures and were unchanged for subsequent imaging of non-permeabilized cultures.

Electrophysiology

Recordings were obtained at room temperature (~25 °C) from cultured rat neurons perfused (2-4 milliliter per min) with recirculating imaging solution consisting of: 1X Hank's balanced salt solution HBSS, 25 millimolar (mM) glucose, 10 mM HEPES, 1 mM pyruvate, 0.74 mM Ca-Cl_2. Osmolarity and pH were adjusted to 300-310 mOsm and 7.3 with double distilled water and sodium hydroxide (Na-OH) respectively, and solution was sterilized with 0.22 μm filter units (EMD Millipore Temecula, CA). Neurons were visualized with infrared differential interference contrast (DIC) and transfected neurons were identified by fluorescence. Patch pipettes (borosilicate glass pipette; Sutter Instruments, CA), with open resistance 3-5 MΩ for whole cell patch experiments and 6-7 MΩ for cell attached or loose cell patch experiments, were filled with an internal solution consisting of (in mM): 147 K-gluconate, 20 KCl, 10 Na_2-phosphocreatine, 10 HEPES, 2 Na-ATP, 0.3 Na-GTP, 5 $MgCl_2$, 0.2 EGTA. Osmolarity and pH were adjusted to 290-300 mOsm and 7.3 with double distilled water and K-OH, respectively.

For whole-cell recordings, series resistance (R_s < 30 MΩ) was uncompensated and recordings were discarded if R_s changed by 20% or more. Current-clamp recordings of spontaneous activity were obtained for two min while simultaneously imaging ASAP3 fluorescence from the soma. For measuring ASAP3 responses to various changes in PM potential, recordings were obtained in voltage-clamp, holding the cell at -65 mV. Current was injected (500 ms pulse duration, three pulses, separated by 5 s) to bring the PM potential to: -85 mV, -65 mV, -55 mV, -45 mV, -35 mV, -25 mV, -5 mV, and +15 mV. The order of pulses was provided at random. ASAP3 was imaged continuously across all voltage sweeps and fluorescence responses from the soma were averaged to generate each cell's fluorescence at set voltages. In some

recordings, the cell died prior to testing all membrane potentials, resulting in different N for some membrane potentials.

For spontaneous activity or bath applied pharmacology experiments with $ASAP3_{ER}$, $NCP\text{-}ASAP_{ER}$, or GFP-ER expressing neurons, cell-attached and loose-patch recordings were performed as previously described. Neurons were recorded from at DIV14-21 to ensure robust network activity and synaptic maturity. Cells were excluded from analysis if they showed no spontaneous spiking activity or if no change in spiking was observed in response to pharmacology. Spontaneous activity recordings were 2 min; bath application of drugs were 6 min.

Drug application

Activity was manipulated via bath application of the following: KCl (40 mM; Sigma-Aldrich, St. Louis, MO), picrotoxin (PTX; 50 μM; Tocris Bioscience, Bristol, UK), sodium tetrodotoxin citrate (TTX; 1 μM; Tocris Bioscience, Bristol, UK), 2-Methyl-6-(phenylethynyl)pyridine hydrochloride (MPEP; 1 μM; Tocris Bioscience, Bristol, UK), 7-(Hydroxyimino)cyclopropa[b]chromen-1a-carboxylate ethyl ester (CPCCOEt; 20 μM; Tocris Bioscience, Bristol, UK), Ryanodine (Ry; 10 μM; Tocris Bioscience, Bristol, UK), Penitrem-A (650 nM; Tocris Bioscience, Bristol, UK), and Paxilline (1 μM; Tocris Bioscience, Bristol, UK), as indicated. Focal drug application was performed through glass pipette, with open resistance of 9-10 MΩ, connected to a Picospritzer II (general valve corporation, Fairfield, NJ) set to minimal pressure (4 PSI). (RS)-3,5-Dihydroxyphenylglycine (DHPG; 500 μM; Tocris Bioscience, Bristol, UK) and caffeine (40 mM; Tocris Bioscience, Bristol, UK) were dissolved neuron imaging media containing Alexa Fluor 594 Biocytin (50 μM; Molecular Probes Inc., Eugene, OR). The pipette tip was placed at a distance of 10 μm from somas or dendrites. DHPG was applied as a single 1 s puff; three puffs of caffeine were applied for the indicated durations with 30 s between puffs. Focal drug applications were repeated while imaging Alexa-594 to visualize application plumes and again with DIC to control for mechanical displacement. If

mechanical movement was detected in any recording, all recordings for that neuron were discarded. Of note, the absolute value of Alexa-594 fluorescence was substantially higher at dendritic regions in comparison to somatic, due to exclusion of the dye from the soma itself

Data acquisition and analysis

Experiments were performed on an Olympus BX51 wide field epifluorescence microscope (Olympus Life Science Solutions) outfitted with a PCO edge4.2 sCMOS camera (PCO, Kelheim, DE). Recordings were obtained with a Multiclamp 700B amplifier (Molecular Devices, Sunnyvale, CA) and National Instruments data acquisition boards (NI PCIe-6259 and BNC-2110; Austin, TX) under control of a 32-bit Windows 7 computer equipped with MATLAB software (Mathworks Inc., Natick, MA) running Scanimage (Pologruto, Sabatini, and Svoboda 2003). Physiology data were sampled at 10 kHz and filtered at 6 kHz. Simultaneous optical data were sampled at either 100 Hz or 10 Hz as indicated in the text. Off-line data analysis was performed using custom software written in MATLAB by E.P.C. or using Neuromatic software (WaveMetrics Igor Pro, Portland, OR). In brief, imaging data were read into MATLAB and used to generate scaled average projection images from all time series images. ROIs were drawn by hand delineating neuronal ROIs (soma or dendrites) and background ROIs. Average intensity values were calculated from background ROIs and subtracted from neuronal ROIs for every image frame. Imaging time series data was interpolated to fit the physiology data sampling frequency and aligned with respect to time.

Voltage-fluorescence response calibration: To calibrate ASAP3 voltage reporting whole-cell patch was used and neurons were discarded if they required more than 300 pA to hold at -65 mV. To quantify ASAP3 fluorescence at different PM potentials, average fluorescence was calculated for each step and normalized to average baseline fluorescence from 1 s immediately preceding the step. To quantify $ASPA3_{ER}$

fluorescence during spontaneous activity, imaging data was normalized to the average fluorescence from the entire 2 min recording

RMSE: For calculating the root mean square error (RMSE) of the fluorescence in spontaneously active neurons, baseline was calculated from the first 10 s, and used to calculate residuals across 90 s of imaging.

Spike rate and cross-correlation: To calculate rolling averages of spike rate, 120 s recordings of spontaneous spiking activity were divided into overlapping time windows of 0.1, 1, or 5 s and were spaced such that each window center was separated by 0.1 s from neighboring windows. Spikes within each window were identified using Neuromatic software and were used to calculate spike frequency within each window. Simultaneously imaged fluorescence from $ASAP3_{ER}$ was normalized to the average fluorescence across the full 120 s and aligned to spike rate windows with respect to time. Cross-correlation between spike rates and fluorescence was calculated across the full 120 s of paired recording and imaging with spike rates shifted with respect to fluorescence data.

Fluorescence quantification: Experiments comparing fluorescence before and after wash-in of a drug, baseline fluorescence was calculated over the 5-15 s prior to wash-in and responses normalized to this baseline. To generate pre- and post-drug application average fluorescence values, 1 s periods centered at 0 s (pre) and 240 s (post) relative to drug application, were averaged for each cell. For focal drug delivery experiments, fluorescence imaging data was generated as above but physiology was not analyzed and imaging data was not interpolated. Imaging data were normalized to baseline fluorescence from 1 s periods directly preceding drug application. Response magnitudes were calculated by fitting an exponential curve to the falling phase of each fluorescence response, beginning at the peak response value, while rise times, and decay constants τ were calculated using Neuromatic software.

Fluorescence signals over dendrites with spontaneous activity: For sliding spatial bin analysis along dendritic branch segments during spontaneous network activity, average projection images from across all

$ASAP3_{ER}$ images were generated and used to manually draw centerlines for sliding bins along longitudinal axes of dendrites, dendrite ROIs, and background ROIs spanning at least 55 μm along dendrites. Dendrite and background ROIs were subdivided into 11 non-overlapping 5 μm wide bins beginning at the start of the dendrite ROI. Average $ASAP3_{ER}$ fluorescence intensities were calculated within dendrite and background sliding bin ROIs and corresponding background was subtracted from dendrite ROIs at every image frame. CCs were calculated for the $ASAP3_{ER}$ fluorescence from each bin with every other bin and reported in an 11-by-11 matrix. CC matrices were averaged across cells.

Fluorescence signals over dendrites with caffeine application: For sliding spatial bin analysis along dendritic segments, average projection images from across all $ASAP3_{ER}$ images were generated and used to manually draw centerlines for sliding bins along longitudinal axes of dendrites. Alexa-594 average projection fluorescence images were referenced to locate the centroid of drug application on dendrites. Dendrite ROIs and background ROIs were drawn on $ASAP3_{ER}$ average fluorescence projections images, spanning the centroid of drug application and 50 μm along dendrites towards the cell body. Dendrite and background ROIs were subdivided into 100 overlapping sliding bins that were 5 μm wide and had centers spaced 0.5 μm apart. Average $ASAP3_{ER}$ fluorescence intensities were calculated within dendrite and background sliding bin ROIs and corresponding background was subtracted from dendrite ROIs at every image frame. Average Alexa-594 fluorescence intensities were also calculated within dendrite sliding bin ROIs at every image frame. $ASAP3_{ER}$ and Alexa-594 fluorescence response peaks were determined by fitting an exponential curve to the falling phase of responses, beginning at the peak response value. Timeframes for detecting peak responses were 1 s or less and ranges of exponential fits were adjusted to maximize R^2 values as needed. Maximal $ASAP3_{ER}$ and Alexa-594 peak responses were plotted at the distances of each spatial bin center.

Confocal and SIM image analysis

Images were analyzed in ImageJ (RRID: SCR_000415; https://imagej.nih.gov/ij/), FIJI (RRID: SCR_002285; https://fiji.sc/) and in custom software written by E.P.C. in MATLAB . Images of permeabilized or non-permeabilized HEK293 cells expressing ASAP3 or $ASAP3_{ER}$ were analyzed in MATLAB . In brief, average intensity projections images were generated, scaled, and used to draw ROIs over transfected cells and background. Average 488 nm and 649 nm fluorescences detected at background ROIs were subtracted from average fluorescences at cell ROIs. Ratios of 649 au / 488 au was calculated and normalized to the average 649 au / 488 au in permeabilized cells. For assessing colocalization by PCC in HEK293 cells, the ImageJ "Coloc 2" plugin for FIJI was used. To assess colocalization in SIM images of neurons by CC, fluorescence profiles were generated in ImageJ software for 1 μm wide sections through neuron somas between nuclear and proximal dendrite structures, and CCs for profiles were calculated in MATLAB .

Mathematical model

Model design: We constructed a 1D partial differential equation model of voltage on the ER membrane, inspired by the linear cable equation (Yihe and Timofeeva 2020; Rinzel and Rall 1974). We assumed that the cable equation was sufficient to capture the dynamics of the voltage at the ER in response to an input current. The ER was taken to be 50 μm long with the ER radius 'a' as a free parameter in our simulations. The control radius is taken to be 25 nm (Wu et al. 2017). The equation was solved for 5 s to capture the spatio-temporal dynamics of voltage across the ER. This timescale was chosen to be sufficiently large when compared to the propagation of electrical signals. We assume that the ER membrane is passive and thus does not actively propagate the voltage signal. We also assume that a change in voltage is proportional to the presence of caffeine along the dendrite. Experimentally we have observed diffusion of the stimulus, caffeine, over time away from the application site. Caffeine activates RyRs in the ER and

releases ions from the ER lumen. We took the spatiotemporal dynamics of the Alexa-594 mixed with caffeine solutions as the stimulus of the model, $I_0(x,t)$. The cable equation is given by:

$$\frac{\partial V}{\partial t} = \frac{\lambda^2}{\tau}\frac{\partial^2 V}{\partial^2 x} - \frac{V}{\tau} + I_0(x,t),$$

where $\tau = C_m R_m$ is the time constant, and $\lambda = \sqrt{\frac{aR_m}{2R_i}}$ is the length constant. C_m is the membrane capacitance (μF/cm^2), R_m is specific membrane resistance (Ω cm^2), R_i is the resistivity of the volume (Ω cm), and a is ER radius (nm).

Model stimulus and fitting: $I_0(x,t)$ represents voltage change due to an injected current from RyR opening as a function of caffeine application. $I_0(x,t)$ is given as:

$$I_0(x,t) = \frac{\beta R_m}{a\tau} I(x,t),$$

where β (mA/μm) is a scaling term and $I(x,t)$ is a dimensionless function that is obtained from the fluorescence measurements as a function of both x and t.

To obtain $I(x,t)$, we plotted all the temporal dynamics of the Alexa-594 at each measured spatial point along the ER. To simplify the fitting, we fit the decay dynamics of each temporal plot from each trace's maximum value to its return to baseline with an exponential decay function ae^{bt}. The majority of the traces peak at 0.5 s, so that is taken as the first time of peak for all the fit dynamics. We then mirror the decay dynamics from 0.5 - 1 s to 0.5 - 0 s, such that the fit fluorescence dynamics show a rise to a peak value at 0.5 s then a decay. The dynamics of the Alexa-594 and the fit traces over time for each spatial location are shown in Supplementary Figure 4A and B.

To make these fits fully a function of x and t, the coefficients for the exponential decay equations are now fit as a function of space, x.

The coefficients a and b are plotted over space and fit as fourth order polynomial functions (see Figure S4C, D). Therefore $I(x,t)$ has the form $I(x,t) = a(x)e^{b(x)t}$.

The coefficient a, for the max value, is given by:

$$a(x) = -2 * 10^{-4}x^4 + 0.022x^3 - 0.554x^2 - 5.379x + 270.185.$$

The coefficient b, for the decay rate, is given by:

$$b(x) = -2.6 * 10^{-6}x^4 - 2.9 * 10^{-4}\,x^3 + 0.01x^2 - 0.052x - 3.917.$$

Initial conditions and boundary conditions: The initial condition for voltage is assumed to be zero everywhere. The boundary conditions at x=0 is prescribed as a no-flux boundary condition $\frac{\partial V}{\partial x}|_{x=0} = 0$ and the boundary condition at x=L=50 μm is prescribed as $V_{(x=50\ \mu m)}=0$. We assume that the caffeine stimulus is applied at x=0 and can then diffuse out from that location. The same dynamics occurring along the positive x axes are mirrored on the negative x axes, justifying the Neumann boundary condition.

Parameter variations: The model has multiple free parameters, notably C_m, R_m, R_i, and β. C_m is the specific membrane capacitance and represents the fact that the cellular membrane acts as a capacitor since the lipid bilayer separates two electrolytic media. R_m is the specific membrane resistance and represents the resistance from the membrane to voltage propagation. R_i is the intraluminal resistivity and represents the resistance to ion flow from the contents of the ER lumen (the reticuloplasm).

Recall that $\tau = C_m R_m$ is the time constant, so τ describes how fast the membrane potential responds to the flow of ions through currents. Also recall that $\lambda = \sqrt{\frac{aR_m}{2R_i}}$ is the length constant and represents the length that a potential will travel down the membrane under only passive electrical conduction.

Values for C_m, R_m and R_i can vary across species and cell types (Roth and Häusser 2001). Currently these parameters are not well known for the ER membrane in rat hippocampal neurons. Therefore, we used four different parameter sets to explore a variety of published parameter values, see Table S1.

β is a free parameter associated with the current injection that acts as the model stimulus. To deal with the uncertainty with this parameter, we fit β for each parameter set such that the maximum value of voltage at x = 0 for each model with radius of 25 nm is equal to the experimentally determined voltage with $ASAP3_{ER}$.

Numerical solver: All simulations are run in MATLAB 2018b using the pdepe solver. Simulations are run for 5s and output at time intervals of 0.001 s. The ER was modeled as 50 μm in length and discretized into 0.005 μm increments. MATLAB files will be made available on Github.

Quantification and Statistical Analysis:

Mean +/- SEM is used as an estimate of center and dispersion of data values throughout this study, with the exception of mean +/- SD reported in Figure 2F. For all experiments "N" reports the number of replicate cells recorded from. Statistical analysis was performed in Prism software (GraphPad Inc, San Diego, CA). Distributions were assessed with Pearson normality tests. For data where sample size was too small to be assessed, normal distributions were assumed. Depending on relationships between experimental populations, significance was determined for experiments with one independent variable by unpaired, paired, or paired ratiometric Student's t tests, or by one-way analysis of variance (ANOVA). For experiments with two independent variables two-way ANOVA was performed. Statistical significance was determined when $p < 0.05$.

Figures and tables:

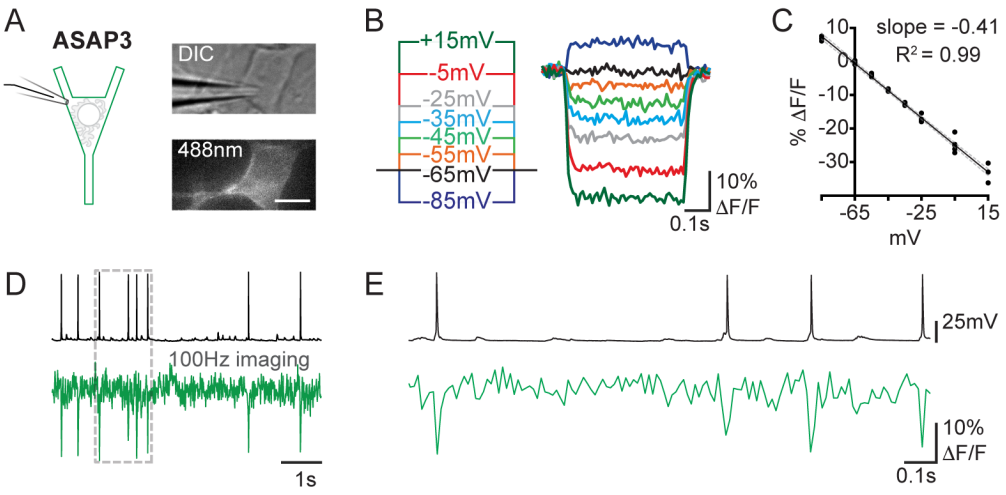

Figure 2.1 ASAP3 retained in the ER reports membrane potential dynamics during spontaneous network activity.

(**A**) Schematic of optical and whole-cell patch clamp recording from a dissociated hippocampal neuron expressing ASAP3 (left). DIC (top, right) and fluorescence (bottom, right) images of a neuron transfected with ASAP3. (**B**) Schematic of voltage steps set by whole-cell patch (0.5 s; left) and corresponding changes in ASAP3 fluorescence imaged over the soma (right). (**C**) Average ASAP3 % ΔF/F responses to changes in PM potential and linear regression (black) with 95% confidence intervals (gray, dashed line; N = 5). (**D**) Example whole-cell recording (top, black), and ASAP3 imaging (bottom, green) of neuronal activity. (**E**) Expanded view of recording and imaging time span denoted by gray dashed box in (D).

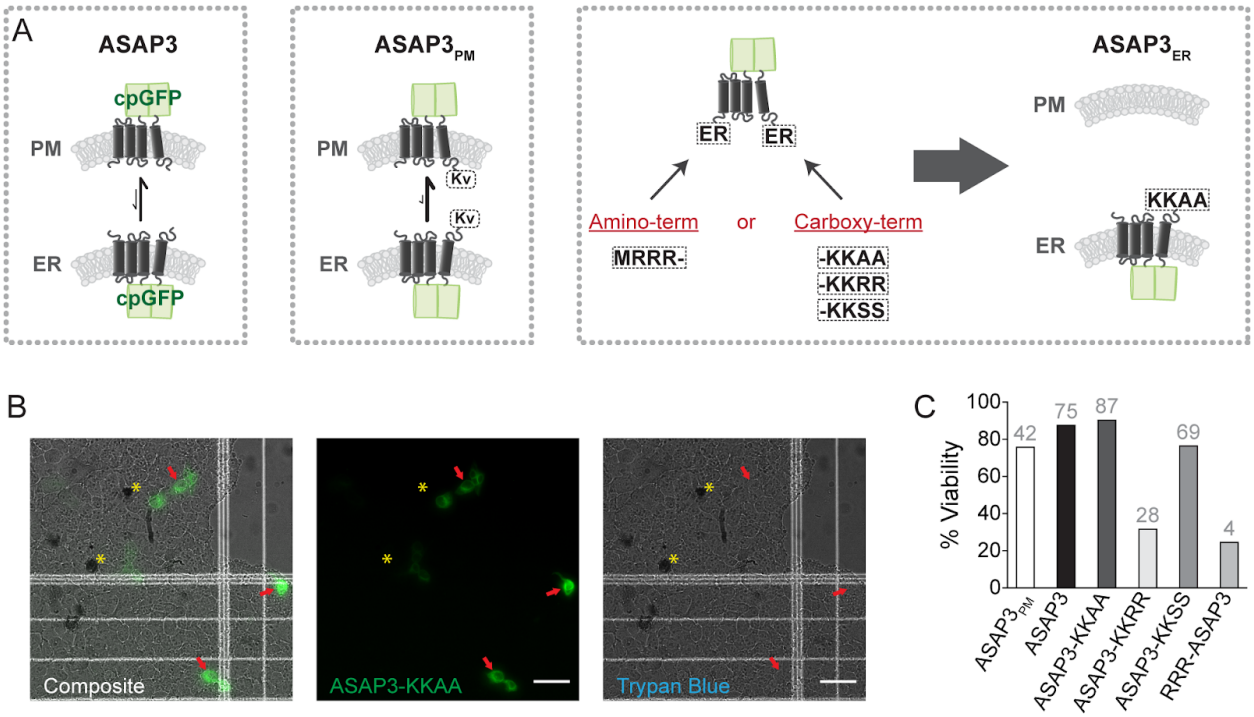

Figure 2.2 Cloning strategy for ER targeted ASAP3 variants.

(**A**) Schematic of ASAP3 and ASAP3$_{PM}$ subcellular localizations, as well as the four ER peptide retention signals tested to generate ASAP3$_{ER}$ and ASAP3$_{ER}$'s subcellular location. (**B**) Composite, fluorescent (488 nm; green), and bright field images (gray) of HEK293 cells expressing ASAP3-KKAA (red arrows) and stained with Trypan Blue (yellow astricies). (**C**) % viability scores for HEK293 cells expressing ASAP3$_{ER}$ with indicated retention signals, N indicated above bars. Image scale bar = 50 µm.

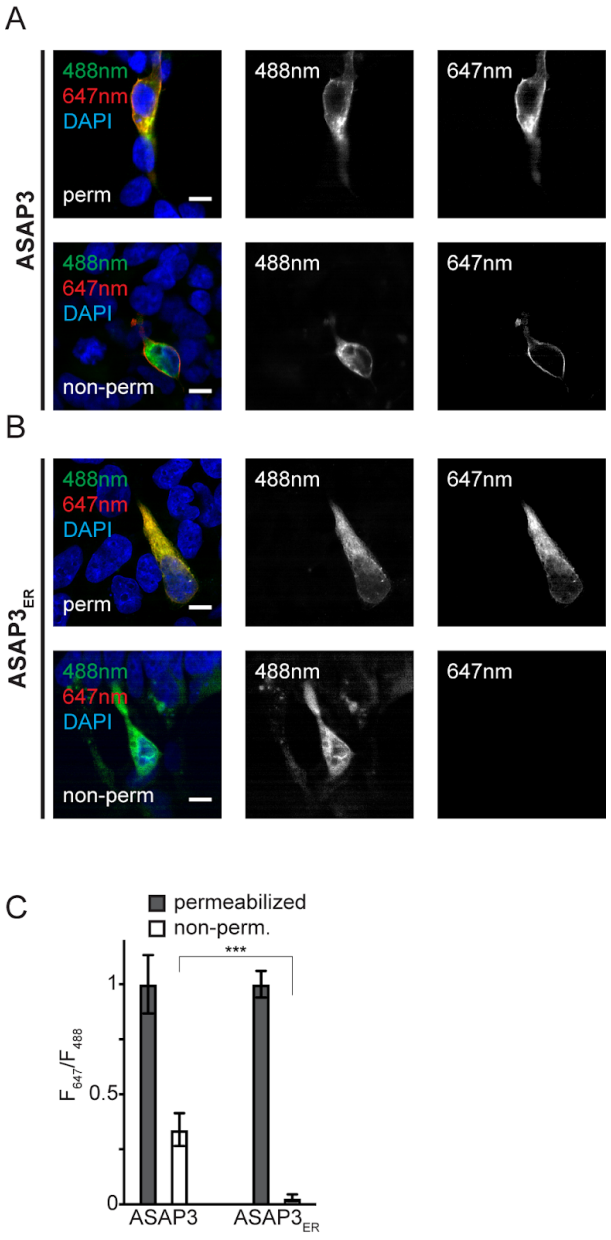

Figure 2.3 Imaging ASAP3$_{ER}$ intracellular localization.

(**A**) Example images of HEK293 cells transfected with ASAP3. Native fluorescence (488 nm), immunostaining for GFP (647 nm) and DAPI are shown for permeabilized (top) and non-permeabilized (bottom) conditions. (**B**) As in (A) but cells are transfected with ASAP3$_{ER}$. (**C**) Quantification of 647 versus 488 fluorescence in HEK293 cells transfected with ASAP3 (N = 19) or ASAP3$_{ER}$ (N = 20) in permeabilized (gray) or non-permeabilized (white) conditions. Data are shown as Avg +/- SEM. Image scale bars = 10 µm. 1-way ANOVA: *** $p < 0.0005$.

Figure 2.4 Imaging $ASAP3_{ER}$ localization at the ER.

(**A**) Example images of HEK293 cells transfected with tdT-ER and $ASAP3_{PM}$ and immunostained with anti-GFP. (**B**) As in (A) but cells transfected with tdT-ER and $ASAP3_{ER}$. (**C**) Quantification of colocalization (PCC) between tdT-ER and ASAP3 (N = 20), $ASAP3_{PM}$ (N = 22), or $ASAP3_{ER}$ (N = 24). (**D**) Example images of HEK293 cells transfected with tdT-ER and $ASAP3_{ER}$, immunostained with anti-GFP and anti-Golga2 (Golgi). (**E**) As in (D) but cells immunostained with anti-GFP and anti-Tomm20 (mitochondria). (**F**) Quantification of colocalization between $ASAP3_{ER}$ and Golga2 (N = 20) or Tomm20 (N = 21). (**G**) Example image of a HEK293 cell transfected with tdT-ER and $ASAP3_{PM}$ and immunostained with anti-GFP. Normalized fluorescence profiles (right) of tdT-ER (red) and ASAP3 (green) taken from within the indicated region (1 μm wide; gray dashed box). (**H**) As in (G) but a HEK293 cell transfected with tdT-ER (red) and $ASAP3_{ER}$ (green). (**I**) Example image of a neuron transfected with tdT-ER and $ASAP3_{PM}$ and immunostained with anti-GFP; magnification of soma is shown (center) with fluorescence profiles (right) of tdT-ER (red) and ASAP3 (green) within boxed region (dashed, gray). (**J**) As in (I) but a neuron transfected with tdT-ER and $ASAP3_{ER}$. (**K**) Quantification of correlation (CC) of tdT-ER fluorescence profiles with ASAP3 (N = 4), $ASAP3_{PM}$ (N = 5), or $ASAP3_{ER}$ (N = 8). Data are shown as Avg +/- SEM. Image scale bars = 10 μm. 1-way ANOVA: *** $p < 0.0005$.

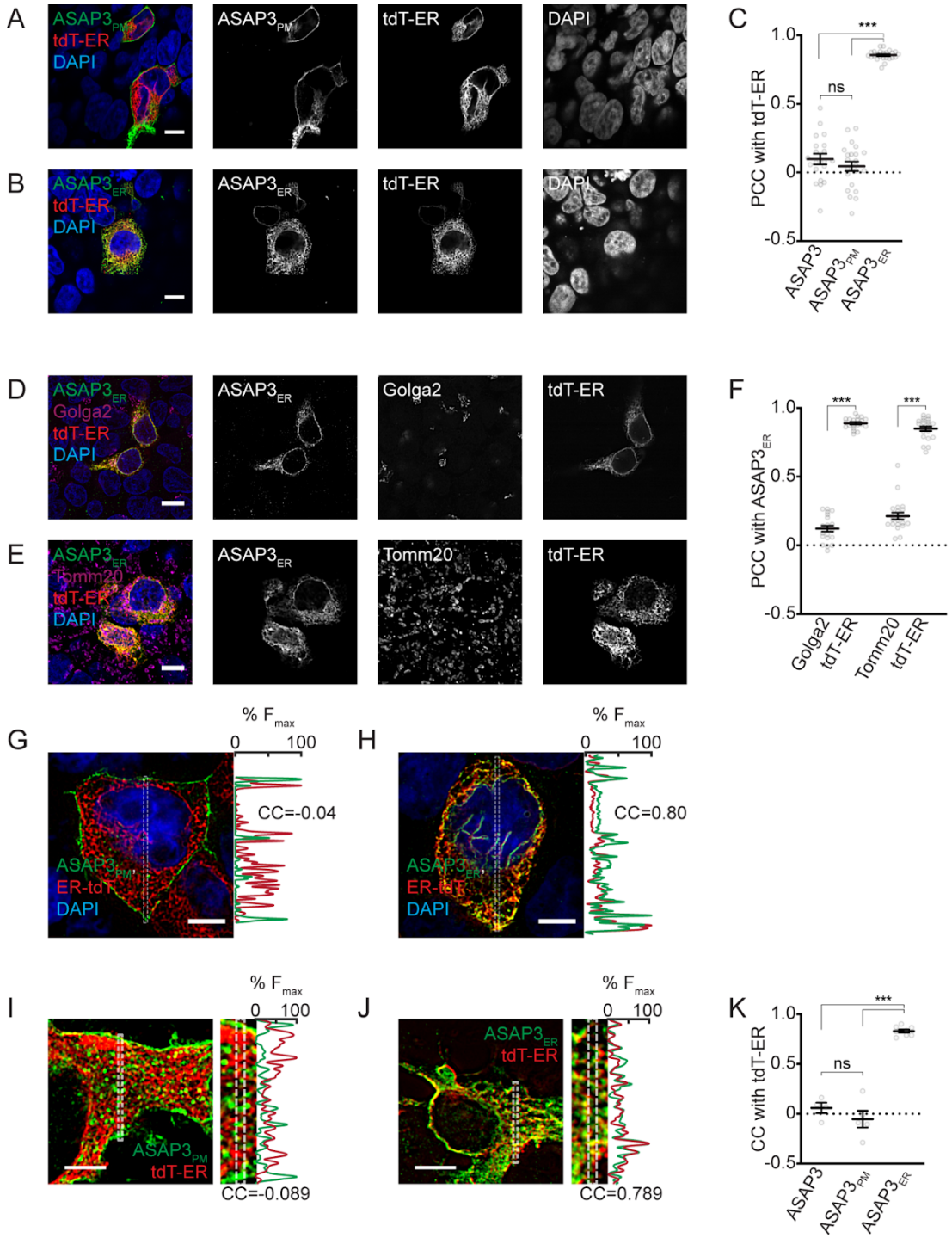
A
ASAP3PM
tdT-ER
DAPI
B
ASAP3ER
C
PCC with tdT-ER
ns
***
ASAP3
ASAP3PM
ASAP3ER
D
Golga2
E
Tomm20
F
PCC with ASAP3ER
Golga2 tdT-ER
Tomm20 tdT-ER
G
% Fmax
0
100
CC=-0.04
H
CC=0.80
I
CC=-0.089
J
CC=0.789
K
CC with tdT-ER

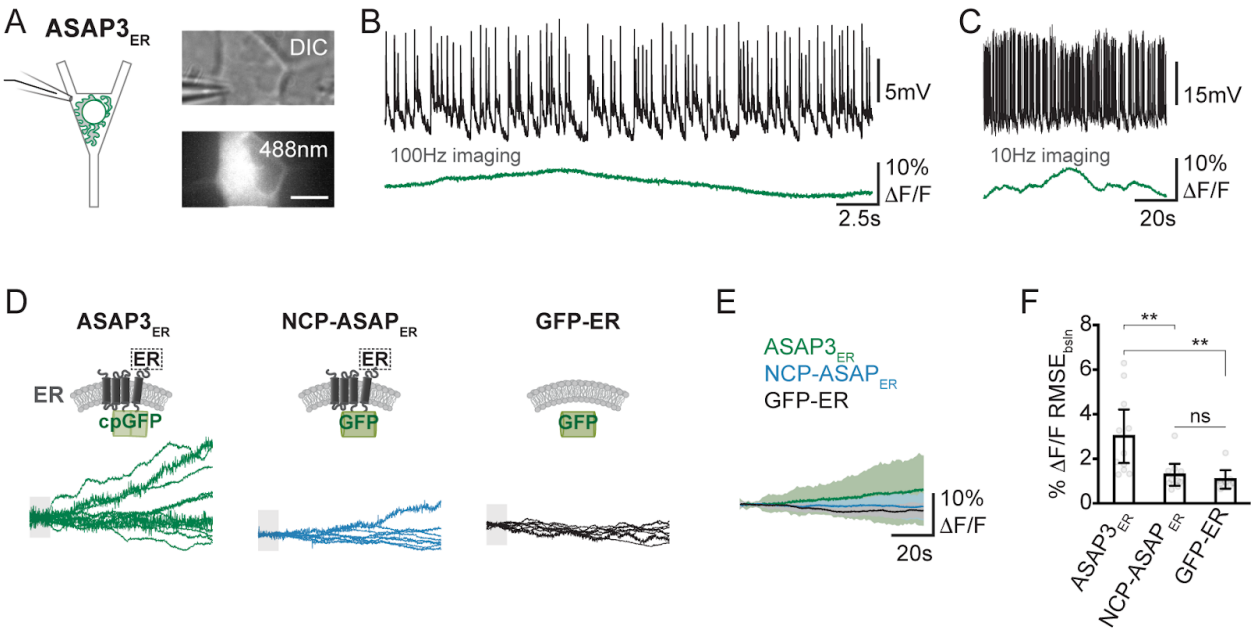

Figure 2.5 ER membrane potential fluctuates during spontaneous network activity.

(**A**) Schematic of optical and cell-attached recording from a neuron expressing ASAP3$_{ER}$ (left). DIC (top, right) and fluorescence (bottom, right) images of a neuron transfected with ASAP3$_{ER}$. (**B**) Example cell-attached recording (top, black) and simultaneous ASAP3$_{ER}$ fluorescence (bottom, green). Imaged at 100 Hz. (**J**) As in (I) but imaged at 10 Hz. (**A**) Fluorescence of neurons transfected with ASAP3$_{ER}$ (N = 11), NCP-ASAP$_{ER}$ (N = 10), or GFP-ER (N = 8) imaged at the soma during spontaneous network activity, aligned to baseline average (initial 10s; gray boxes). (**B**) Avg +/- SD for (A). (**C**) Quantification of the root mean square error (RMSE) from baseline in (A). Data are shown as Avg +/- SEM. Image scale bar = 10 μm. 1-way ANOVA: ** $p < 0.005$.

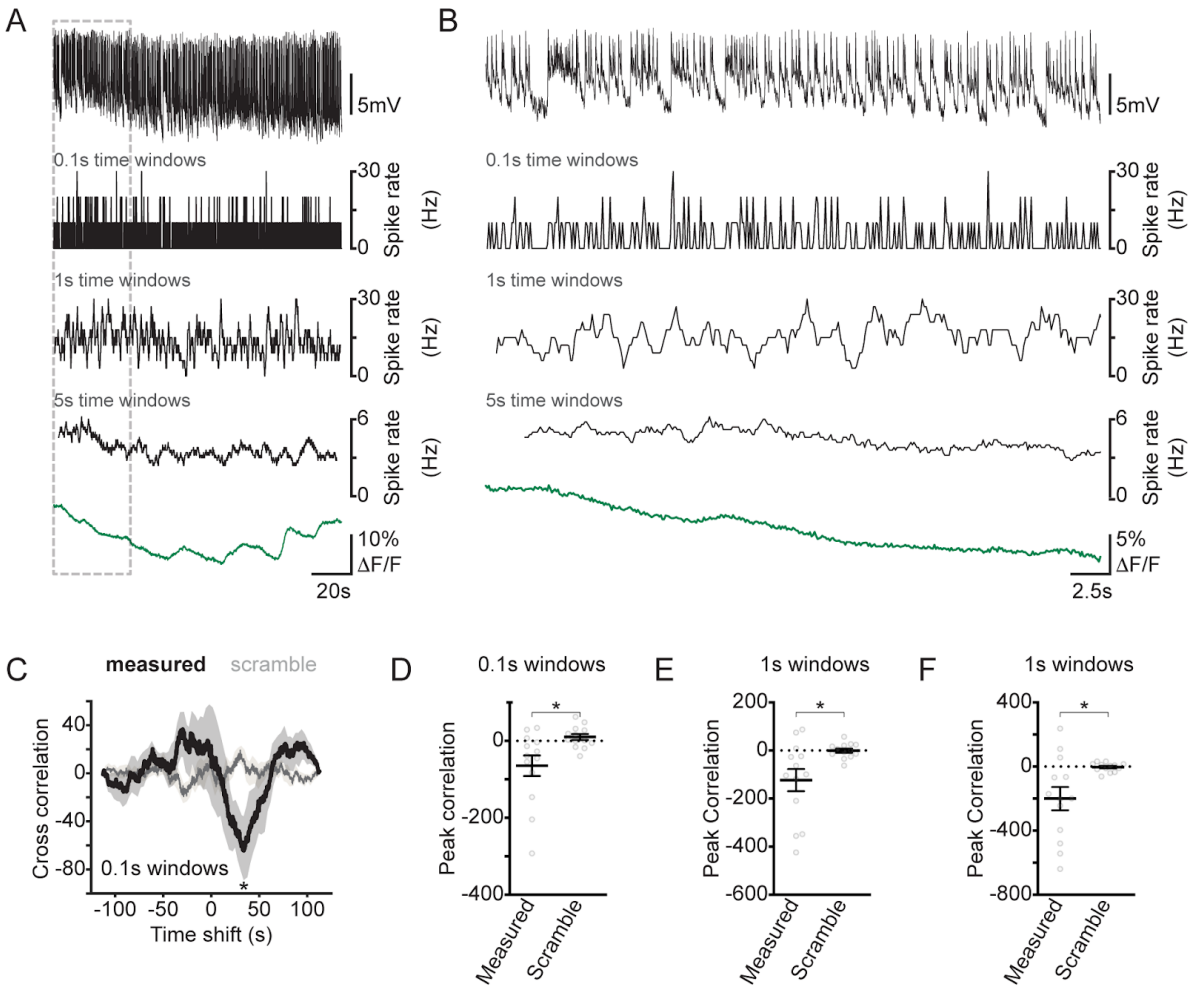

Figure 2.6 ER membrane potential fluctuations correlate with spike rates.

(**A**) Example cell-attached recording (top, black), with 0.1, 1, and 5 s widow rolling averages spike rates (middle, black), and concurrent $ASAP3_{ER}$ fluorescence (bottom, green). (**B**) Expanded view of the region of time denoted by box in (A; gray, dashed). (**C**) Average cross-correlation between $ASAP3_{ER}$ % ΔF/F and rolling average spike rate (black line; spike rate calculated in 0.1 s time windows), or scrambled spike rate (gray line; N=13). (**D**) Quantification of inverse correlation peak in (C). (**E, F**) As in (C) but spike rates calculated from 1, or 5 s time windows, respectively. Data are shown as Avg +/- SEM and imaging performed at 10 Hz frame rate. Paired t test: * $p < 0.05$.

Figure 2.7 ER membrane potential changes in response to manipulation of network activity.

(**A)** Electrical recording (top, black) and $ASAP3_{ER}$ fluorescence (top, green) in response to wash-inof KCl (40 mM; at grey bar). Average $ASAP3_{ER}$ response (bottom) to wash-inof KCl (green; N=8) or no addition (control; gray; N=12). (**B**) Same as (A), but wash-inof PTX (50 μM; N=11) or DMSO vehicle (DMSO; N=9). (**C**) Same as (A), but wash-inof TTX (1 μM; N=7) or control (replotted from A for comparison). (**D**) Same as (A), but sequential wash-inof PTX followed by TTX (N=3). (**E-G**) Quantification of %F in (A-C), and (**H**) comparison of %ΔF/F changes across conditions. (**I**) Quantification of %F in (D). (**J**) Average response of NCP-$ASAP_{ER}$ (N=8) and GFP-ER (N=7) to PTX. (**K**) Quantification of %ΔF/F in (J). (**L**) $ASAP3_{ER}$ response to PTX with MPEP (1 μM; left; N=10), CPCCOEt (20 μM; right; N=17), or MPEP + CPCCOEt (right; N=3) in the bath. (**M**) Quantification of %ΔF/F in (L). In (J, L), $ASAP3_{ER}$ PTX and DMSO replotted from (C) for comparison. Data are shown as Avg +/- SEM; imaging performed at a 10 Hz frame rate; ratiometric paired t test or 1-way ANOVA: * $p < 0.05$, ** $p < 0.005$, *** $p < 0.0005$.

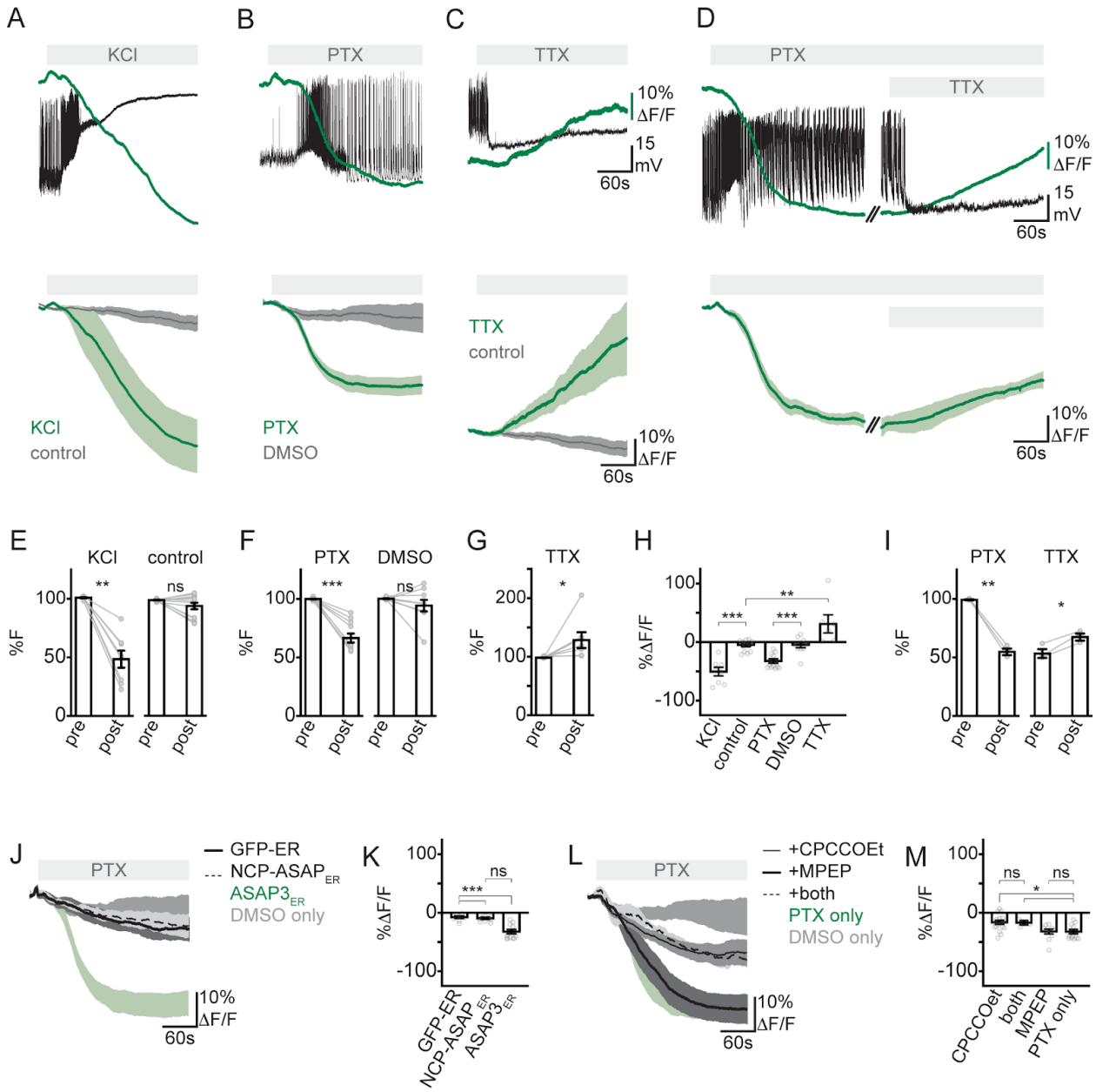
A
KCl
KCl
control
B
PTX
PTX
DMSO
C
TTX
10%
ΔF/F
15
mV
60s
TTX
control
10%
ΔF/F
60s
D
PTX
TTX
10%
ΔF/F
15
mV
60s
10%
ΔF/F
60s
E
KCl
control
%F
**
ns
pre
post
F
PTX
DMSO
%F
***
ns
G
TTX
%F
*
H
%ΔF/F
***
***
**
KCl
control
PTX
DMSO
TTX
I
PTX
TTX
%F
**
*
J
PTX
GFP-ER
NCP-ASAP$_{ER}$
ASAP3$_{ER}$
DMSO only
10%
ΔF/F
60s
K
%ΔF/F
***
ns
GFP-ER
NCP-ASAP$_{ER}$
ASAP3$_{ER}$
L
PTX
+CPCCOEt
+MPEP
+both
PTX only
DMSO only
10%
ΔF/F
60s
M
%ΔF/F
ns
ns
*
CPCCOEt
both
MPEP
PTX only

Figure 2.8 ER membrane generates linear stimulus-voltage response curves in somas and dendrites.

(**A**) DIC (top) and fluorescence (bottom) images of a neuron expressing $ASAP3_{ER}$. The picospritzer pipette (blue) and region of interest (ROI, red) are indicated. (**B**) Average $ASAP3_{ER}$ responses to 1 s puffs (black, above) of DHPG (500 μM; N=7) or caffeine (caff; 40 mM; N=10). (**C**) Quantification of peak, rise time, and decay time constants (τ) for (B). (**D**) Average $ASAP3_{ER}$ (green) and Alexa-594 (red) responses to caffeine puffs of indicated durations (black; N=6). (**E**) Average $ASAP3_{ER}$ response to 500 ms caffeine puff imaged at 100 Hz (N=3). (**F**) Quantification of $ASAP3_{ER}$ response peaks from (D-E) versus puff duration with linear fit (black, solid) and 95% CI (gray, dashed). (**G**) as in (F) but versus Alexa-594 peak fluorescence (**H**) Max $ASAP3_{ER}$ response rates versus caffeine puff durations. (**I**) as in (A) but at dendrites. (**J-M**) As in (D-H) but with stimulation and imaging of dendrites (N=9). (**N**) Quantification of somatic and dendritic $ASAP3_{ER}$ peak, (**O**) rise time, and (**P**) decay τ values. (**Q**) Decay τ vs peak for somatic and dendritic ROIs (N=15). Data are shown as Avg +/- SEM, and imaged at 10 Hz except in (E), which is imaged at 100 Hz. Green circle in (F) quantified from (E). Image scale bars=10 μm. 2-way ANOVA: * $p < 0.05$, ** $p < 0.005$, *** $p < 0.0005$. Puff duration effect is significant in N-P ($p < 0.0005$).

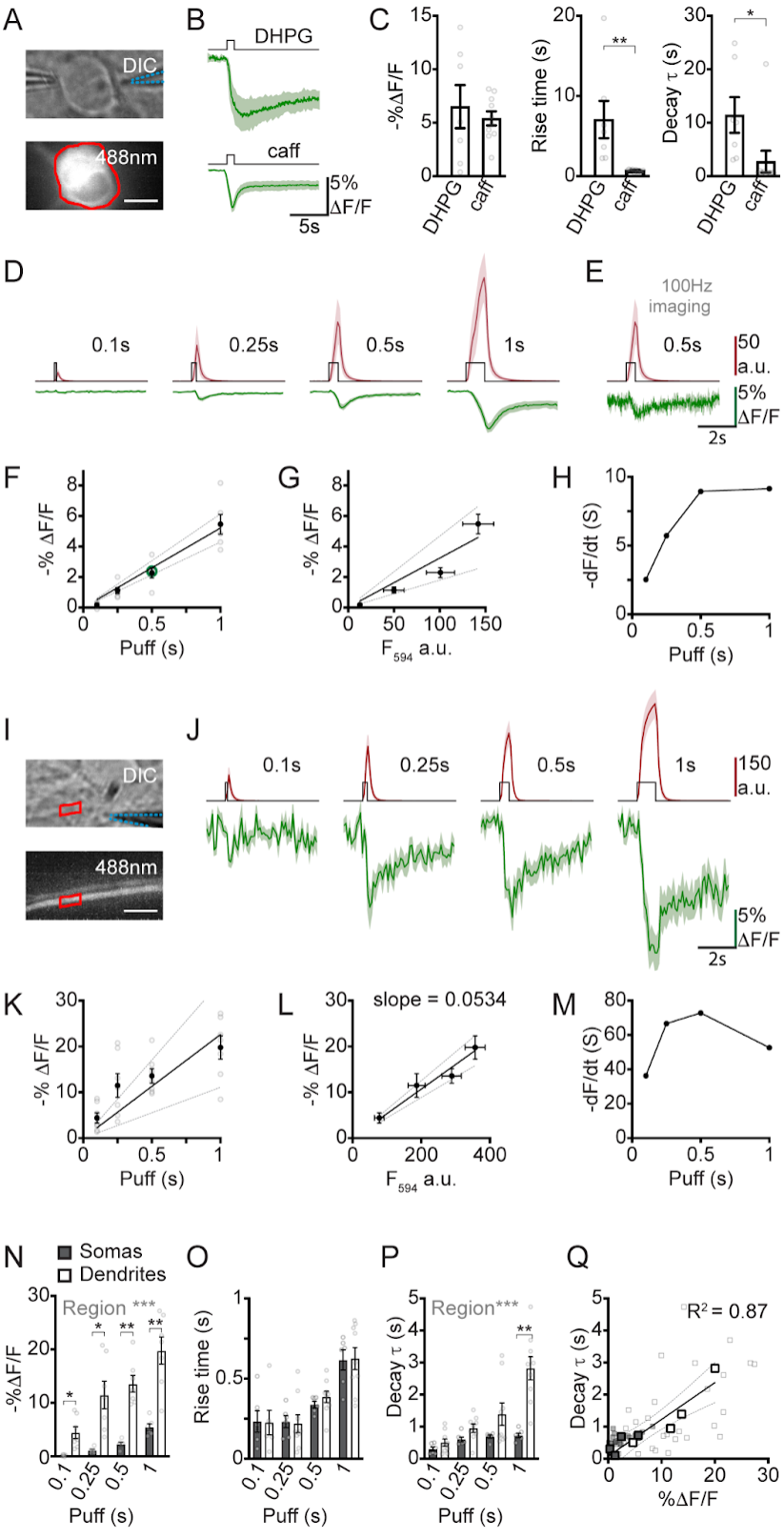
A
DIC
488nm
B
DHPG
caff
5%
ΔF/F
5s
C
-%ΔF/F
Rise time (s)
Decay τ (s)
DHPG
caff
D
0.1s
0.25s
0.5s
1s
E
100Hz
imaging
0.5s
50
a.u.
5%
ΔF/F
2s
F
-% ΔF/F
Puff (s)
G
-% ΔF/F
F594 a.u.
H
-dF/dt (S)
Puff (s)
I
DIC
488nm
J
0.1s
0.25s
0.5s
1s
150
a.u.
5%
ΔF/F
2s
K
-% ΔF/F
Puff (s)
L
slope = 0.0534
-% ΔF/F
F594 a.u.
M
-dF/dt (S)
Puff (s)
N
Somas
Dendrites
Region ***
-%ΔF/F
Puff (s)
O
Rise time (s)
Puff (s)
P
Region***
Decay τ (s)
Puff (s)
Q
R² = 0.87
Decay τ (s)
%ΔF/F

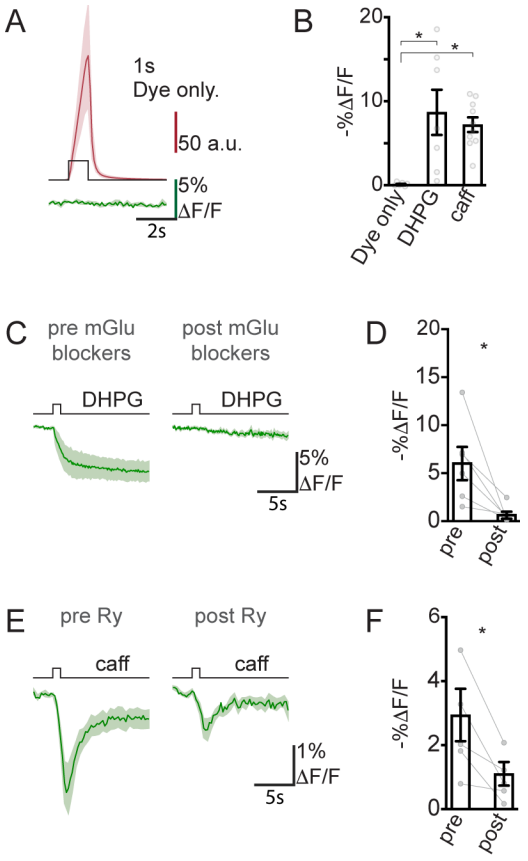

Figure 2.9 Specificity of ASAP3$_{ER}$ responses to DHPG and caffeine.

(**A**) Average ASAP3$_{ER}$ (green) and Alexa-594 (red) peaks generated by a 1 s puff (black) of vehicle solution containing Alexa-594. (**B**). Quantification of (A; N = 6). DHPG and caffeine data in (B) replotted from Figure 3C for comparison. (**C**) Average ASAP3$_{ER}$ response to 1 s puffs of DHPG (500 µM) pre and post bath application of MPEP + CPCCOEt (1 µM and 20µM, respectively). (**D**) Quantification of peak fluorescence in (C; N = 6). (**E**) Average ASAP3$_{ER}$ response to 0.5 s puffs of caff (40 mM) pre and post bath application of ryanodine (10 µM). (**F**) Quantification of fluorescence response peaks in (E; N = 5). Data are shown as Avg +/- SEM; imaging performed at 10 Hz frame rate; ratiometric paired t test * $p < 0.05$.

Figure 2.10 ER membrane potential fluctuations across dendritic branches.

(**A**) Fluorescence image of an example dendrite expressing $ASAP3_{ER}$ (top), ROIs (red) with centers spaced 5 μm apart along the dendrite, spanning 0-50 μm. Example $ASAP3_{ER}$ fluorescence (green; bottom) from ROIs at indicated distances during wash-in of PTX (at gray bar; 50 μM). (**B**) CCs for $ASAP3_{ER}$ fluorescence compared between each pair of ROIs in (A). (**C**) Average CCs from dendritic ROIs as in (A-B; N = 6). (**D-F**) As in (A-C) except for neurons stimulated by spontaneous network activity, without wash-in of PTX (N=11).

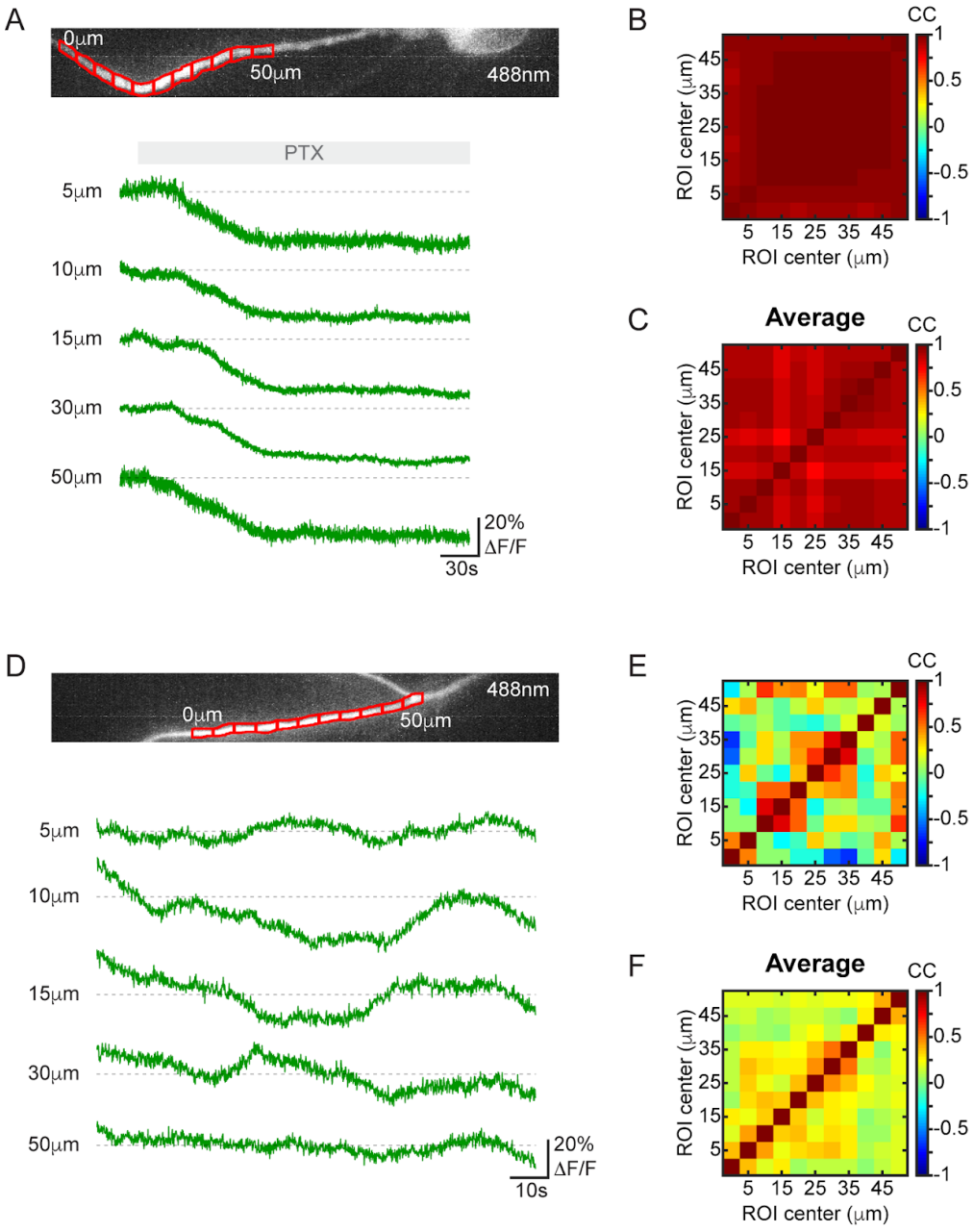
A
0μm
50μm
488nm
PTX
5μm
10μm
15μm
30μm
50μm
20%
ΔF/F
30s
B
CC
1
0.5
0
-0.5
-1
ROI center (μm)
5 15 25 35 45
C
Average
D
E
F
10s

Figure 2.11 Stimulus-evoked ER membrane potential fluctuations are restricted to the site of stimulation in dendrites.

(**A**) DIC (top) and fluorescence (below) images of an example dendrite expressing $ASAP3_{ER}$, picrospritzer pipette (blue) is shown and 4 of 100 sliding-bin ROIs (red) centered at indicated distances from the centroid of a 0.5 s caffeine puff. Average fluorescence (bottom) of Alexa-594 (red) or $ASAP3_{ER}$ (green) from ROIs at indicated distances (N=18). (**B**) Average profiles of $ASAP3_{ER}$ (green, left Y axis) and Alexa-594 (red, right Y axis) peaks across all ROIs (N=18). (**C**) Quantification of $ASAP3_{ER}$ peaks at puff centers. (**D**) Normalized profiles of average $ASAP3_{ER}$ peaks measured (green) or expected from Alexa-594 fluorescence (black). Insert is quantification of CCs between measured and expected $ASAP3_{ER}$ profiles. (**E**) As in (C) but for expected $ASAP3_{ER}$ peaks. (**F**) Circuit schematic of the passive cable ER model with membrane capacitance C_m (0.75 $\mu F/cm^2$) and resistance R_m, luminal resistivity R_i, and an injected current I(x,t). (**G**) Model results of peak voltage across time and distance, using an ER diameter of 50 nm and parameters in set 1 (see Table S1 for details). (**H**) Model predictions for different diameters (d), R_m, and R_i values. (**I**) Profiles of average $ASAP3_{ER}$ peaks pre (green) or post (black) wash-in of penitrem (pen; N=6), normalized to peak at puff center. (**J**) Quantification of $ASAP3_{ER}$ response peaks at puff centers from (I). (**K,L**) As in (I,J) but paxilline (pax; N=8). (**M**) Distance at which $ASAP3_{ER}$ peaks are 50% max; pre and post wash-in of pen (grey) or pax (white). Data are shown as Avg +/- SEM, and imaged at 10 Hz; ratiometric t test: * $p < 0.05$, *** $p < 0.0005$.

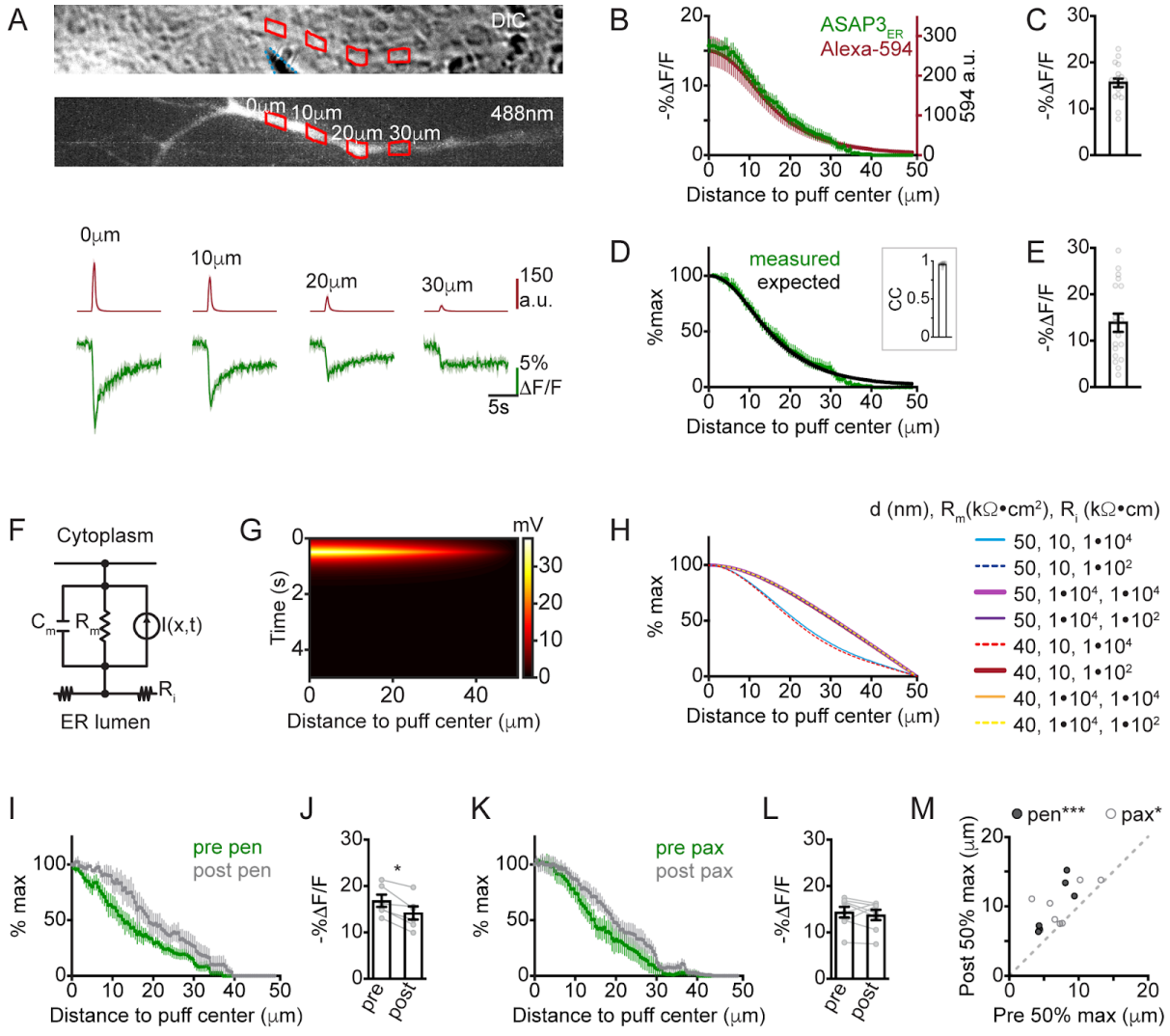
A
DIC
0μm 10μm 20μm 30μm
488nm
0μm
10μm
20μm
30μm
150 a.u.
5% ΔF/F
5s
B
ASAP3ER
Alexa-594
-%ΔF/F
594 a.u.
Distance to puff center (μm)
C
-%ΔF/F
D
measured
expected
%max
CC
Distance to puff center (μm)
E
-%ΔF/F
F
Cytoplasm
Cm
Rm
I(x,t)
Ri
ER lumen
G
mV
Time (s)
Distance to puff center (μm)
H
d (nm), Rm(kΩ•cm2), Ri (kΩ•cm)
50, 10, 1•10^4
50, 10, 1•10^2
50, 1•10^4, 1•10^4
50, 1•10^4, 1•10^2
40, 10, 1•10^4
40, 10, 1•10^2
40, 1•10^4, 1•10^4
40, 1•10^4, 1•10^2
% max
Distance to puff center (μm)
I
pre pen
post pen
% max
Distance to puff center (μm)
J
-%ΔF/F
pre
post
K
pre pax
post pax
% max
Distance to puff center (μm)
L
-%ΔF/F
pre
post
M
pen***
pax*
Post 50% max (μm)
Pre 50% max (μm)

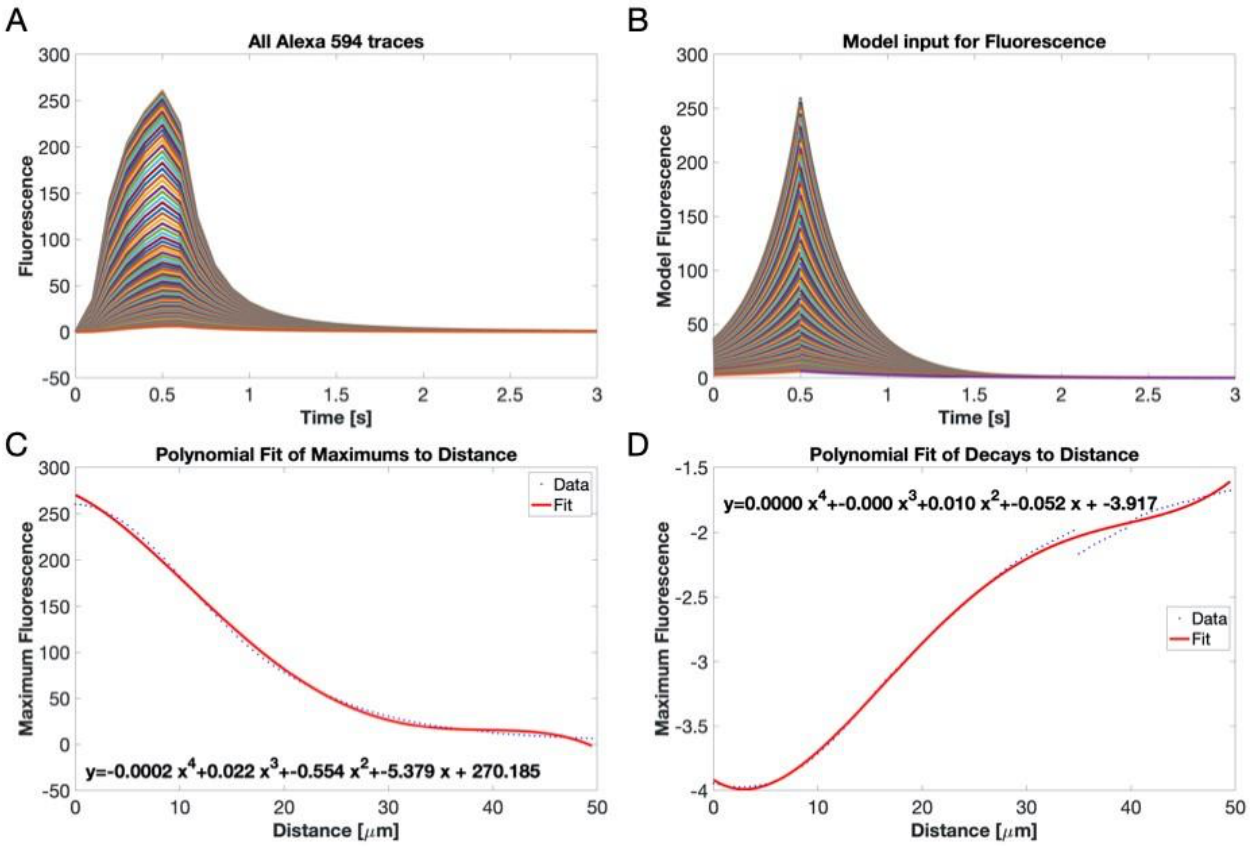

Figure 2.12 Model fitting of injected current over time and distance.

(**A**) Experimental temporal dynamics of Alexa-594 recorded at 0.5 μm intervals along the ER. (**B**) The model input for I(x,t) which mimics the experimental Alexa Fluor 594 maximums and decay dynamics. (**C**) Polynomial fit of the maximum values of the Alexa temporal traces over distance. R^2 value of 0.998. (**D**) Polynomial fit of the decay constants of the Alexa temporal traces over distance. R^2 value of 0.998.

Table 2.1 Parameter values for model

Parameter	Units	Definition	Parameter set 1 (Original)	Parameter set 2 (Monai)	Parameter set 3 (Roth)	Parameter set 4 (Major)
Cm	$\frac{\mu F}{cm^2}$	Specific membrane capacitance	1	1.5	0.77	0.75
Rm	$k\Omega\ cm^2$	Specific membrane resistance	10	30	122	160
Ri	$\Omega\ cm$	Specific intracellular resistance	100	200	115	255
β	$\frac{mV}{\mu m\ \Omega}$ or $\frac{mA}{\mu m}$	Injection current scaling	7.6044×10^{-14}	3.7501×10^{-14}	6.1981×10^{-14}	2.8126×10^{-14}

Original: (Bekkers 2013; Omori et al. 2006)

Monai: (Monai et al. 2010)

Roth: (Roth and Häusser 2001)

Major: (Major et al. 1994).

Table 2.2 Key Resources table

REAGENT or RESOURCE	SOURCE	IDENTIFIER
Antibodies		
Chicken polyclonal anti-GFP	ThermoFisher Scientific	Cat# A10262; RRID: AB_2534023
Rabbit polyclonal anti-GOLGA2	Proteinetech	Cat# 11308-1-AP; RRID: AB_2115327
Rabbit polyclonal anti-TOMM20	Proteinetech	Cat# 11802-1-AP; RRID: AB_2207530
Goat anti-Chicken AlexaFluor 647	ThermoFisher Scientific	Cat# A-21449; RRID: AB_2535866
Goat anti-Chicken AlexaFluor 488	ThermoFisher Scientific	Cat# A-11039; RRID: AB_2534096
Goat anti-Rabbit AlexaFluor 647	ThermoFisher Scientific	Cat#A-21244; RRID: AB_2535812
Bacterial and virus strains		
E. coli: JM109	Promega	L2005
Chemicals, peptides, and recombinant proteins		
Picrotoxin (PTX)	Tocris Bioscience	1128
2-Methyl-6-(phenylethynyl)pyridine hydrochloride (MPEP)	Tocris Bioscience	1212
7-(Hydroxyimino)cyclopropa[b]chromen-1a-carboxylate ethyl ester (CPCCOEt)	Tocris Bioscience	1028
Ryanodine (Ry)	Tocris Bioscience	1329
(RS)-3,5-Dihydroxyphenylglycine (DHPG)	Tocris Bioscience	0342
3,7-Dihydro-1,3,7-trimethyl-1H-purine-2,6-dione (Caffeine)	Tocris Bioscience	2793

Table 2.2 Key Resources table, continued

REAGENT or RESOURCE	SOURCE	IDENTIFIER
Chemicals, peptides, and recombinant proteins		
Tetrodotoxin Citrate (TTX)	Tocris Bioscience	1069
Biocytin AlexaFluor594, sodium salt (AlexaFluor594)	Molecular Probes	A12922
Trypan Blue Stain	Gibco	15250-061
Deposited data		
Original MATLAB code for image analysis	GitHub	
Original MATLAB code for computational model	GitHub	
Experimental models: Cell lines		
Human: HEK293T	ATCC	CRL-3216; RRID:CVCL_0063
Experimental models: Organisms/strains		
Rattus norvegicus: Sprague Dawley	Envigo	240F
Oligonucleotides		
Primer: pCAG-WT Forward: CGCTAGCCGCCACCATGGA	This paper	N/A
Primer: pCAG-WT Reverse: AAGCTTTCATTAGGTTACCACTTCAAGTTGTTTCTTCTGTG	This paper	N/A
Primer: pCAG-MRRR Forward: CGCTAGCCGCCACCATGAGGAGGAGGATGGAGACGACTGTGAGGTATGAAC	This paper	N/A

Table 2.2 Key Resources table, continued

REAGENT or RESOURCE	SOURCE	IDENTIFIER
Oligonucleotides		
Primer: pCAG-KKAA Reverse: CAAGCTTTTACGCCGCCTTCTTGGTTACCACTTCAAGTTGTTTCTTCTGTG	This paper	N/A
Primer: pCAG-KKRR Reverse: CAAGCTTTCATTACCTCCTCTTCTTGGTTACCACTTCAAGTTGTTTCTTCTGTG	This paper	N/A
Primer: pCAG-KKSS Reverse: CAAGCTTTCATTAAGAAGACTTCTTGGTTACCACTTCAAGTTGTTTCTTCTGTG	This paper	N/A
Primer: hSyn Forward: CGTCGACCGCCACCATGGAGACGACT	This paper	N/A
Primer: hSyn Reverse: CCGAGCTCGGTACCAAGCTT	This paper	N/A
Recombinant DNA		
Plasmid: pCAG-backbone	DOI: 10.1038/nmeth.2171	Addgene 40257; RRID:Addgene_40257
Plasmid: Puro-CAG-ASAP3	DOI: 10.1016/j.cell.2019.11.004	N/A
Plasmid: hSyn-ASAP3	DOI: 10.1016/j.cell.2019.11.004	Addgene 132331; RRID:Addgene_132331
Plasmid: Puro-CAG-ASAP3Kv (pCAG-ASAP3$_{PM}$)	DOI: 10.1016/j.cell.2019.11.004	N/A
Plasmid: pAAV-hSyn-ASAP3Kv-WPRE (hSyn-ASAP3$_{PM}$)	DOI: 10.1016/j.cell.2019.11.004	Addgene 132332; RRID:Addgene_132332

Table 2.2 Key Resources table, continued

REAGENT or RESOURCE	SOURCE	IDENTIFIER
Recombinant DNA		
Plasmid: Puro-CAG-ASAP1-NCP (pCAG-NCP-ASAP)	DOI: 10.7554/eLife.25690	N/A
Plasmid: CMV- tdTomato-ER-3 (CMV-tdT-ER)	Addgene	Addgene 58097; RRID:Addgene_58097
pMH4-SYN-EGFP-ER	DOI: 10.1073/pnas.0905110106	Addgene 22285; RRID:Addgene_22285
Puro-CAG-ASAP3-KKAA (pCAG-ASAP3$_{ER}$)	This paper	N/A
pAAV-hSyn-ASAP3-KKAA-WPRE (hSyn-ASAP3$_{ER}$)	This paper	N/A
Puro-CAG-ASAP3-KKRR	This paper	N/A
Puro-CAG-ASAP3-KKSS	This paper	N/A
Puro-CAG-MRRR-ASAP3	This paper	N/A
Puro-CAG-NCP-ASAP$_{ER}$	This paper	N/A
Software and algorithms		
MATLAB (R2009b)	Mathworks Inc	https://www.mathworks.com/
ScanImage	Pologruto et al., 2003	http://scanimage.vidriotechnologies.com/display/SIH/ScanImage+Home
Igor Pro	WaveMetrics	https://www.wavemetrics.com/
Fiji	Schindelin et al., 2012	RRID: SCR_002285; https://fiji.sc/

Table 2.2 Key Resources table, continued

REAGENT or RESOURCE	SOURCE	IDENTIFIER
Software and algorithms		
ImageJ	Schindelin et al., 2012	RRID: SCR_000415; https://imagej.nih.gov/ij/
Illustrator CC	Adobe Systems Inc.	https://www.adobe.com/products/illustrator.html
Prism	GraphPad Inc.	https://www.graphpad.com/scientific-software/prism/
Other		
PDL coated German coverslips	Neuvitro Corporation	GG-12-PDL-Ulaval
DAPI Fluoromount-G®	SouthernBiotech	Cat# 0100-20

Acknowledgements:

We thank Brittney Trinh for technical contributions, Michael Lin for the kind gift of ASAP3 and Dr. St-Pierre for the kind gift of NCP-ASAP1. We also thank David Keinfeld (UC San Diego), Massimo Scanziani (UC San Francisco), and members of the Bloodgood lab for ongoing discussion and careful reading of the manuscript. This work was supported by a National Defense Science and Engineering Graduate (NDSEG) Fellowship to M.K.B., Air Force Office of Scientific Research FA9550-18-1-0051 to P.R, NIH NIBIB T32 EB 9380-8 to E.P.C., and NIH NINDS 1DP2NS097029 and B.L.B.

Chapter 2 is material appearing in E.P. Campbell, A.A. Abushawish, M.K. Bell, M. Haryono, P. Rangamani, B.L. Bloodgood. Electrical signals in neuronal ER: large, linear, and spatially restricted. In revision. The dissertation author was the primary investigator and author of this paper.

Author Contributions:

Conceptualization: E.P.C. and B.L.B.; Methodology: E.P.C., M.K.B., P.R., and B.L.B.; Formal Analysis: E.P.C., A.A.A.; Investigation: E.P.C., A.A.A., M.H.; Resources: P.R., B.L.B.; Writing Original draft: E.P.C., M.K.B., P.R., B.L.B.; Visualization: E.P.C., M.K.B., P.R., B.L.B.; Supervision: E.P.C., P.R., B.L.B.; Funding Acquisition: P.R., B.L.B.

References:

Ahern, G. P., & Laver, D. R. (1998). ATP inhibition and rectification of a Ca2+-activated anion channel in sarcoplasmic reticulum of skeletal muscle. *Biophysical Journal*, *74*(5), 2335–2351.

Andersson, H., Kappeler, F., & Hauri, H. P. (1999). Protein targeting to endoplasmic reticulum by dilysine signals involves direct retention in addition to retrieval. *The Journal of Biological Chemistry*, *274*(21), 15080–15084.

Ashrafpour, M., Eliassi, A., Sauve, R., Sepehri, H., & Saghiri, R. (2008). ATP regulation of a large conductance voltage-gated cation channel in rough endoplasmic reticulum of rat hepatocytes. *Archives of Biochemistry and Biophysics*, *471*(1), 50–56.

Barlowe, C. (1997). Coupled ER to Golgi transport reconstituted with purified cytosolic proteins. *The Journal of Cell Biology*, *139*(5), 1097–1108.

Bekkers, J. (2013). Resistivity, Axial. In D. Jaeger & R. Jung (Eds.), *Encyclopedia of Computational Neuroscience* (pp. 1–2). Springer New York.

Broadwell, R. D., & Cataldo, A. M. (1983). The neuronal endoplasmic reticulum: its cytochemistry and contribution to the endomembrane system. I. Cell bodies and dendrites. *The Journal of Histochemistry and Cytochemistry: Official Journal of the Histochemistry Society*, *31*(9), 1077–1088.

Buyse, G., Trouet, D., Voets, T., Missiaen, L., Droogmans, G., Nilius, B., & Eggermont, J. (1998). Evidence for the intracellular location of chloride channel (ClC)-type proteins: co-localization of ClC-6a and ClC-6c with the sarco/endoplasmic-reticulum Ca2+ pump SERCA2b. *Biochemical Journal*, *330 (Pt 2)*, 1015–1021.

Casey, J. R., Grinstein, S., & Orlowski, J. (2010). Sensors and regulators of intracellular pH. *Nature Reviews. Molecular Cell Biology*, *11*(1), 50–61.

Chamberland, S., Yang, H. H., Pan, M. M., Evans, S. W., Guan, S., Chavarha, M., Yang, Y., Salesse, C., Wu, H., Wu, J. C., Clandinin, T. R., Toth, K., Lin, M. Z., & St-Pierre, F. (2017). Fast two-photon imaging of subcellular voltage dynamics in neuronal tissue with genetically encoded indicators. *eLife*, *6*. https://doi.org/10.7554/eLife.25690

Chen-Engerer, H.-J., Hartmann, J., Karl, R. M., Yang, J., Feske, S., & Konnerth, A. (2019). Two types of functionally distinct Ca2+ stores in hippocampal neurons. *Nature Communications*, *10*(1), 3223.

Cornejo, V. H., Ofer, N., & Yuste, R. (2021). Voltage compartmentalization in dendritic spines in vivo. *Science*, eabg0501.

Cui-Wang, T., Hanus, C., Cui, T., Helton, T., Bourne, J., Watson, D., Harris, K. M., & Ehlers, M. D. (2012). Local zones of endoplasmic reticulum complexity confine cargo in neuronal dendrites. *Cell*, *148*(1-2), 309–321.

Daigle, T. L., Madisen, L., Hage, T. A., Valley, M. T., Knoblich, U., Larsen, R. S., Takeno, M. M., Huang, L., Gu, H., Larsen, R., Mills, M., Bosma-Moody, A., Siverts, L. A., Walker, M., Graybuck, L. T.,

Yao, Z., Fong, O., Nguyen, T. N., Garren, E., Lenz G. H., Chavarha M., Pendergraft J., Harrington J., Hirokawa K. E., Harris J. A., Nicovich P. R., McGraw M. J., Ollerenshaw D. R., Smith K. A., Baker C. A., Ting J. T., Sunkin S. M., Lecoq J., Lin M. Z., Boyden E. S., Murphy G. J., da Costa N. M., Waters J., Li L., Tasic B., Zeng, H. (2018). A Suite of Transgenic Driver and Reporter Mouse Lines with Enhanced Brain-Cell-Type Targeting and Functionality. *Cell*, *174*(2), 465–480.e22.

Dayel, M. J., Hom, E. F., & Verkman, A. S. (1999). Diffusion of green fluorescent protein in the aqueous-phase lumen of endoplasmic reticulum. *Biophysical Journal*, *76*(5), 2843–2851.

Dogic, D., Dubois, A., de Chassey, B., Lefkir, Y., & Letourneur, F. (2001). ERGIC-53 KKAA signal mediates endoplasmic reticulum retrieval in yeast. *European Journal of Cell Biology*, *80*(2), 151–155.

Duncan, R. R., Westwood, P. K., Boyd, A., & Ashley, R. H. (1997). Rat brain p64H1, expression of a new member of the p64 chloride channel protein family in endoplasmic reticulum. *The Journal of Biological Chemistry*, *272*(38), 23880–23886.

Fitzpatrick, J. S., Hagenston, A. M., Hertle, D. N., Gipson, K. E., Bertetto-D'Angelo, L., & Yeckel, M. F. (2009). Inositol-1,4,5-trisphosphate receptor-mediated Ca2+ waves in pyramidal neuron dendrites propagate through hot spots and cold spots. *The Journal of Physiology*, *587*(Pt 7), 1439–1459.

Gao, C., Cai, Y., Wang, Y., Kang, B.-H., Aniento, F., Robinson, D. G., & Jiang, L. (2014). Retention mechanisms for ER and Golgi membrane proteins. *Trends in Plant Science*, *19*(8), 508–515.

Gaynor, E. C., te Heesen, S., Graham, T. R., Aebi, M., & Emr, S. D. (1994). Signal-mediated retrieval of a membrane protein from the Golgi to the ER in yeast. *The Journal of Cell Biology*, *127*(3), 653–665.

Gillespie, D., Chen, H., & Fill, M. (2012). Is ryanodine receptor a calcium or magnesium channel? Roles of K+ and Mg2+ during Ca2+ release. *Cell Calcium*, *51*(6), 427–433.

Gillespie, D., & Fill, M. (2009). Intracellular calcium release channels mediate their own countercurrent: The ryanodine receptor case study. *Biophysical Journal*, *96*(3), 114a.

GOSLIN, & K. (1998). Rat hippocampal neurons in low density culture. *Culturing Nerve Cells*. https://ci.nii.ac.jp/naid/10019273197/

Holbro, N., Grunditz, A., & Oertner, T. G. (2009). Differential distribution of endoplasmic reticulum controls metabotropic signaling and plasticity at hippocampal synapses. *Proceedings of the National Academy of Sciences of the United States of America*, *106*(35), 15055–15060.

Kawano, S., Nakamura, F., Tanaka, T., & Hiraoka, M. (1992). Cardiac sarcoplasmic reticulum chloride channels regulated by protein kinase A. *Circulation Research*, *71*(3), 585–589.

Kim, J. H., Johannes, L., Goud, B., Antony, C., Lingwood, C. A., Daneman, R., & Grinstein, S. (1998). Noninvasive measurement of the pH of the endoplasmic reticulum at rest and during calcium release. *Proceedings of the National Academy of Sciences of the United States of America*, *95*(6), 2997–3002.

Klier, P. E. Z., Martin, J. G., & Miller, E. W. (2021). Imaging Reversible Mitochondrial Membrane

Potential Dynamics with a Masked Rhodamine Voltage Reporter. *Journal of the American Chemical Society*, *143*(11), 4095–4099.

Kneen, M., Farinas, J., Li, Y., & Verkman, A. S. (1998). Green fluorescent protein as a noninvasive intracellular pH indicator. *Biophysical Journal*, *74*(3), 1591–1599.

Kong, H., Jones, P. P., Koop, A., Zhang, L., Duff, H. J., & Chen, S. R. W. (2008). Caffeine induces Ca2+ release by reducing the threshold for luminal Ca2+ activation of the ryanodine receptor. *Biochemical Journal*, *414*(3), 441–452.

Kulawiak, B., Kudin, A. P., Szewczyk, A., & Kunz, W. S. (2008). BK channel openers inhibit ROS production of isolated rat brain mitochondria. *Experimental Neurology*, *212*(2), 543–547.

Kuum, M., Veksler, V., Liiv, J., Ventura-Clapier, R., & Kaasik, A. (2012). Endoplasmic reticulum potassium-hydrogen exchanger and small conductance calcium-activated potassium channel activities are essential for ER calcium uptake in neurons and cardiomyocytes. *Journal of Cell Science*, *125*(Pt 3), 625–633.

Lam, A. J., St-Pierre, F., Gong, Y., Marshall, J. D., Cranfill, P. J., Baird, M. A., McKeown, M. R., Wiedenmann, J., Davidson, M. W., Schnitzer, M. J., Tsien, R. Y., & Lin, M. Z. (2012). Improving FRET dynamic range with bright green and red fluorescent proteins. *Nature Methods*, *9*(10), 1005–1012.

Li, B., Jie, W., Huang, L., Wei, P., Li, S., Luo, Z., Friedman, A. K., Meredith, A. L., Han, M.-H., Zhu, X.-H., & Gao, T.-M. (2014). Nuclear BK channels regulate gene expression via the control of nuclear calcium signaling. *Nature Neuroscience*, *17*(8), 1055–1063.

Losonczy, A., & Magee, J. C. (2006). Integrative properties of radial oblique dendrites in hippocampal CA1 pyramidal neurons. *Neuron*, *50*(2), 291–307.

Major, G., Larkman, A. U., Jonas, P., Sakmann, B., & Jack, J. J. (1994). Detailed passive cable models of whole-cell recorded CA3 pyramidal neurons in rat hippocampal slices. *The Journal of Neuroscience: The Official Journal of the Society for Neuroscience*, *14*(8), 4613–4638.

Martone, M. E., Zhang, Y., Simpliciano, V. M., Carragher, B. O., & Ellisman, M. H. (1993). Three-dimensional visualization of the smooth endoplasmic reticulum in Purkinje cell dendrites. *The Journal of Neuroscience: The Official Journal of the Society for Neuroscience*, *13*(11), 4636–4646.

Matamala, E., Castillo, C., Vivar, J. P., Rojas, P. A., & Brauchi, S. E. (2021). Imaging the electrical activity of organelles in living cells. *Communications Biology*, *4*(1), 389.

Miller, C. (1978). Voltage-gated cation conductance channel from fragmented sarcoplasmic reticulum: steady-state electrical properties. *The Journal of Membrane Biology*, *40*(1), 1–23.

Monai, H., Omori, T., Okada, M., Inoue, M., Miyakawa, H., & Aonishi, T. (2010). An analytic solution of the cable equation predicts frequency preference of a passive shunt-end cylindrical cable in response to extracellular oscillating electric fields. *Biophysical Journal*, *98*(4), 524–533.

Nixon-Abell, J., Obara, C. J., Weigel, A. V., Li, D., Legant, W. R., Xu, C. S., Pasolli, H. A., Harvey, K., Hess, H. F., Betzig, E., Blackstone, C., & Lippincott-Schwartz, J. (2016). Increased spatiotemporal resolution reveals highly dynamic dense tubular matrices in the peripheral ER. *Science*, *354*(6311).

https://doi.org/10.1126/science.aaf3928

Oetliker, H. (1989). Energetical considerations related to calcium release from the sarcoplasmic reticulum in skeletal muscle. *Biomedica Biochimica Acta*, *48*(5-6), S313–S318.

Omori, T., Aonishi, T., Miyakawa, H., Inoue, M., & Okada, M. (2006). Estimated distribution of specific membrane resistance in hippocampal CA1 pyramidal neuron. *Brain Research*, *1125*(1), 199–208.

Perkins, K. L. (2006). Cell-attached voltage-clamp and current-clamp recording and stimulation techniques in brain slices. *Journal of Neuroscience Methods*, *154*(1-2), 1–18.

Pologruto, T. A., Sabatini, B. L., & Svoboda, K. (2003). ScanImage: flexible software for operating laser scanning microscopes. *Biomedical Engineering Online*, *2*, 13.

Pozzo-Miller, L. D., Pivovarova, N. B., Leapman, R. D., Buchanan, R. A., Reese, T. S., & Andrews, S. B. (1997). Activity-dependent calcium sequestration in dendrites of hippocampal neurons in brain slices. *The Journal of Neuroscience: The Official Journal of the Society for Neuroscience*, *17*(22), 8729–8738.

Reiner, A., & Levitz, J. (2018). Glutamatergic Signaling in the Central Nervous System: Ionotropic and Metabotropic Receptors in Concert. *Neuron*, *98*(6), 1080–1098.

Rinzel, J., & Rall, W. (1974). Transient response in a dendritic neuron model for current injected at one branch. *Biophysical Journal*, *14*(10), 759–790.

Ross, W. N. (2012). Understanding calcium waves and sparks in central neurons. *Nature Reviews. Neuroscience*, *13*(3), 157–168.

Roth, A., & Häusser, M. (2001). Compartmental models of rat cerebellar Purkinje cells based on simultaneous somatic and dendritic patch-clamp recordings. *The Journal of Physiology*, *535*(Pt 2), 445–472.

Saminathan, A., Devany, J., Veetil, A. T., Suresh, B., Pillai, K. S., Schwake, M., & Krishnan, Y. (2021). A DNA-based voltmeter for organelles. *Nature Nanotechnology*, *16*(1), 96–103.

Sanchez, C., Berthier, C., Allard, B., Perrot, J., Bouvard, C., Tsutsui, H., Okamura, Y., & Jacquemond, V. (2018). Tracking the sarcoplasmic reticulum membrane voltage in muscle with a FRET biosensor. *The Journal of General Physiology*, *150*(8), 1163–1177.

Schoepp, D. D., Goldsworthy, J., Johnson, B. G., Salhoff, C. R., & Baker, S. R. (1994). 3,5-dihydroxyphenylglycine is a highly selective agonist for phosphoinositide-linked metabotropic glutamate receptors in the rat hippocampus. *Journal of Neurochemistry*, *63*(2), 769–772.

Schoepp, D. D., Jane, D. E., & Monn, J. A. (1999). Pharmacological agents acting at subtypes of metabotropic glutamate receptors. *Neuropharmacology*, *38*(10), 1431–1476.

Schutze, M. P., Peterson, P. A., & Jackson, M. R. (1994). An N-terminal double-arginine motif maintains type II membrane proteins in the endoplasmic reticulum. *The EMBO Journal*, *13*(7), 1696–1705.

Selezneva, A., Yoshida, M., Gibb, A., & Willis, D. (2021). Nuclear BK channels regulate CREB phosphorylation in RAW264.7 macrophages. *Pharmacological Reports: PR*, *73*(3), 881–890.

Sepehri Rad, M., Cohen, L. B., Braubach, O., & Baker, B. J. (2018). Monitoring voltage fluctuations of intracellular membranes. *Scientific Reports*, *8*(1), 6911.

Shemer, I., Brinne, B., Tegnér, J., & Grillner, S. (2008). Electrotonic signals along intracellular membranes may interconnect dendritic spines and nucleus. *PLoS Computational Biology*, *4*(3), e1000036.

Shin, J., Dunbrack, R. L., Jr, Lee, S., & Strominger, J. L. (1991). Signals for retention of transmembrane proteins in the endoplasmic reticulum studied with CD4 truncation mutants. *Proceedings of the National Academy of Sciences of the United States of America*, *88*(5), 1918–1922.

Shruti, S., Urban-Ciecko, J., Fitzpatrick, J. A., Brenner, R., Bruchez, M. P., & Barth, A. L. (2012). The brain-specific Beta4 subunit downregulates BK channel cell surface expression. *PloS One*, *7*(3), e33429.

Somlyo, A. V., Gonzalez-Serratos, H. G., Shuman, H., McClellan, G., & Somlyo, A. P. (1981). Calcium release and ionic changes in the sarcoplasmic reticulum of tetanized muscle: an electron-probe study. *The Journal of Cell Biology*, *90*(3), 577–594.

Spacek, J., & Harris, K. M. (1997). Three-dimensional organization of smooth endoplasmic reticulum in hippocampal CA1 dendrites and dendritic spines of the immature and mature rat. *The Journal of Neuroscience: The Official Journal of the Society for Neuroscience*, *17*(1), 190–203.

Sugiyama, H., Ito, I., & Hirono, C. (1987). A new type of glutamate receptor linked to inositol phospholipid metabolism. *Nature*, *325*(6104), 531–533.

Takei, K., Stukenbrok, H., Metcalf, A., Mignery, G. A., Südhof, T. C., Volpe, P., & De Camilli, P. (1992). Ca2+ stores in Purkinje neurons: endoplasmic reticulum subcompartments demonstrated by the heterogeneous distribution of the InsP3 receptor, Ca(2+)-ATPase, and calsequestrin. *The Journal of Neuroscience: The Official Journal of the Society for Neuroscience*, *12*(2), 489–505.

Tanifuji, M., Sokabe, M., & Kasai, M. (1987). An anion channel of sarcoplasmic reticulum incorporated into planar lipid bilayers: single-channel behavior and conductance properties. *The Journal of Membrane Biology*, *99*(2), 103–111.

Teasdale, R. D., & Jackson, M. R. (1996). Signal-mediated sorting of membrane proteins between the endoplasmic reticulum and the golgi apparatus. *Annual Review of Cell and Developmental Biology*, *12*, 27–54.

Terasaki, M., Slater, N. T., Fein, A., Schmidek, A., & Reese, T. S. (1994). Continuous network of endoplasmic reticulum in cerebellar Purkinje neurons. *Proceedings of the National Academy of Sciences of the United States of America*, *91*(16), 7510–7514.

Thillaiappan, N. B., Chavda, A. P., Tovey, S. C., Prole, D. L., & Taylor, C. W. (2017). Ca2+ signals initiate at immobile IP3 receptors adjacent to ER-plasma membrane junctions. *Nature Communications*, *8*(1), 1505.

Tsukita, S., & Ishikawa, H. (1976). THREE-DIMENSIONAL DISTRIBUTIONOF SMOOTH ENDOPLASMIC RETICULUM IN MYELINATED AXONS. *Journal of Electron Microscopy*, *25*(3), 141–149.

Villette, V., Chavarha, M., Dimov, I. K., Bradley, J., Pradhan, L., Mathieu, B., Evans, S. W., Chamberland,

S., Shi, D., Yang, R., Kim, B. B., Ayon, A., Jalil, A., St-Pierre, F., Schnitzer, M. J., Bi, G., Toth, K., Ding, J., Dieudonné, S., & Lin, M. Z. (2019). Ultrafast Two-Photon Imaging of a High-Gain Voltage Indicator in Awake Behaving Mice. *Cell*, *179*(7), 1590–1608.e23.

Walton, P. D., Airey, J. A., Sutko, J. L., Beck, C. F., Mignery, G. A., Südhof, T. C., Deerinck, T. J., & Ellisman, M. H. (1991). Ryanodine and inositol trisphosphate receptors coexist in avian cerebellar Purkinje neurons. *The Journal of Cell Biology*, *113*(5), 1145–1157.

Wang, X.-H., Su, M., Gao, F., Xie, W., Zeng, Y., Li, D.-L., Liu, X.-L., Zhao, H., Qin, L., Li, F., Liu, Q., Clarke, O. B., Lam, S. M., Shui, G.-H., Hendrickson, W. A., & Chen, Y.-H. (2019). Structural basis for activity of TRIC counter-ion channels in calcium release. *Proceedings of the National Academy of Sciences of the United States of America*, *116*(10), 4238–4243.

Weigel, A. V., Chang, C.-L., Shtengel, G., Xu, C. S., Hoffman, D. P., Freeman, M., Iyer, N., Aaron, J., Khuon, S., Bogovic, J., Qiu, W., Hess, H. F., & Lippincott-Schwartz, J. (2021). ER-to-Golgi protein delivery through an interwoven, tubular network extending from ER. *Cell*, *184*(9), 2412–2429.e16.

Wu, Y., Whiteus, C., Xu, C. S., Hayworth, K. J., Weinberg, R. J., Hess, H. F., & De Camilli, P. (2017). Contacts between the endoplasmic reticulum and other membranes in neurons. *Proceedings of the National Academy of Sciences of the United States of America*, *114*(24), E4859–E4867.

Yazawa, M., Ferrante, C., Feng, J., Mio, K., Ogura, T., Zhang, M., Lin, P.-H., Pan, Z., Komazaki, S., Kato, K., Nishi, M., Zhao, X., Weisleder, N., Sato, C., Ma, J., & Takeshima, H. (2007). TRIC channels are essential for Ca2+ handling in intracellular stores. *Nature*, *448*(7149), 78–82.

Yihe, L., & Timofeeva, Y. (2020). Exact solutions to cable equations in branching neurons with tapering dendrites. *Journal of Mathematical Neuroscience*, *10*(1), 1.

Zorova, L. D., Popkov, V. A., Plotnikov, E. Y., Silachev, D. N., Pevzner, I. B., Jankauskas, S. S., Babenko, V. A., Zorov, S. D., Balakireva, A. V., Juhaszova, M., Sollott, S. J., & Zorov, D. B. (2018). Mitochondrial membrane potential. *Analytical Biochemistry*, *552*, 50–59.

Chapter III: What Comes Next?

The primary efforts of my doctoral studies presented in Chapter II have elucidated membrane potential dynamics of the ER in neurons. This has included developing and validating a novel approach for targeting a GEVI to the ER membrane, identifying stimuli that drive changes in ER membrane potential, and providing initial descriptions of the ER's electrical properties in neurons. Here in Chapter III, I will discuss the implications of these findings as well as how they advance understanding of ER biology and neuronal signaling.

Targeting ASAP3 with an -KKAA ER retention signal provided multiple advantages:

For many decades, the membrane potential of the ER has been assumed to be fixed at zero and inert. This assumption has become an established convention, chiefly due to the absence of any direct description of ER membrane potential and a lack of methodology capable of measuring electrical signals that are specific to the ER membrane (Oetliker 1982). Even recent attempts to measure ER membrane potential have been unable to provided definitive descriptions, due to the inconsistency of their measurements and the uncertainty arising from their techniques (Sepehri Rad et al. 2018; Sanchez et al. 2018; Matamala et al. 2021). The difficulty of developing techniques to reliably measure the membrane potential of the ER is understandable in light of the ER's rapidly dynamic and nanometer-scale structure (C. Lee and Chen 1988; Nixon-Abell et al. 2016; Valm et al. 2017; Wu et al. 2017; Perez-Alvarez et al. 2020). The fluctuating morphology and small diameter of ER tubules preclude electrode-based recordings, as well as the ability of light microscopy techniques to distinguish ER membrane from other organelles. Such technical challenges have set a barrier to unambiguously measuring electrical activity of the ER and to understanding how membrane potential participates in larger ER biology.

To circumvent the technical barriers of measuring ER-specific voltage, I have targeted ASAP3 to the ER membrane using a highly selective and endogenous ER retention peptide sequence for transmembrane proteins, a carboxy terminus -KKAA (Figure 2.2). The functionality of this peptide signal is largely conserved from yeast to mammals, demonstrating that its mechanism of subcellular targeting is essential and tightly regulated (Dogic et al. 2001; Townsley and Pelham 1994). Integral membrane proteins that have the -KKAA sequence are directly retained in the ER (Andersson, Kappeler, and Hauri 1999) and maintain their orientation with the -KKAA signal in the cytoplasm (Shin et al. 1991). By leveraging this endogenous protein targeting, the location and orientation of $ASAP3_{ER}$ was predictable, such that its cpGFP was in the ER lumen and both of its termini remained in the cytoplasm. This allowed me to collect photons from large cellular volumes with confidence that they originated from the ER. Further, $ASAP3_{ER}$'s unambiguous orientation allowed me to distinguish between relative depolarizations and hyperpolarizations of the ER membrane. Although $ASAP3_{ER}$ cannot be used to define the absolute membrane potential, its bright fluorescence during baseline activity suggested that the cytoplasm is negatively charged relative to the ER lumen. Also, changes in $ASAP3_{ER}$ fluorescence provided measurements of kinetics and the dynamic range of the ER membrane potential in neurons. Thus, the strategy of measuring changes in ER membrane potential with $ASAP3_{ER}$, as presented in this dissertation, enables assessment of key biophysical properties of the ER. Further, because of the conserved function of the -KKAA ER-retention signal, I suggest that $ASAP3_{ER}$ may also be broadly applicable to other cellular systems, such as cardiomyocytes where SR membrane potential remains controversial (Oetliker 1989; Sanchez et al. 2018; Gillespie and Fill 2009).

Validating the subcellular location of GEVIs targeted to the ER and avoiding non-voltage based artifacts are critical challenges to optically measuring ER membrane potential (Sepehri Rad et al. 2018; Sanchez et al. 2018; Oetliker 1982). The ER-retention signal based targeting technique that I used, as well as the structure of ASAP3, also provided advantages for validating ER-specific voltage signals. In particular, the difference between the extracellular position of ASAP3's cpGFP while at the PM, and the intraluminal position of $ASAP3_{ER}$'s cpGFP at the ER membrane, allowed me to leverage immunostaining

with and without permeabilization to confirm the intracellular localization of ASAP3$_{ER}$ (Figure 2.3). Furthermore, while GFP fluorescence is sensitive to low pH (Kneen et al. 1998), the lumen of the ER is known to be consistently neutral (Kim et al. 1998; for review see Casey, Grinstein, and Orlowski 2010). Yet, to further confirm the voltage basis for changes in ASAP3$_{ER}$ fluorescence, and to dispel concerns of non-voltage artifacts, comparison with non voltage sensitive fluorophores like NCP-ASAP$_{ER}$ and GFP-ER may be readily assessed. The use of these control fluorophores abrogates pH-related or other artifact-based concerns for interpreting changes in ASAP3$_{ER}$ fluorescence. ASAP3$_{ER}$ therefore provides a means to reliably measure and validate changes in ER membrane potential.

Imaging ASAP3$_{ER}$ elucidated fundamental properties of the ER's membrane potential:

In neurons, ASAP3$_{ER}$ reports modest but ongoing changes in ER membrane potential during spontaneous activity (Figure 2.5-2.6) and substantial, bidirectional changes in response to explicit manipulations of network activity and synaptic transmission (Figure 2.8). In this way, the ER appears similar to the PM and different from organelles like lysosomes and Golgi (Saminathan et al. 2021; Matamala et al. 2021). The magnitudes of changes in ER membrane potential that occur in response to altered network activity also indicate that the ER's dynamic range is large, on par with that of the PM. This opens the possibility that fluctuation in ER membrane potential activate many resident voltage-gated ion channels in the ER, which may occur in concert with or apart from the BK channels that I have tested in my own studies (Figure 2.11). Accordingly, many ion channels of the ER may be gated by voltage, including trimeric intracellular cation channels (Yazawa et al. 2007) or Cl^- intracellular channels (Duncan et al. 1997; Dulhunty et al. 2005; Buyse et al. 1998). Contingent on the equilibrium potentials for the ion species conducted by these channels, this may also serve as the basis for the ER membrane potential's large dynamic range. Timescales over which the ER membrane potential changes, however, are much slower than those observed at the PM and more closely resemble timescales of membrane potential dynamics in

lysosomes and Golgi (Saminathan et al. 2021; Matamala et al. 2021). Thus, the ER membrane system generates unique electrical dynamics that cannot be simply inferred from those observed at the PM or other organelles.

Focally stimulating specific receptors also showed that activation of IP3Rs or RyRs can trigger changes in ER membrane potential that have distinct kinetics. Activation of IP3Rs provided longer lasting depolarizations than those resulting from activation of RyRs, which fits the expected relationship between the different response timescales resulting from stimulation of the G_q signaling transduction pathway versus directly activating ion channels in the ER membrane, respectively (Figure 2.8A-C; Sugiyama, Ito, and Hirono 1987; Schoepp et al. 1994; for review see Reiner and Levitz 2018; Ross 2012). Receptor-mediated depolarization of the ER through the action of group I mGluRs also illuminated a synaptic mechanism for depolarizing the ER during large-scale increases in network activity, such as those induced by PTX stimulation. Indeed, my studies demonstrated that $mGluR_1$s are a principal driver for synaptically depolarizing the ER membrane during PTX application (Figure 2.7L-M). However, the observation that $mGluR_1$s and not $mGluR_5$s drive PTX-induced ER depolarization at the soma was unanticipated (Figure 2.7-K). This supports the notion that $mGluR_1$ and $mGluR_5$ drive different cellular functions and have different subcellular localizations (Mannaioni et al. 2001; Merlin 2002; Purgert et al. 2014). My observations suggest that $mGlu_1$s may be preferentially localized or active on the soma of neurons or in the ER membrane itself.

From focal stimulation of RyRs, I also observed a correlation between the magnitude of electrical responses in the ER membrane and corresponding decay time constants (Figure 2.8Q). This linear relationship was observed from electrical responses recorded across both somatic and dendritic compartments, even though dendritic ER displayed substantially larger and longer lasting responses in membrane potential. The increase in duration with magnitude of electrical responses of the ER may be attributable to local Ca^{2+} induced Ca^{2+} release from RyRs (Fabiato 1983; Bezprozvanny, Watras, and Ehrlich 1991) or possible saturation of ER Ca^{2+} store refilling machinery, which increases the duration of

Ca^{2+} transients in neurons (Hirabayashi et al. 2017). However, even from the largest amplitude depolarizations generated by stimulating RyRs in the ER, I did not observe a steep increase in the rate of $ASAP3_{ER}$ fluorescence changes (Figure 2.8D-M). These data suggest that unlike the PM, the ER membrane does engage active conductances that facilitate superlinear changes in membrane potential (Losonczy and Magee 2006), at least, not to the stimuli that I have assessed in this dissertation.

Despite the observation that ER membrane potential is responsive to stimulation across entire lengths of dendritic branches (Figure 2.10A-C), I detected low correlation between the membrane potential fluctuations of the ER in neighboring regions of dendrite during spontaneous network activity (Figure 2.10D-F). This provided the first indication that although the ER membrane may be highly electrically dynamic, it may also act independently of ER in directly adjoining regions of dendrite. The substantial degree of electrical compartmentalization in the ER became clear from focal application of caffeine, which showed no detectable spread of electrical signals in the ER beyond the direct sites of RyR stimulation (Figure 2.11A-E). These data demonstrated that propagation of electrical activity is highly restricted along the ER membrane, and further experiments showed that active conductance through BK channels was one factor that added to this restriction (Figure 2.11I-M). These findings suggest a compartmentalized model of ER membrane potential, in which electrical propagation is restricted from influencing voltage potential of the ER in adjoining sections of dendrite, and thereby preserving the driving force for Ca^{2+} efflux from ER stores at those locations. Thus, localized changes in ER membrane potential may be one mechanism that is necessary for providing region-specific Ca^{2+} signaling from the ER.

Membrane potential of the ER may be compartmentalized by many mechanisms:

The extreme extent to which electrotonic spread is restricted along the ER membrane (Figure 2.11A-E, I-M) suggests that conductance through BK channels is only one of many features that suppresses electrical propagation; another likely feature is the ER's structure itself. Small diameter ER tubules (often

~50 nm; Nixon-Abell et al. 2016) will inevitably have large axial resistances, which will rapidly attenuate electrical signal propagation (Rall 1962). Also, areas of increased ER complexity, such as those frequently observed at dendritic branch points and at the base of active spines, may have particularly short apparent length constants. In fact, proteins in the ER membrane show restricted mobility at these regions, due to the intricacy of the membrane and its surface area (Cui-Wang et al. 2012). Thus, the sinuous and interwoven ER tubules at these points may similarly dissipate electrical currents. Indeed, the geometry of membrane structures highly influences how electrical signals propagate along them (Rall 1962; Jack and Redman 1971; Rall and Rinzel 1973; Mainen et al. 1996). In this regard, the ER's intricate and heterogeneous morphology may be a primary source of attenuating electrical propagation within it.

In addition to the activity of BK channels, there may also be a variety of active currents that shunt or repolarize the ER membrane (Meissner and McKinley 1982), thereby repressing the spread of depolarizations along it. Many types of ER ion channels have been proposed to supply countercurrent exchange, including voltage-gated K^+ channels (Yazawa et al. 2007; X.-H. Wang et al. 2019), Cl^- channels (Zhu, Yan, and Thornhill 2014; Tanifuji, Sokabe, and Kasai 1987), and even RyRs themselves (Gillespie and Fill 2009; Gillespie, Chen, and Fill 2012). However, if the opening of IP3Rs or RyRs were strictly yoked to counter currents, the ER membrane would be unlikely to generate stimulus-evoked potentials of the magnitude and duration that I observed. An alternative possibility is that the electrical environment of the ER membrane is composed of multiple subdomains that have unique behaviors delineated by specific receptor populations or associations between receptors. If this were the case, origin points or boundaries of electrical compartments in the ER may be defined by subdomains that possess unique ion channels and conductances. The ER is well known to have subdomains with unique ionic currents and receptors, such as contact points with mitochondria (Hirabayashi et al. 2017; K.-S. Lee et al. 2018) or ER-PM contact points where RyRs couple with Kv2.1 channels and LTCCs (Schulien et al. 2016; Vierra et al. 2021). Indeed, my own observation that only one type of group I mGluR depolarizes somatic ER in response to PTX supports this notion of receptor-specific control of ER membrane potential (Figure 2.7L, M). More extensive

descriptions of ER ion channels and advancements in methods for achieving higher spatial resolution in voltage imaging are called for to examine the full extent of these possibilities.

Membrane potential in the ER has many implications for Ca^{2+} signaling:

The importance of ER membrane potential for proper Ca^{2+} signaling is evident from studies that disrupt it by knocking out voltage-gated K^+ channels and report impaired Ca^{2+} release through IP3Rs and RyRs (Yazawa et al. 2007). By a similar mechanism, pharmacological studies have shown that Ca^{2+} activated small-conductance potassium channels are necessary for proper refilling of ER Ca^{2+} stores (Kuum et al. 2012; Kuum, Veksler, and Kaasik 2015). These studies support the conclusions of calculations made from studies in cardiomyocytes, which illustrated that some regulation of ER membrane potential is necessary to account for Ca^{2+} dynamics regulated by the ER. Without regulation of ER membrane potential to relieve the electrical build-up from Ca^{2+} handling by the ER, Ca^{2+} conductance known to be enacted by the ER would be prohibited (Oetliker 1989). The model that my own studies have contributed to understanding the ER's membrane potential is one with highly dynamic voltage fluctuations, which are specific to the receptor activities that generate them, and are compartmentalized to the cellular regions they are generated within. This gives rise to a view of the ER membrane system wherein electrical activity can respond independently to stimuli at each cellular location, as well as be regulated differently across cellular compartments. This model suggests that the ER membrane potential provides local control of the driving force for Ca^{2+} release from the ER, yet suppress the spread of electrical changes into ER at other regions of the cell, where membrane potential may be regulated differently. I put forward that these electrical properties of the ER may be an essential framework for the ER's richly diverse and adaptable Ca^{2+} signaling roles across cellular compartments.

Specialized ER Ca^{2+} signaling has been observed at branch points (Fitzpatrick et al. 2009), at PM-ER junctions (Vierra et al. 2019; Thillaiappan et al. 2017), and in dendritic spines (Perez-Alvarez et al.

2020; Basnayake et al. 2021). It remains to be seen if the ER is imbued with unique electrical properties at dendritic regions like branch points where enriched IP3R population generates Ca^{2+} signaling "hot spots" (Fitzpatrick et al. 2009), or PM-ER junctions where clustered KV2.1, LTCCs, and RyRs generate Ca^{2+} "sparks" (Thillaiappan et al. 2017). Electrical properties of the ER at these regions may be important for preserving the driving force for Ca^{2+} release at critical regions for global Ca^{2+} signaling events, such as branch point hot spots that fuel the propagation of Ca^{2+} waves across dendritic trees (Nakamura et al. 1999; Wild et al. 2019; Larkum et al. 2003). A subset of dendritic spines also contain ER, which can either transiently occupy small less-active dendritic spines or persist at more active synapses (Holbro, Grunditz, and Oertner 2009; Toresson and Grant 2005; Perez-Alvarez et al. 2020), forming large spine apparatus structures (Spacek and Harris 1997). Specialized ER electrical properties, particularly within dendritic compartments like spines, are positioned to shape signaling that is important for functions like preventing runaway excitation (Perez-Alvarez et al. 2020), refilling of ER Ca^{2+} stores (Basnayake et al. 2021; Maneshi et al. 2020), or regulating synaptic plasticity (Holbro, Grunditz, and Oertner 2009).

ER membrane potential may also be important for functions beyond Ca^{2+} signaling:

In this dissertation I have focused heavily on the implications of ER membrane potential to Ca^{2+} signaling of the ER, however, membrane potential dynamics may be vital to a variety of other ER functions as well. For example, mutations in the *Clcc1* gene, which encodes a Cl^- channel of the ER, have been associated with neurodegeneration of granule cells in the cerebellum. The proposed mechanism of cellular pathology from such mutations is an imbalance of Cl^- ions across the ER membrane, which leads to an accumulation of misfolded proteins and an increased sensitivity to ER stress (Jia et al. 2015). These findings suggest that ER membrane potential regulated by Cl^- gradients may be important for proper protein folding and quality control preformed in the ER.

Roles of membrane potential in other organelles may also provide insight into the possible functions of ER membrane potential. For example, lysosomes maintain membrane potentials that are cell type specific, dependent on metabolic state, and may range in magnitude during basal activity from ~40 to ~115 mV (Saminathan et al. 2021). In this way lysosomes and the ER are alike, in that they both maintain large magnitude voltage gradients with a relatively positive charge in the lumen and negative charge in the cytoplasm. Among the many functions ascribed to lysosomal membrane potential, it is proposed to modulate fusion of their membrane structures (X. Wang et al. 2012). This raises the possibility that membrane potential of the ER may similarly regulate fusogenic potential of its membrane structure. Indeed, the fusion, fission, and remodeling of distal ER tubules is highly active (Orso et al. 2009; Espadas et al. 2019; Guo et al. 2018), which provides abundant opportunity for regulation by electrical potential of the ER membrane at these regions. By similar mechanisms, regulation of ER membrane potential may be important for preventing fusion between the ER membrane and the membranes of other organelles at ER contact points. The ER maintains abundant contact points with every other organelle (Valm et al. 2017; H. Wu, Carvalho, and Voeltz 2018), and the ER's membrane potential may be essential for maintaining its proper distance at these close appositions of organellar membranes. Thus, regulation of ER membrane potential may be important for its role at the center of the organelle interactome and therefore many organelle functions within cells.

Further insights to ER membrane potential may come from mitochondria, which highly regulate membrane potential across both their inner and outer membranes (Tedeschi, Mannella, and Bowman 1987; Sorgato, Keller, and Stühmer 1987). Mitochondria are best known for using electrical potential to generate proton motive force during ATP synthesis (Mitchell 1961; Stock, Leslie, and Walker 1999). However, mitochondria also leverage membrane potential to shutte metabolites past their outer membrane, in order to meet their high metabolic demands (Colombini 1979; A. C. Lee et al. 1998). The ER also maintains a high metabolic demand due to functions like protein synthesis and modification, as well as lipid synthesis (Redman and Sabatini 1966; Omura, Siekevitz, and Palade 1967; Dawidowicz 1987). Therefore, like

mitochondria, the ER membrane system may similarly rely on membrane potential to facilitate the import of small molecules and nutrients into its lumen. Clearly, there are many and diverse functions of the ER that may depend on membrane potential.

Concluding perspective:

Using a novel approach to target a voltage indicator specifically to the ER membrane, the work of my doctorate has shown, for the first time, that the ER's membrane potential is highly dynamic in neurons. Changes in ER membrane potential occur across magnitudes of many tens of millivolts and over time scales of hundreds of milliseconds to tens of seconds. These findings demonstrate a departure from the conventional assumption that the ER membrane potential is inert. They also provide a basis for other studies that have suggested that the ER membrane may be highly polarized and change rapidly (Matamala et al. 2021; Sepehri Rad et al. 2018). The method of using $ASAP3_{ER}$ to investigate ER membrane potential that I have presented in this dissertation also provides a reliable approach for studying ER membrane potential in other cell types or during other neuronal functions.

My measurements using $ASAP3_{ER}$ have shown that the ER membrane potential in neurons is bidirectionally responsive to increases or decreases in network activity, and responds with unique kinetics and magnitudes to the specific receptor activities that change it. These findings suggest that multiple receptors and functions contribute to generating ER membrane potential, which opens a wealth of possible avenues for investigating cellular functions pertaining to ER membrane potential dynamics. This is especially the case within neurons, where electrical signaling and cellular function are so intimately linked.

An additional effort of my doctoral studies has been to leverage the direct stimulation of RyRs to describe electrical properties of the ER membrane. Increasing stimulation strength and measuring the spread of electrical responses away from focal simulation of RyRs has illuminated characteristics of

summation and spread of electrical responses in the ER membrane. These studies have noted an absence of facilitatory conductances that might generate superlinear responses, as is known to occur at the PM. My measurements instead describe linear stimulus-response relationships as well as active suppression of electrotonic spread along the ER membrane. These data provide the first definitive descriptions of electrical properties of the ER.

Membrane potential of the ER may have numerous mechanisms of regulation and functional implications across cell types, functions, and signaling modalities. The work of my doctoral thesis has provided a means to further investigate membrane potential of the ER, and has laid a foundation for understanding its role within neurons.

References:

Andersson, H., Kappeler, F., & Hauri, H. P. (1999). Protein targeting to endoplasmic reticulum by dilysine signals involves direct retention in addition to retrieval. *The Journal of Biological Chemistry*, *274*(21), 15080–15084.

Basnayake, K., Mazaud, D., Kushnireva, L., Bemelmans, A., Rouach, N., Korkotian, E., & Holcman, D. (2021). Nanoscale molecular architecture controls calcium diffusion and ER replenishment in dendritic spines. *Science Advances*, *7*(38), eabh1376.

Bezprozvanny, I., Watras, J., & Ehrlich, B. E. (1991). Bell-shaped calcium-response curves of Ins(1,4,5)P3- and calcium-gated channels from endoplasmic reticulum of cerebellum. *Nature*, *351*(6329), 751–754.

Buyse, G., Trouet, D., Voets, T., Missiaen, L., Droogmans, G., Nilius, B., & Eggermont, J. (1998). Evidence for the intracellular location of chloride channel (ClC)-type proteins: co-localization of ClC-6a and ClC-6c with the sarco/endoplasmic-reticulum Ca2+ pump SERCA2b. *Biochemical Journal*, *330 (Pt 2)*, 1015–1021.

Casey, J. R., Grinstein, S., & Orlowski, J. (2010). Sensors and regulators of intracellular pH. *Nature Reviews. Molecular Cell Biology*, *11*(1), 50–61.

Colombini, M. (1979). A candidate for the permeability pathway of the outer mitochondrial membrane. *Nature*, *279*(5714), 643–645.

Cui-Wang, T., Hanus, C., Cui, T., Helton, T., Bourne, J., Watson, D., Harris, K. M., & Ehlers, M. D. (2012). Local zones of endoplasmic reticulum complexity confine cargo in neuronal dendrites. *Cell*, *148*(1-2), 309–321.

Dawidowicz, E. A. (1987). Dynamics of membrane lipid metabolism and turnover. *Annual Review of Biochemistry*, *56*, 43–61.

Dogic, D., Dubois, A., de Chassey, B., Lefkir, Y., & Letourneur, F. (2001). ERGIC-53 KKAA signal mediates endoplasmic reticulum retrieval in yeast. *European Journal of Cell Biology*, *80*(2), 151–155.

Dulhunty, A. F., Pouliquin, P., Coggan, M., Gage, P. W., & Board, P. G. (2005). A recently identified member of the glutathione transferase structural family modifies cardiac RyR2 substate activity, coupled gating and activation by Ca2+ and ATP. *Biochemical Journal*, *390*(Pt 1), 333–343.

Duncan, R. R., Westwood, P. K., Boyd, A., & Ashley, R. H. (1997). Rat brain p64H1, expression of a new member of the p64 chloride channel protein family in endoplasmic reticulum. *The Journal of Biological Chemistry*, *272*(38), 23880–23886.

Espadas, J., Pendin, D., Bocanegra, R., Escalada, A., Misticoni, G., Trevisan, T., Velasco Del Olmo, A., Montagna, A., Bova, S., Ibarra, B., Kuzmin, P. I., Bashkirov, P. V., Shnyrova, A. V., Frolov, V. A., & Daga, A. (2019). Dynamic constriction and fission of endoplasmic reticulum membranes by reticulon. *Nature Communications*, *10*(1), 5327.

Fabiato, A. (1983). Calcium-induced release of calcium from the cardiac sarcoplasmic reticulum. *The American Journal of Physiology*, *245*(1), C1–C14.

Fitzpatrick, J. S., Hagenston, A. M., Hertle, D. N., Gipson, K. E., Bertetto-D'Angelo, L., & Yeckel, M. F. (2009). Inositol-1,4,5-trisphosphate receptor-mediated Ca2+ waves in pyramidal neuron dendrites propagate through hot spots and cold spots. *The Journal of Physiology*, *587*(Pt 7), 1439–1459.

Gillespie, D., Chen, H., & Fill, M. (2012). Is ryanodine receptor a calcium or magnesium channel? Roles of K+ and Mg2+ during Ca2+ release. *Cell Calcium*, *51*(6), 427–433.

Gillespie, D., & Fill, M. (2009). Intracellular calcium release channels mediate their own countercurrent: The ryanodine receptor case study. *Biophysical Journal*, *96*(3), 114a.

Guo, Y., Li, D., Zhang, S., Yang, Y., Liu, J.-J., Wang, X., Liu, C., Milkie, D. E., Moore, R. P., Tulu, U. S., Kiehart, D. P., Hu, J., Lippincott-Schwartz, J., Betzig, E., & Li, D. (2018). Visualizing Intracellular Organelle and Cytoskeletal Interactions at Nanoscale Resolution on Millisecond Timescales. *Cell*, *175*(5), 1430–1442.e17.

Hirabayashi, Y., Kwon, S.-K., Paek, H., Pernice, W. M., Paul, M. A., Lee, J., Erfani, P., Raczkowski, A., Petrey, D. S., Pon, L. A., & Polleux, F. (2017). ER-mitochondria tethering by PDZD8 regulates Ca2+ dynamics in mammalian neurons. *Science*, *358*(6363), 623–630.

Holbro, N., Grunditz, A., & Oertner, T. G. (2009). Differential distribution of endoplasmic reticulum controls metabotropic signaling and plasticity at hippocampal synapses. *Proceedings of the National Academy of Sciences of the United States of America*, *106*(35), 15055–15060.

Jack, J. J., & Redman, S. J. (1971). The propagation of transient potentials in some linear cable structures. *The Journal of Physiology*, *215*(2), 283–320.

Jia, Y., Jucius, T. J., Cook, S. A., & Ackerman, S. L. (2015). Loss of Clcc1 results in ER stress, misfolded protein accumulation, and neurodegeneration. *The Journal of Neuroscience: The Official Journal of the Society for Neuroscience*, *35*(7), 3001–3009.

Kim, J. H., Johannes, L., Goud, B., Antony, C., Lingwood, C. A., Daneman, R., & Grinstein, S. (1998). Noninvasive measurement of the pH of the endoplasmic reticulum at rest and during calcium release. *Proceedings of the National Academy of Sciences of the United States of America*, *95*(6), 2997–3002.

Kneen, M., Farinas, J., Li, Y., & Verkman, A. S. (1998). Green fluorescent protein as a noninvasive intracellular pH indicator. *Biophysical Journal*, *74*(3), 1591–1599.

Kuum, M., Veksler, V., & Kaasik, A. (2015). Potassium fluxes across the endoplasmic reticulum and their role in endoplasmic reticulum calcium homeostasis. *Cell Calcium*, *58*(1), 79–85.

Kuum, M., Veksler, V., Liiv, J., Ventura-Clapier, R., & Kaasik, A. (2012). Endoplasmic reticulum potassium-hydrogen exchanger and small conductance calcium-activated potassium channel activities are essential for ER calcium uptake in neurons and cardiomyocytes. *Journal of Cell Science*, *125*(Pt 3), 625–633.

Larkum, M. E., Watanabe, S., Nakamura, T., Lasser-Ross, N., & Ross, W. N. (2003). Synaptically activated Ca2+ waves in layer 2/3 and layer 5 rat neocortical pyramidal neurons. *The Journal of Physiology*,

549(Pt 2), 471–488.

Lee, A. C., Xu, X., Blachly-Dyson, E., Forte, M., & Colombini, M. (1998). The role of yeast VDAC genes on the permeability of the mitochondrial outer membrane. *The Journal of Membrane Biology*, *161*(2), 173–181.

Lee, C., & Chen, L. B. (1988). Dynamic behavior of endoplasmic reticulum in living cells. *Cell*, *54*(1), 37–46.

Lee, K.-S., Huh, S., Lee, S., Wu, Z., Kim, A.-K., Kang, H.-Y., & Lu, B. (2018). Altered ER-mitochondria contact impacts mitochondria calcium homeostasis and contributes to neurodegeneration in vivo in disease models. *Proceedings of the National Academy of Sciences of the United States of America*, *115*(38), E8844–E8853.

Losonczy, A., & Magee, J. C. (2006). Integrative properties of radial oblique dendrites in hippocampal CA1 pyramidal neurons. *Neuron*, *50*(2), 291–307.

Mainen, Z. F., Carnevale, N. T., Zador, A. M., Claiborne, B. J., & Brown, T. H. (1996). Electrotonic architecture of hippocampal CA1 pyramidal neurons based on three-dimensional reconstructions. *Journal of Neurophysiology*, *76*(3), 1904–1923.

Maneshi, M. M., Toth, A. B., Ishii, T., Hori, K., Tsujikawa, S., Shum, A. K., Shrestha, N., Yamashita, M., Miller, R. J., Radulovic, J., Swanson, G. T., & Prakriya, M. (2020). Orai1 Channels Are Essential for Amplification of Glutamate-Evoked Ca2+ Signals in Dendritic Spines to Regulate Working and Associative Memory. *Cell Reports*, *33*(9), 108464.

Mannaioni, G., Marino, M. J., Valenti, O., Traynelis, S. F., & Conn, P. J. (2001). Metabotropic glutamate receptors 1 and 5 differentially regulate CA1 pyramidal cell function. *The Journal of Neuroscience: The Official Journal of the Society for Neuroscience*, *21*(16), 5925–5934.

Matamala, E., Castillo, C., Vivar, J. P., Rojas, P. A., & Brauchi, S. E. (2021). Imaging the electrical activity of organelles in living cells. *Communications Biology*, *4*(1), 389.

Meissner, G., & McKinley, D. (1982). Permeability of canine cardiac sarcoplasmic reticulum vesicles to K+, Na+, H+, and Cl-. *The Journal of Biological Chemistry*, *257*(13), 7704–7711.

Merlin, L. R. (2002). Differential roles for mGluR1 and mGluR5 in the persistent prolongation of epileptiform bursts. *Journal of Neurophysiology*, *87*(1), 621–625.

Mitchell, P. (1961). Coupling of phosphorylation to electron and hydrogen transfer by a chemi-osmotic type of mechanism. *Nature*, *191*, 144–148.

Nakamura, T., Barbara, J. G., Nakamura, K., & Ross, W. N. (1999). Synergistic release of Ca2+ from IP3-sensitive stores evoked by synaptic activation of mGluRs paired with backpropagating action potentials. *Neuron*, *24*(3), 727–737.

Nixon-Abell, J., Obara, C. J., Weigel, A. V., Li, D., Legant, W. R., Xu, C. S., Pasolli, H. A., Harvey, K., Hess, H. F., Betzig, E., Blackstone, C., & Lippincott-Schwartz, J. (2016). Increased spatiotemporal resolution reveals highly dynamic dense tubular matrices in the peripheral ER. *Science*, *354*(6311). https://doi.org/10.1126/science.aaf3928

Oetliker, H. (1982). An appraisal of the evidence for a sarcoplasmic reticulum membrane potential and its relation to calcium release in skeletal muscle. *Journal of Muscle Research and Cell Motility*, *3*(3), 247–272.

Oetliker, H. (1989). Energetical considerations related to calcium release from the sarcoplasmic reticulum in skeletal muscle. *Biomedica Biochimica Acta*, *48*(5-6), S313–S318.

Omura, T., Siekevitz, P., & Palade, G. E. (1967). Turnover of constituents of the endoplasmic reticulum membranes of rat hepatocytes. *The Journal of Biological Chemistry*, *242*(10), 2389–2396.

Orso, G., Pendin, D., Liu, S., Tosetto, J., Moss, T. J., Faust, J. E., Micaroni, M., Egorova, A., Martinuzzi, A., McNew, J. A., & Daga, A. (2009). Homotypic fusion of ER membranes requires the dynamin-like GTPase atlastin. *Nature*, *460*(7258), 978–983.

Perez-Alvarez, A., Yin, S., Schulze, C., Hammer, J. A., Wagner, W., & Oertner, T. G. (2020). Endoplasmic reticulum visits highly active spines and prevents runaway potentiation of synapses. *Nature Communications*, *11*(1), 5083.

Purgert, C. A., Izumi, Y., Jong, Y.-J. I., Kumar, V., Zorumski, C. F., & O'Malley, K. L. (2014). Intracellular mGluR5 can mediate synaptic plasticity in the hippocampus. *The Journal of Neuroscience: The Official Journal of the Society for Neuroscience*, *34*(13), 4589–4598.

Rall, W. (1962). Theory of physiological properties of dendrites. *Annals of the New York Academy of Sciences*, *96*, 1071–1092.

Rall, W., & Rinzel, J. (1973). Branch input resistance and steady attenuation for input to one branch of a dendritic neuron model. *Biophysical Journal*, *13*(7), 648–687.

Redman, C. M., & Sabatini, D. D. (1966). Vectorial discharge of peptides released by puromycin from attached ribosomes. *Proceedings of the National Academy of Sciences of the United States of America*, *56*(2), 608–615.

Reiner, A., & Levitz, J. (2018). Glutamatergic Signaling in the Central Nervous System: Ionotropic and Metabotropic Receptors in Concert. *Neuron*, *98*(6), 1080–1098.

Ross, W. N. (2012). Understanding calcium waves and sparks in central neurons. *Nature Reviews. Neuroscience*, *13*(3), 157–168.

Saminathan, A., Devany, J., Veetil, A. T., Suresh, B., Pillai, K. S., Schwake, M., & Krishnan, Y. (2021). A DNA-based voltmeter for organelles. *Nature Nanotechnology*, *16*(1), 96–103.

Sanchez, C., Berthier, C., Allard, B., Perrot, J., Bouvard, C., Tsutsui, H., Okamura, Y., & Jacquemond, V. (2018). Tracking the sarcoplasmic reticulum membrane voltage in muscle with a FRET biosensor. *The Journal of General Physiology*, *150*(8), 1163–1177.

Schoepp, D. D., Goldsworthy, J., Johnson, B. G., Salhoff, C. R., & Baker, S. R. (1994). 3,5-dihydroxyphenylglycine is a highly selective agonist for phosphoinositide-linked metabotropic glutamate receptors in the rat hippocampus. *Journal of Neurochemistry*, *63*(2), 769–772.

Schulien, A. J., Justice, J. A., Di Maio, R., Wills, Z. P., Shah, N. H., & Aizenman, E. (2016). Zn(2+) -induced Ca(2+) release via ryanodine receptors triggers calcineurin-dependent redistribution of

cortical neuronal Kv2.1 K(+) channels. *The Journal of Physiology*, *594*(10), 2647–2659.

Sepehri Rad, M., Cohen, L. B., Braubach, O., & Baker, B. J. (2018). Monitoring voltage fluctuations of intracellular membranes. *Scientific Reports*, *8*(1), 6911.

Shin, J., Dunbrack, R. L., Jr, Lee, S., & Strominger, J. L. (1991). Signals for retention of transmembrane proteins in the endoplasmic reticulum studied with CD4 truncation mutants. *Proceedings of the National Academy of Sciences of the United States of America*, *88*(5), 1918–1922.

Sorgato, M. C., Keller, B. U., & Stühmer, W. (1987). Patch-clamping of the inner mitochondrial membrane reveals a voltage-dependent ion channel. *Nature*, *330*(6147), 498–500.

Spacek, J., & Harris, K. M. (1997). Three-dimensional organization of smooth endoplasmic reticulum in hippocampal CA1 dendrites and dendritic spines of the immature and mature rat. *The Journal of Neuroscience: The Official Journal of the Society for Neuroscience*, *17*(1), 190–203.

Stock, D., Leslie, A. G., & Walker, J. E. (1999). Molecular architecture of the rotary motor in ATP synthase. *Science*, *286*(5445), 1700–1705.

Sugiyama, H., Ito, I., & Hirono, C. (1987). A new type of glutamate receptor linked to inositol phospholipid metabolism. *Nature*, *325*(6104), 531–533.

Tanifuji, M., Sokabe, M., & Kasai, M. (1987). An anion channel of sarcoplasmic reticulum incorporated into planar lipid bilayers: single-channel behavior and conductance properties. *The Journal of Membrane Biology*, *99*(2), 103–111.

Tedeschi, H., Mannella, C. A., & Bowman, C. L. (1987). Patch clamping the outer mitochondrial membrane. *The Journal of Membrane Biology*, *97*(1), 21–29.

Thillaiappan, N. B., Chavda, A. P., Tovey, S. C., Prole, D. L., & Taylor, C. W. (2017). Ca2+ signals initiate at immobile IP3 receptors adjacent to ER-plasma membrane junctions. *Nature Communications*, *8*(1), 1505.

Toresson, H., & Grant, S. G. N. (2005). Dynamic distribution of endoplasmic reticulum in hippocampal neuron dendritic spines. *The European Journal of Neuroscience*, *22*(7), 1793–1798.

Townsley, F. M., & Pelham, H. R. (1994). The KKXX signal mediates retrieval of membrane proteins from the Golgi to the ER in yeast. *European Journal of Cell Biology*, *64*(1), 211–216.

Valm, A. M., Cohen, S., Legant, W. R., Melunis, J., Hershberg, U., Wait, E., Cohen, A. R., Davidson, M. W., Betzig, E., & Lippincott-Schwartz, J. (2017). Applying systems-level spectral imaging and analysis to reveal the organelle interactome. *Nature*, *546*(7656), 162–167.

Vierra, N. C., Kirmiz, M., van der List, D., Santana, L. F., & Trimmer, J. S. (2019). Kv2.1 mediates spatial and functional coupling of L-type calcium channels and ryanodine receptors in mammalian neurons. *eLife*, *8*. https://doi.org/10.7554/eLife.49953

Vierra, N. C., O'Dwyer, S. C., Matsumoto, C., Santana, L. F., & Trimmer, J. S. (2021). Regulation of neuronal excitation-transcription coupling by Kv2.1-induced clustering of somatic L-type Ca2+ channels at ER-PM junctions. *Proceedings of the National Academy of Sciences of the United States of America*, *118*(46). https://doi.org/10.1073/pnas.2110094118

Wang, X.-H., Su, M., Gao, F., Xie, W., Zeng, Y., Li, D.-L., Liu, X.-L., Zhao, H., Qin, L., Li, F., Liu, Q., Clarke, O. B., Lam, S. M., Shui, G.-H., Hendrickson, W. A., & Chen, Y.-H. (2019). Structural basis for activity of TRIC counter-ion channels in calcium release. *Proceedings of the National Academy of Sciences of the United States of America*, *116*(10), 4238–4243.

Wang, X., Zhang, X., Dong, X.-P., Samie, M., Li, X., Cheng, X., Goschka, A., Shen, D., Zhou, Y., Harlow, J., Zhu, M. X., Clapham, D. E., Ren, D., & Xu, H. (2012). TPC proteins are phosphoinositide-activated sodium-selective ion channels in endosomes and lysosomes. *Cell*, *151*(2), 372–383.

Wild, A. R., Sinnen, B. L., Dittmer, P. J., Kennedy, M. J., Sather, W. A., & Dell'Acqua, M. L. (2019). Synapse-to-Nucleus Communication through NFAT Is Mediated by L-type Ca2+ Channel Ca2+ Spike Propagation to the Soma. *Cell Reports*, *26*(13), 3537–3550.e4.

Wu, H., Carvalho, P., & Voeltz, G. K. (2018). Here, there, and everywhere: The importance of ER membrane contact sites. *Science*, *361*(6401). https://doi.org/10.1126/science.aan5835

Wu, Y., Whiteus, C., Xu, C. S., Hayworth, K. J., Weinberg, R. J., Hess, H. F., & De Camilli, P. (2017). Contacts between the endoplasmic reticulum and other membranes in neurons. *Proceedings of the National Academy of Sciences of the United States of America*, *114*(24), E4859–E4867.

Yazawa, M., Ferrante, C., Feng, J., Mio, K., Ogura, T., Zhang, M., Lin, P.-H., Pan, Z., Komazaki, S., Kato, K., Nishi, M., Zhao, X., Weisleder, N., Sato, C., Ma, J., & Takeshima, H. (2007). TRIC channels are essential for Ca2+ handling in intracellular stores. *Nature*, *448*(7149), 78–82.

Zhu, J., Yan, J., & Thornhill, W. B. (2014). The Kv1.3 potassium channel is localized to the cis-Golgi and Kv1.6 is localized to the endoplasmic reticulum in rat astrocytes. *The FEBS Journal*, *281*(15), 3433–3445.